Record 2002/02

GAWLER CRATON MINERAL PROMOTION PROJECT

Interpretation of Airborne Electromagnetic Data:

Summary report on the Challenger Workshop

Richard Lane and Lisa Worrall

With contributions from Roger Skirrow, Patrick Lyons, Tony Poustie, David Frances, Andrew Tomkins, Peter Williams, Sue Daly, Baohong Hou, David Gray, John Wilford, Ross Brodie, Peter Milligan, Matti Peljo and Lindsay Highet.

In collaboration with:

MINERALS & ENERGY RESOURCES

Government of South Australia

CRCLEME

Dominion Mining Limited

GEOSCIENCE AUSTRALIA

GEOSCIENCE Australia

SPATIAL INFORMATION FOR THE NATION

Geoscience Australia

Chief Executive Officer: Dr Neil Williams

Department of Industry, Tourism & Resources

Minister for Industry, Tourism & Resources: The Hon. Ian Macfarlane MP
Parliamentary Secretary: The Hon. Warren Entsch, MP

ISBN: 0 642 467315

Bibliographic reference: Lane, R.. & Worrall, L. 2002. Interpretation of Airborne Electromagnetic Data: Summary Report on the Challenger Workshop. Geoscience Australia Record 2002/02.

Table of Contents

List of Figures

1 Executive Summary

This report details the outcomes of a 2-day interpretation workshop for TEMPEST airborne electromagnetic data acquired in the Challenger area, northern Gawler Craton, South Australia. The purpose of the workshop was to bring together representatives of GA, PIRSA, CRC LEME, and the mineral explorers at Challenger, to integrate products of the AEM survey with existing information and commence the process of evaluating the AEM data for mineral exploration in the Challenger environment. The workshop was expected to result in a new understanding of the geology and mineralising systems in the prospect area.

The report contains (1) the principal findings of the workshop, (2) recommended processing strategies for the AEM data, with examples of processed data, (3) recommended interpretation strategies and (4) a summary interpretation.

The AEM data proved to have good signal to noise ratio, and the conductivity depth inversion algorithm produced results which were consistent with the available drillhole data. The derived conductivity distribution was relatively simple, allowing plan view summary products to be used for interpretation (e.g., Figure 1). However, it became apparent in the course of the workshop that these products are less than ideal for the interpretation of conductivity variation in three-dimensional space. Further development of software tools to facilitate the integrated analysis of geological and geophysical data is required.

There is no outcrop in the Challenger area. Observed conductivity patterns were used to sub-divide the regolith into areas dominated by the presence of transported materials and areas dominated by the presence of *in situ* materials. This partition has important implications for the interpretation of surface geochemical data. If available at an earlier stage of exploration of the Challenger area, this partition would have helped to divert sampling and drilling away from areas with greater thickness of transported material. The areas dominated by transported materials were further subdivided into areas of relatively shallow cover (less than 30 m) and thicker cover (greater than 100 m). The areas dominated by *in situ* materials were further subdivided into large areas (1-5 km) of homogeneous resistive regolith, smaller round areas (< 1km) of homogeneous resistive regolith and areas of conductive regolith. The latter generally surrounded the round homogeneous resistive areas or formed along inferred structures. The Challenger deposit is located in one of the areas where conductive *in situ* regolith materials are present.

A further iteration of geological investigations in the Challenger area is recommended in the light of the AEM interpretation. Foremost in this regard would be a re-mapping of the subtle variations in basement lithology, comparison of conductivity data with drillhole regolith logging carried out by CRC LEME (Lintern and Sheard, 1999) and a re-evaluation of the interpretive mapping of surficial deposits.

Analysis of ground EM and resistivity data presented at the workshop led to the conclusion that conductivity mapping would not pinpoint the Challenger deposit or a deposit like it. At best, this mineralisation style may be weakly conductive in contrast to resistive surrounds. Despite this finding, an analysis of the AEM data (in profile form) for discrete conductors was carried out, and a number of third (low) priority targets were established.

A 200 m deep trough of transported material was identified by the AEM survey 2 km to the west of the Challenger deposit. Subsequent drilling confirmed the predicted depth of this trough and established the presence of groundwater that could be used during mining of Challenger.

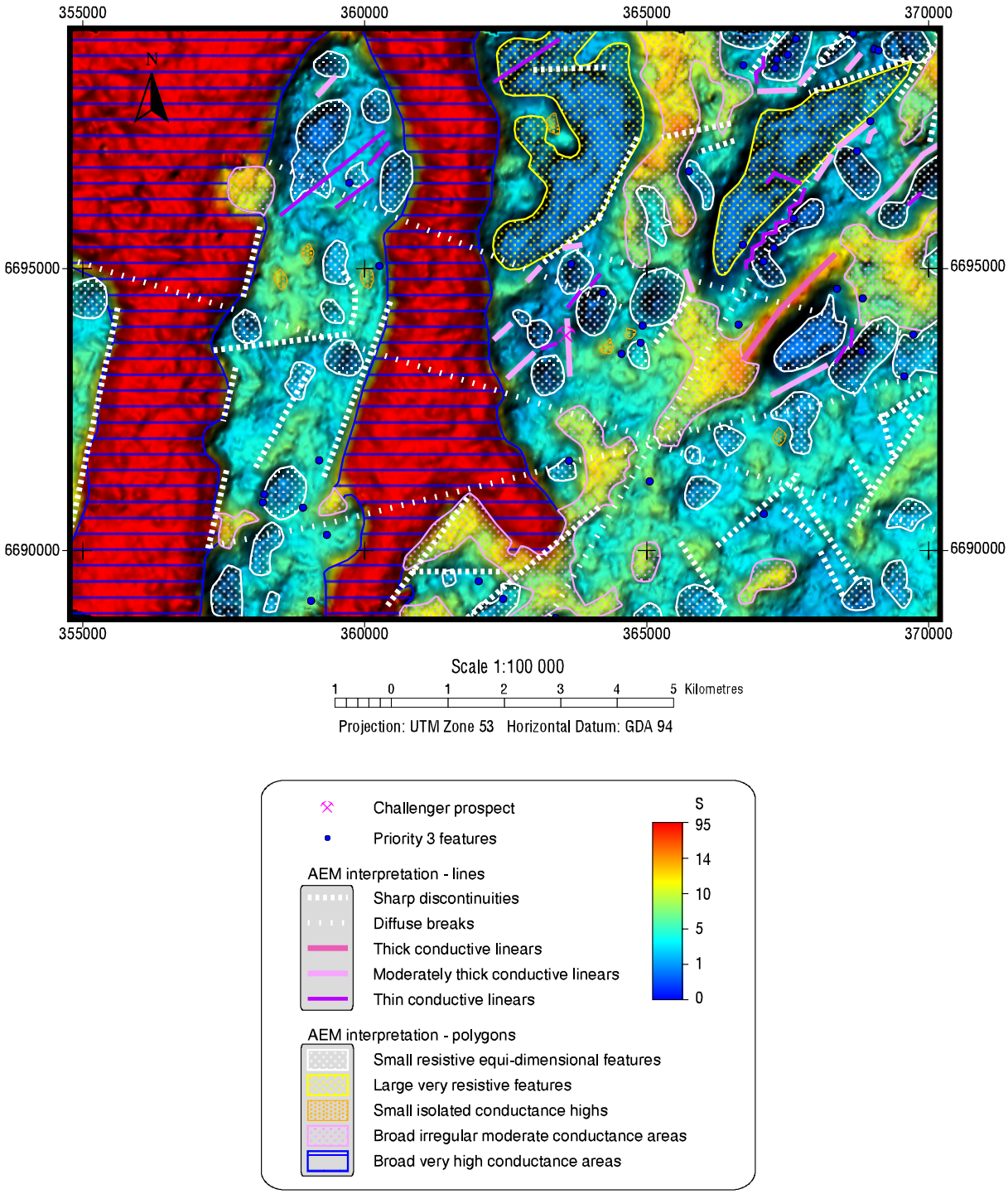

Figure 1. Conductance of the "conductive unit" derived from the AEM survey data overlain by the AEM interpretation .

2 Introduction

2.1 Gawler Craton Mineral Promotion Project (Roger Skirrow)

The Gawler Craton Mineral Promotion Project is a collaborative program between the n Geoscience Australia (GA), Primary Industries and Resources South Australia (PIRSA) and the Cooperative Research Centre for Landscape Evolution and Mineral Exploration (CRC LEME) operating within the National Geoscience Agreement. The planned outcome of the Project is the enhancement of the global attractiveness of Australia's exploration investment opportunities by the development of a new geoscientific framework for the Gawler Craton. The three-year program involves multidisciplinary teams from the Minerals Division in GA, the Office of Minerals and Energy Resources in PIRSA and CSIRO CRC LEME. The Project aims to develop a new regional geological framework to underpin discovery of economic mineral deposits in the Gawler Craton, focussing on Proterozoic Cu-Au, Archean Au, and Archean Ni-Cu ore-forming systems in three regions (Modules A, B, C, Figure 2).

The crystalline Archean to Mesoproterozoic basement of the Gawler Craton (Drexel et al., 1993) is extensively obscured by sedimentary basins and regolith cover, which have hindered both geological mapping and exploration. Despite major advances in the understanding of basement geology through interpretation of high-resolution aeromagnetics, this method is less effective for geological mapping where there is poor magnetic contrast in the basement rocks. Alternative geophysical imaging techniques include high-resolution gravity, 3D seismic and airborne electromagnetics (AEM), all of which have been implemented or are planned in the Gawler Craton Project.

The program of regolith studies (Module D) is an integral part of the Gawler Craton Project and is aimed at improved recognition of Cu-Au, Ni-Cu and Au ore-forming systems within and through the regolith. The regolith program involves the acquisition and interpretation of AEM data and integration of these data with geological investigations and geochemical studies of gold and base metal dispersion within the regolith. The application of AEM to mapping of both regolith and basement geology in an area of gold-mineralised Archean metamorphic rocks is described in this report. AEM also has considerable promise as a tool for mapping hydrological features that control geochemical dispersion within the regolith. This latter application of AEM is the subject of ongoing studies in Module D, and is reported elsewhere.

Proterozoic Cu-Au systems are the focus of Project investigations in the Olympic Cu-Au-Fe province (Module A), a region extending along the eastern margin of the Gawler Craton northwards from the Moonta-Wallaroo Cu-Au district, via Olympic Dam to the Mt Woods Inlier. In a related study, gold systems of the central Gawler Craton (Tarcoola – Tunkillia – Myall-Sheoak) and their relationship to granites are being investigated as part of a Ph.D. by an GA team member. Module B is focussed on Archean Au systems of the Mulgathing Complex, represented by the Challenger deposit in the northwestern Gawler Craton. PIRSA are currently investigating the Ni-Cu potential of Archean mafic-ultramafic rocks in the central Gawler Craton, in collaboration with GA (Module C).

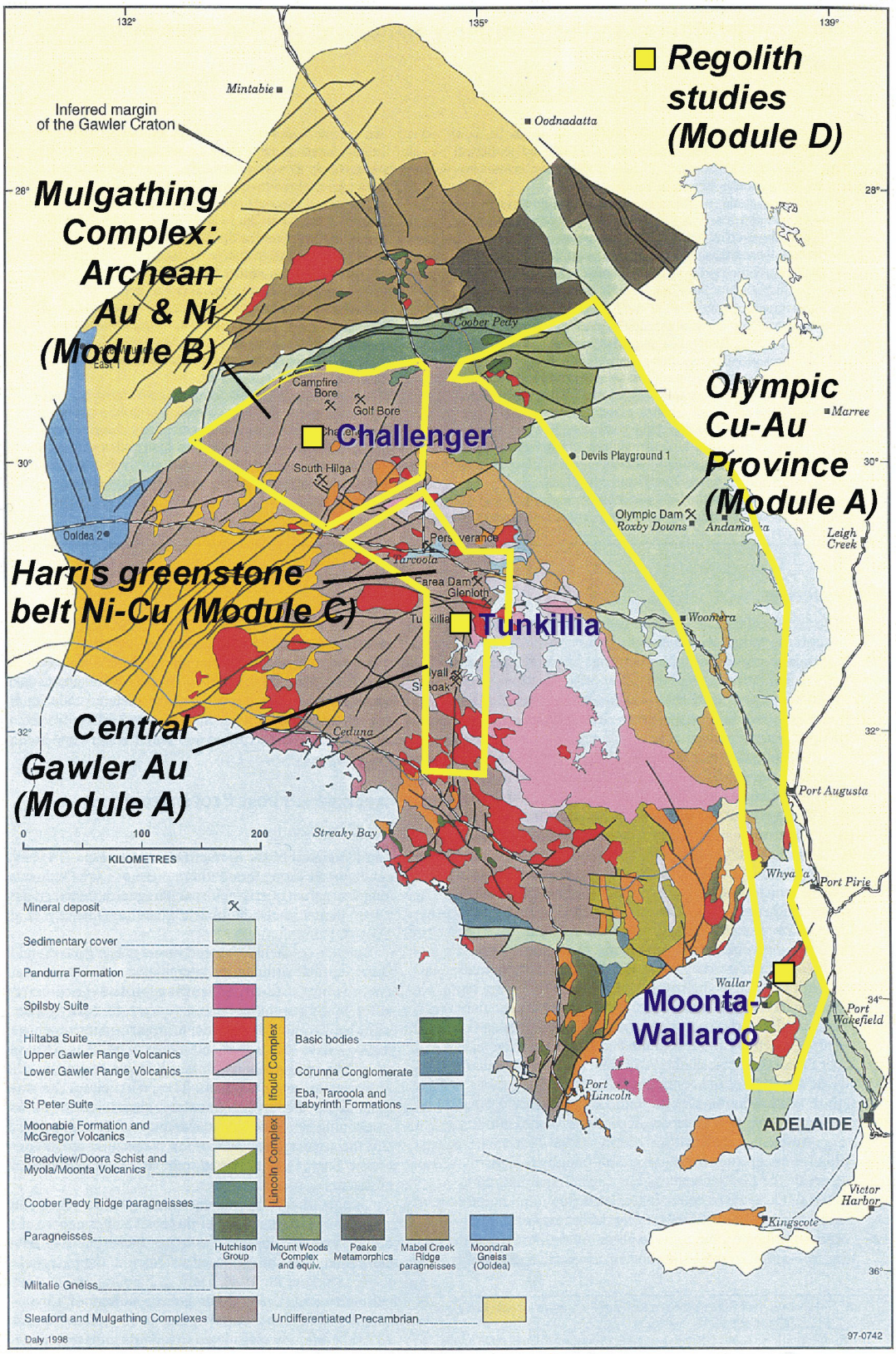

Figure 2. Areas of focus in the Gawler Craton Mineral Promotion Project. Project AEM Surveys (yellow boxes) are also shown

2.2 AEM Data Acquisition and Processing

In order to investigate the potential of AEM as a regolith and bedrock geological mapping tool in the Gawler Craton, three AEM surveys were flown in contrasting geological settings (Figure 2). The areas selected were (1) in the vicinity of Moonta-Wallaroo on the Yorke Peninsula in the eastern Gawler (1055 line km), (2) over the Tunkillia prospect in the central Gawler (3215 line km), and (3) over the Challenger deposit in the central northwestern Gawler (1130 line km).

The Moonta-Wallaroo area is representative of Mesoproterozoic Cu-Au mineralisation, and also Pb-Zn mineralisation hosted by the Paleoproterozoic basement. The basement rocks have been deeply weathered and are overlain by a variably thick cover of transported materials that dates back to the Cambrian. Regolith thickness (transported plus *in situ* materials) varies from a few metres to over 200 m. The Tunkillia area is the site of recent Au-in-calcrete discoveries that relate to Mesoproterozoic(?) processes, but which have yet to yield significant ore reserves. The area is blanketed by sand dunes and there is no outcrop. At the time of the survey little was known about the extent of weathering or the nature of the transported cover, however drilling did indicate that the thickness of regolith varies from a few metres to around 55 m. The Challenger area is representative of Au mineralisation in Archean metamorphic rocks. Drilling in the vicinity of the Challenger deposit indicated that the regolith, which comprises both transported and *in situ* materials, varies in thickness from a few metres to around 50 m.

The AEM surveys were flown in June 2000 by Fugro Airborne Surveys (FAS) using the TEMPEST AEM system, a low base frequency, broad bandwidth, time domain system developed by CRC AMET (Lane et al., 2000). The surveys were flown at 150 m line spacing along east-southeast/west-northwest (Moonta-Wallaroo and Challenger) and northeast/southwest (Tunkillia) lines (Appendix 1). The nominal height of the aircraft (transmitter loop) was 110 m. The three component dB/dt receiver was towed 109 m behind and 43 m below the aircraft. Streamed data were recorded then stacked into 0.2s (12 m) samples. The stacked data were deconvolved and the primary field removed. The deconvolved data were transformed into an equivalent B-field response for a perfect 100% duty cycle square wave, then binned into 15 windows with centres ranging from 13 µs to 16.2 ms. The data were also transformed to conductivity using EMFlow. The windowed data and the inverted data were received from FAS in September 2000 and released to the public on the 1st of December 2000.

2.3 Interpretation Workshops

In order to facilitate the interpretation of the AEM data from the three survey areas, three two day workshops were held at GA in Canberra between the 5th and 16th of February 2001. These workshops brought together the collaborators in the Gawler Craton Mineral Promotion Project (GA, PIRSA and CRC LEME), and the mineral explorers operating in the area under consideration. A technical facilitator (Richard Lane) was on hand to provide assistance with details of AEM data acquisition, processing and interpretation.

Prior to the workshop all available regolith geological, geological, geophysical and geochemical data from each survey area were compiled in a Geographic Information System (GIS). As many of the datasets are confidential, all participants were required to sign a confidentiality agreement which recognised data ownership, and imposed a confidentially condition on the release of the workshop outcomes

The workshops were a mix of lectures on the TEMPEST AEM system, the use of TEMPEST data in discrete conductor detection and geological mapping, sessions with participants investigating the relationships between various data sets, and sessions when interpretation was carried out jointly by all participants.

In general terms, the outcomes of the workshops were a better understanding of the role of AEM in mapping regolith and geology in the Gawler Craton, and a preliminary assessment of the conductivity information derived from the TEMPEST surveys. The preliminary interpretation of the data is presented in three reports, each with an accompanying GIS. The reports contain a number of recommendations regarding further investigations in the survey areas.

2.4 Participants in the Challenger Workshop

The Challenger workshop was attended by Tony Poustie and David Frances (Dominion Mining Limited), Peter Williams (Resolute Limited), Andrew Tomkins (ANU), Sue Daly and Baohong Hou (PIRSA), David Gray and John Wilford (CRC LEME), and Roger Skirrow, Lisa Worrall and Patrick Lyons (GA). Richard Lane was the facilitator and Ross Brodie, Peter Milligan, Matti Peljo and Lindsay Highet (GA) provided geophysical and GIS support.

2.5 Participant Expectations of the Challenger Workshop

The expectations of the participants were surveyed at the start of the workshop. This helped focus the workshop and provided a basis for assessing progress made during workshop sessions.

Some of the responses are given below.

- A previous experience with AEM involved looking for bumps at the base of profiles, most of which turned out to be caused by fences. Has anything changed?
- I would like to take away from this workshop a better understanding of AEM, for both discrete target detection and mapping.
- Imaging of AEM data is relatively new – what are the artifacts in this process?
- What do AEM data map in this environment?
- What is the relationship of the regolith units derived from interpretation of AEM data with what is observed at surface?
- If regolith units can be mapped from the AEM data, does this help to understand the dispersion of metals and the interpretation of geochemical patterns?
- Do AEM data provide a means of prioritising the more than 500 calcrete surface geochemical anomalies (> 5 ppb Au) that exist around Challenger?
- Can AEM assist in locating groundwater for mineral processing?
- Can AEM detect and map the regional distribution of palaeochannels?
- Is it possible to integrate 3D conductivity data with existing drilling and what does this tell us?
- Can any new targets be identified from the AEM data?
- Does it work? Is it cost effective?
- What are the relationships between conductivity, geology and groundwater?
- What is the regional mapping capability of AEM?
- Recent applications of TEMPEST (e.g., Lawrie et al., 2000; Lane and Pracillio, 2000) have compared conductivity derived from AEM measurements with conductivity measured in drillholes. Can conductivity information from AEM be relied upon without drillhole calibration? Can it be interpreted without correlation to lithological and fluid information obtained from drillholes?
- I would like to learn about methods of AEM data display and how the data can be integrated with other data.
- What is the AEM signature of Challenger and does this complement the magnetic and geochemical signatures? Will AEM data be useful for exploration in this environment?

3 Exploration, Geology, and Mineralisation in the Challenger Area

3.1 Exploration and Geology (Tony Poustie and Patrick Lyons)

The Challenger gold deposit was discovered in May 1995 following more than three years of exploration in the Gawler Craton, initially by Dominion Mining Limited and later by Dominion in Joint Venture with Resolute Limited. The discovery can be attributed both to exploration initiatives (including bedrock drilling and airborne geophysical programs) undertaken by the South Australian Government, and to the innovatory application of calcrete geochemistry by the Joint Venture. To date, resources totalling 1.79 Mt grading 8.6 g/t Au (495,000 ounces of contained Au) have been outlined to a maximum depth of 480 m. The mineralisation is open at depth.

The deposit is hosted in the Christie Gneiss of the Mulgathing Complex, an assemblage of garnet-rich paragneiss, amphibolite, and meta-norite and -pyroxenite, which underwent polyphase deformation and metamorphism to granulite facies during the Sleafordian Orogeny (~2440 Ma). As mafic and ultramafic protoliths of the Mulgathing Complex lost magnetite during granulite facies metamorphism, the Christie Gneiss in the Challenger area is non-magnetic and shows a uniform character in TMI images. This makes the lithological distribution difficult to resolve via magnetics. High-grade Au mineralisation is associated with quartz-feldspar rich leucosomes that form shoots plunging approximately 30° to 030°. It is believed that this plunge is defined by an asymmetric fold closure in the gneissic foliation. Au mineralisation is associated with arsenopyrite (with löllingite), pyrrhotite, pyrite, and rare graphite. Chalcopyrite and bismuth compounds are also noted. Gold occurs as single grains or aggregates in arsenopyrite (commonly at the interface with löllingite cores) and as inclusions in quartz, K-feldspar, and plagioclase.

Dominion Mining Limited (now 100% owners of the Challenger property) is currently carrying out a feasibility study to commence development of the Challenger deposit. The proposed development will involve an initial open pit to recover approximately 100,000 ounces of Au, followed by underground development. The discovery of any additional resources close to Challenger could provide a significant boost to the chances of the proposed development. In the past, there has been a significant exploration effort focussed on the Challenger area but no additional resources with economic potential have been outlined.

3.2 Mineralisation (Andy Tomkins)

Challenger is an Archaean Au deposit that was metamorphosed at granulite facies conditions of 800°C and 7.5kbar about 2440 Ma. The pelitic host rock underwent partial melting at this time. Simultaneously, much of the gold and bismuth and some arsenopyrite (and other minor sulfides) melted. The silicate and metal-sulfide melt were redistributed together to form leucosomes. Ptygmatic folding was synchronous with leucosome formation and may have developed in an S-vergent dilatant shear system. This resulted in the development of the fold-parallel ore shoots which plunge ~30°/030°. Some time later mafic dykes and sills intruded the deposit but did not remobilise the mineralisation. Competency contrasts developed between mafic dykes/sills and pelitic gneiss caused fracturing along their contact. This allowed fluid infiltration, which altered both the dykes/sills and the pelitic gneiss and caused some redistribution of gold.

Apart from the dominant pelitic gneiss and the mafic dykes/sills some 2-pyroxene mafic granulite has also been intersected by drilling. This rock is also significantly mineralised. Importantly, because mineralisation was introduced prior to peak metamorphism, Challenger could represent a typical Archaean Au deposit, many of which are hosted in mafic rocks as well as BIF. The presence of mineralised mafic rock at Challenger is further encouragement

that Au mineralisation in the northwest Gawler is not necessarily only hosted in pelitic gneisses.

There are strong indications that the late fluid infiltration event caused redistribution of gold and sulfides. Throughout the northwest Gawler there are many late shear zones, which have acted as fluid pathways well after peak metamorphism. Given the degree of gold anomalism in the region, small splays of these major shears that intersect appropriate rock types (i.e., the general Yilgarn model) could represent exploration targets.

Based on examples in the Glenelg River Complex, western Victoria (Kemp, AGC 2000) and at Cooma (Ellis and Obata, 1992), it is possible that silicate melt, which escaped from leucosomes at Challenger, ponded nearby in a small granitic accumulation (although, it could well have escaped entirely to upper crustal levels). Some gold-rich metallic melt would have left the system with escaping silicate melt. Consequently, such small granitic accumulations could contain significant gold.

Finally, based on mineral assemblages associated with gold in unweathered rock at Challenger, an appropriate multi-element geochemical sampling suite would include: Au, Bi, As, Co, Ni, Cu, S, Te, Zn in order of importance.

3.3 Geophysics (Peter Williams and Richard Lane)

The Joint Venture partners acquired ultra-detailed aeromagnetic data (25 m and 50 m line spacing, 20m terrain clearance) over the deposit. A low order northeast trending anomaly (6nT) is associated with the main area of mineralisation due to the presence of a halo of pyrrhotite. The magnetic fabric of the area is dominated, however, by a number of dyke suites. Prominent amongst these are northeast striking dolerite dykes and northwest striking lamprophyre dykes. The anomaly associated with mineralisation is subtly different to the northeast trending anomalies associated with dolerite dykes in that the strike is a few degrees more to the north and the anomaly is slightly broader. The latter is probably a reflection of greater depth of weathering over mineralisation relative to that present over dolerite dykes. The Kelpie mineralisation trend also has a low order anomaly associated with it. Again this is due to pyrrhotite associated with late stage remobilised Au. This trend strikes NNE, 10° to 20° anti-clockwise from the main NE dolerite dyke trend.

Drilling information in the main area of mineralisation suggested that a weathering trough over the deposit might give rise to a patch of conductive cover that could be mapped using EM or other electrical techniques. Bonwick (1997) reports that the depth of weathering over the deposit is 40 m to 50 m and around 10 m elsewhere. The quality of gradient array resistivity and induced polarisation measurements was affected by difficulties getting current into the ground through a very thin highly resistive layer at surface. A total of 4 lines of Zonge nanoTEM ground electromagnetic data were acquired along east-west lines over the deposit in 1997. This revealed a N/S striking conductive feature to 200 mS/m in a 5 mS/m background. The subcrop of the ore shoots falls within the N/S conductive trough. However, the trough is far more extensive than the ore shoots, reducing the value of this observation for identifying targets in the surrounding area.

A swath of GEOTEM AEM data was acquired over the deposit by the Joint Venture partners (Geoterrex Job 776). These data were inspected for discrete conductors at the time of the survey but none were identified. No further analysis of these data was carried out in a mapping sense.

4 Interpretation Process

4.1 Assessment of Data Integrity

4.1.1 Data repeatability

The reliability of the complete acquisition and processing system was tested by repeating one line within the survey area on each flight. The data from this line were processed in the same manner as the rest of the data from the flight. The repeat line chosen in the Challenger area was an east-west line passing over the deposit (at 363500 m E 6693700 m N, MGA Zone 53, GDA94 datum).

The comparison of results obtained along the repeat line could be carried out using (i) window amplitude profiles prior to approximate correction for variations in system geometry (e.g., transmitter loop terrain clearance, transmitter loop attitude, and transmitter loop to receiver coil geometry), (ii) window amplitude profiles after application of the approximate corrections or (iii) conductivity sections. The latter were chosen because as many of the incidental variations have been removed as is possible. Also, conductivity data were the principal end product used for interpretation of data from the main survey, so it made sense to use this product for assessing system repeatability. Terrain clearance variations have a significant effect on the amplitude of the response profiles. This is particularly so at the early times, and especially in areas such as this which are dominated by near surface (top 50 m) conductive material. Hence, comparison of window response profiles prior to correcting for these variations is far more difficult than comparison of conductivity sections. Response variations due to changes in the system geometry and some of system-specific features in the data (e.g., waveform, recorded quantity (dB/dt or B-field)) are removed prior to or during the transformation to conductivity.

The most striking feature of the repeat line (Figure 3) is an extremely broad (2 km), deep (150 m), conductive (300-400 mS/m) zone west of 362300mE. There are indications of slightly greater conductivity on the flanks than in the centre.

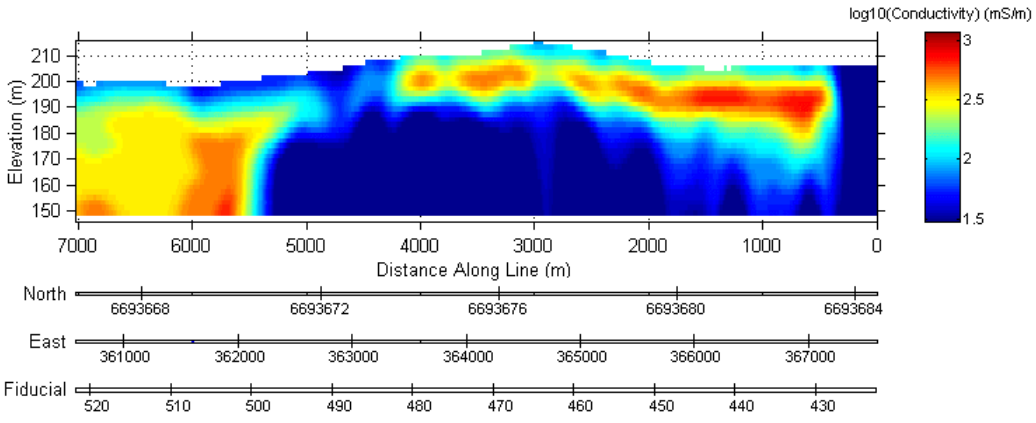

Figure 3. Conductivity section from flight 12 for the repeat line (360600mE 6693650mN to 367600mE 6693650mN) shown with a minimum depth extent of 70 m.

The overall pattern from around 363300 m E to 367200 m E is of a near surface conductive wedge increasing in thickness (and conductance) to the east from 20 m to 50 m. Within this wedge, a discrete patch of near surface conductive material 100 m to 200 m wide is evident,

centred at 363500 m E. This coincides with the location of the upper part of the main body of mineralisation at Challenger.

A narrow, more resistive zone occurs between 364500 m E and 364900 m E, over the crest of the slight rise. A weakly elevated conductivity artifact is present at depths of 20 m to 50 m below this resistive zone. The extreme eastern end of the line, beyond the sharp termination of the near-surface conductive unit, is significantly more resistive than the remainder of the line.

Figure 4 shows the conductivity section to greater depth and with less vertical exaggeration than in Figure 3. A grey mask has been applied to the section to indicate the effective limit of useful and reliable conductivity prediction.

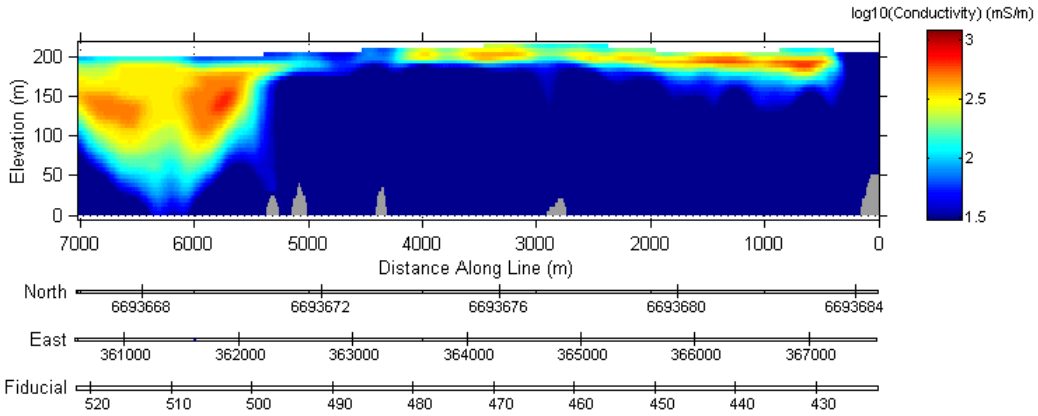

Figure 4. Conductivity section from flight 12 for the repeat line (360600mE 6693650mN to 367600mE 6693650mN) shown with a minimum depth extent of 220m. A grey mask has been applied to the section below the depth of last signal return.

Conductivity sections for the four passes over the repeat line are shown in Figures 5 and 6. The deep conductive trough on the western end of the line is approximately 2 km wide and more than 150 m deep. Predicting the conductivity near the base of such high conductance features is difficult, but the general uncertainty from pass to pass of at most a few 10's of metres to the base of this feature is an indication of good quality data. The pattern of higher conductivity values towards the flanks of the trough is not uncommon in large channels filled with transported material. At Toolibin this reflected a greater proportion of conductive clays towards the margins and slightly more resistive sandy material in the central part of the channel (Lane and Pracilio, 2000).

The thinner surficial conductors in the centre and eastern end of the line show excellent repeatability. There is no evidence of any bedrock conductors along this line, in either the window amplitude profiles or the conductivity sections.

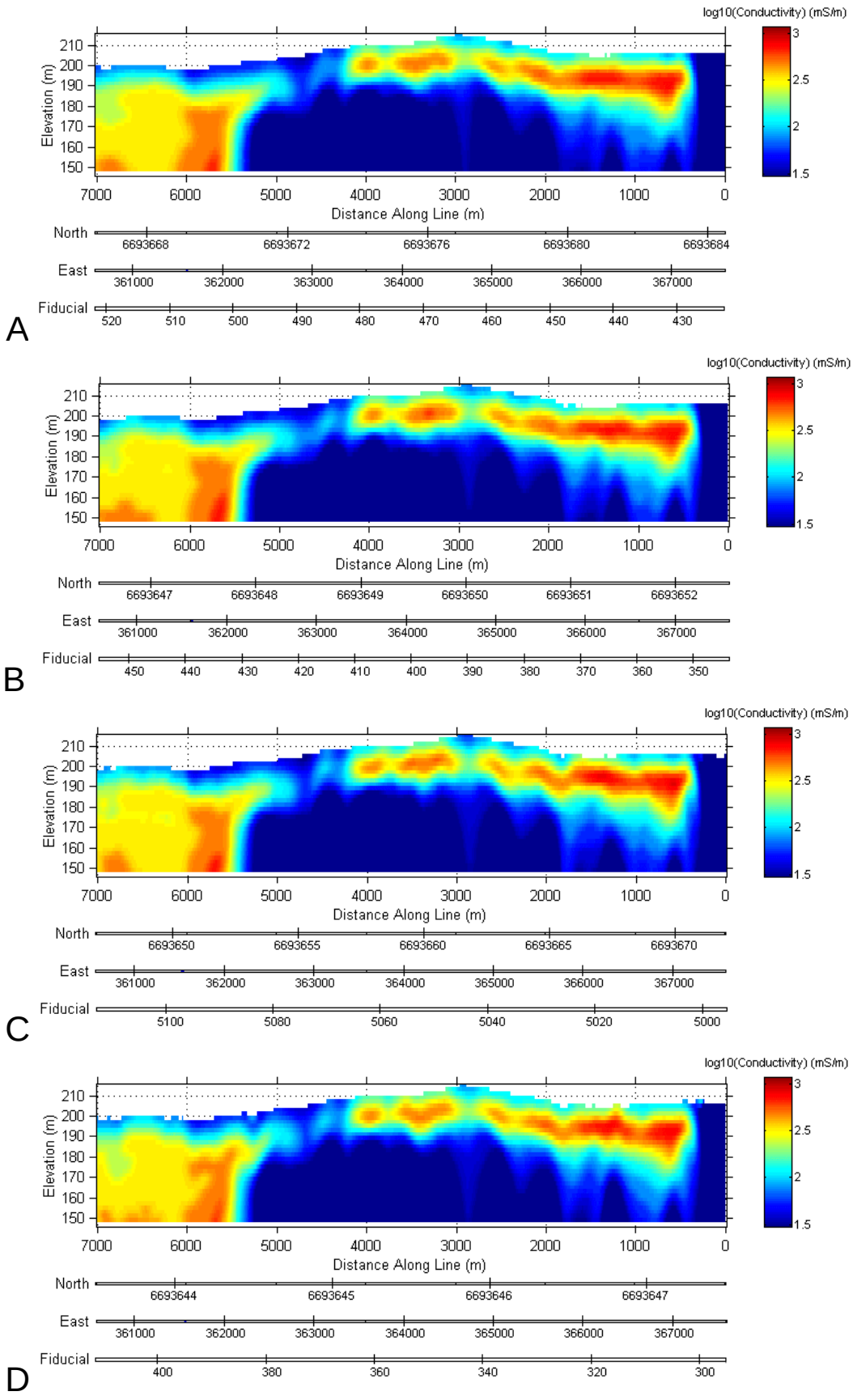

Figure 5. Conductivity sections for the repeat line (360600mE 6693650mN to 367600mE 6693650mN) shown with a minimum depth extent of 70 m. (A) flight 12, (B) flight 14, (C) flight 15 and (D) flight 16.

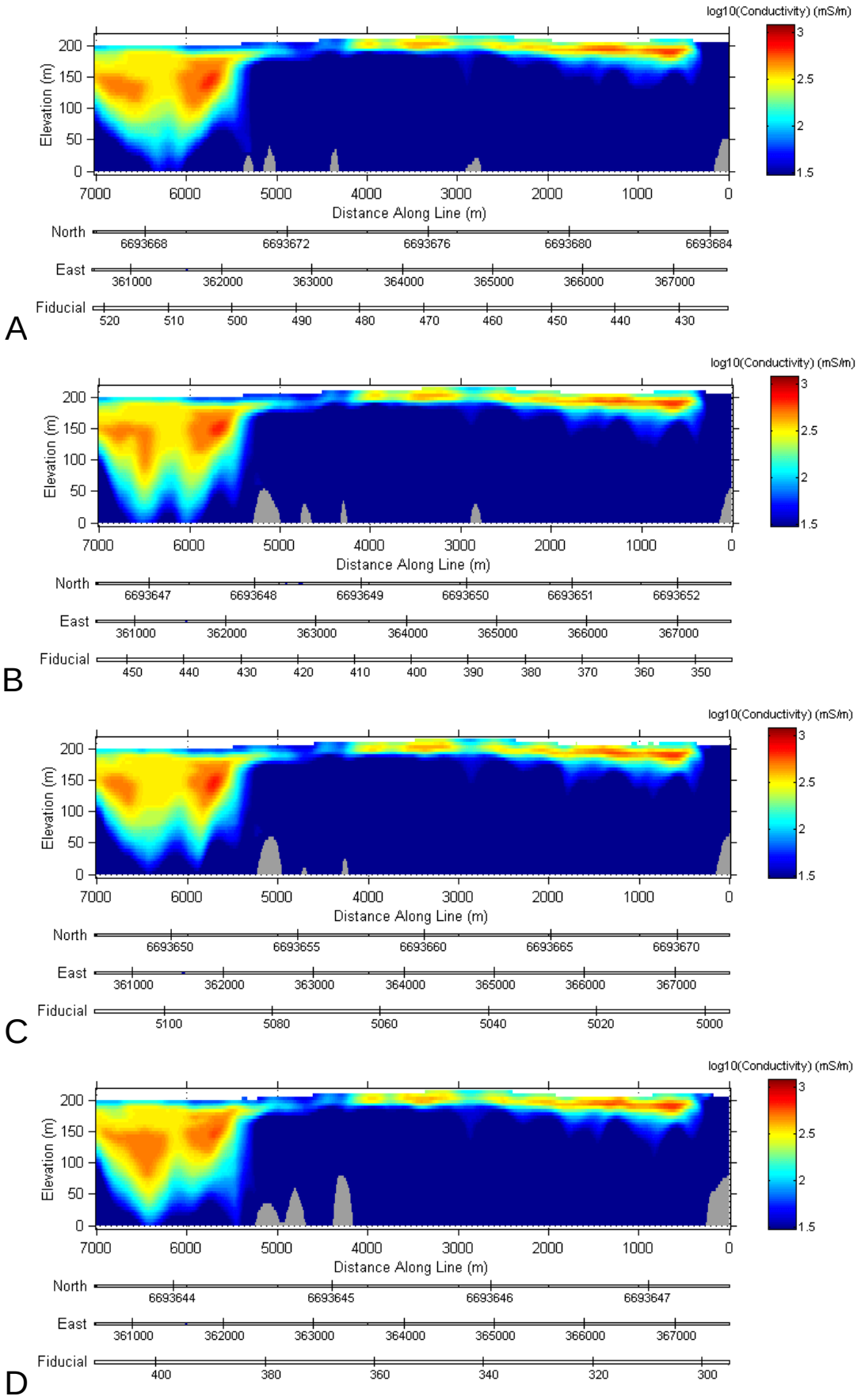

Figure 6. Conductivity sections for the repeat line (360600mE 6693650mN to 367600mE 6693650mN) shown with a minimum depth extent of 220 m. (A) flight 12, (B) flight 14, (C) flight 15 and (D) flight 16. A grey mask has been applied to the section below the depth of last signal return.

4.1.2 Forward Modelling

Figure 7 shows a CDI section produced from X component synthetic data. The forward model response was calculated using a 3D program, Marco_air, developed as part of AMIRA Project P223 (Raiche, 1998). The forward model was based on a 2-layer sequence (15 m of 200 mS/m over a 2 mS/m halfspace). A 3D block of 200 mS/m material was positioned from 15 to 65 m depth (50 m in depth extent), between 499950 m E and 500050 m E (100 m wide), extending 250 m to the north and south of the flight line (500 m strike extent). The position of the layer interface and the 3D body is shown on the CDI section.

Viewed in totality, CDI sections are a tremendous aid in interpretation of the response from AEM systems such as TEMPEST. Under the right circumstances, they provide a good first order quantification of sub-surface conductivity. However, there are artifacts in the sections. The CDI section in Figure 7 illustrates a number of typical features of such sections:

- it is difficult to predict the true conductivity of an extensive resistive layer below a conductive layer. The predicted basement conductivity is 0.1 mS/m or less compared with the true value of 2 mS/m.
- the conductivity of discrete features is underestimated as a result of the 1D approximation used in the conductivity transformation.
- the anomalous conductivity associated with a discrete feature is smeared out both above and below the true position of the feature.
- the complex spatial response function of the asymmetirc transmitter loop and receiver coil geometry of an AEM system such as TEMPEST is not accounted for in the conductivity transformation, leading to a number of artifacts. The anomalous feature around 499700 m E is one such artifact.
- the break-up of the predicted conductivity at low conductivity values and with increasing depth is an artifact of the conductivity transformation implementation.

It is interesting to compare the enhancement in predicted conductivity above the 3D body shown in Figure 7 with the similar, localised, second-order enhancement in near-surface CDI conductivity above the Challenger deposit (see 0-20 m depth, 363400-363600 m E in Figure 3). It could be surmised that the true anomalous conductivity at this location has greater conductivity contrast and depth extent than is indicated in the CDI section.

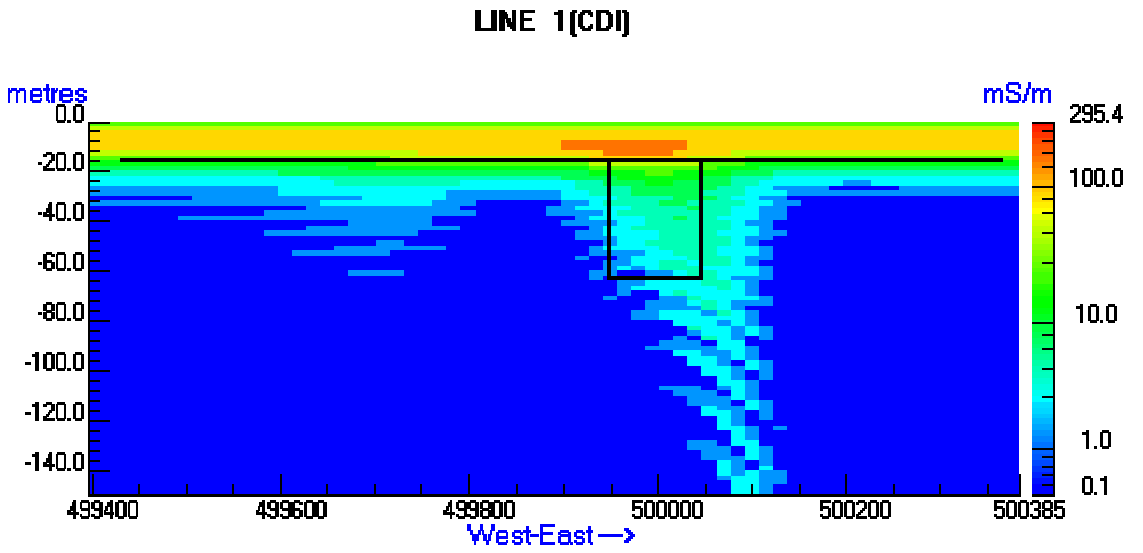

Figure 7. CDI section for Marco_air model output. A 15 m thick layer of 5 ohm.m (200 mS/m) is present over 500 ohm.m (2 mS/m) basement. The discrete target, shown as a black rectangle, has a resistivity of 5 ohm.m (200 mS/m), 100 m horizontal extent by 50 m vertical extent, and 500 m strike length.

4.1.3 Comparison of conductivity sections derived from ground EM and AEM

The Joint Venture partners acquired ground EM data along 4 traverses in September 1997 using the Zonge NanoTEM system. A single turn 20 m by 20 m transmitter loop and single turn 5 m by 5 m receiver loop were used with a transmitter waveform repetition rate of 32 Hz and station spacing of 20 m. The traverses were:

- 6693500 m N, 363200 - 363900 m E
- 6693600 m N, 363200 - 363880 m E
- 6693700 m N, 363200 - 363720 m E
- 6693800 m N, 363200 - 363880 m E

These values are assumed to be AMG coordinates on an AGD datum, either AGD66 or AGD84. The AEM survey data are in MGA94 coordinates (GDA94 datum, Zone 53), which have values around 200 m northeast of their AMG counterparts. In MGA94 coordinates, these lines are approximately (i.e., to 10m accuracy)

- “line 6693500 m N” 6693670 m N, 363330 - 364030 m E
- “line 6693600 m N” 6693770 m N, 363330 - 364010 m E
- “line 6693700 m N” 6693870 m N, 363330 - 363850 m E
- “line 6693800 m N” 6693970 m N, 363330 - 364010 m E

The NanoTEM data were transformed by the contractor to resistivity values using the Zonge “smooth-model” 1D inversion method. The resistivity section for “line 6693500 m N” is shown in Figure 8. This line coincides with the repeat line from the AEM survey. The location of the NanoTEM resistivity section along the conductivity section for the repeat line from Flight 12 is shown in Figure 9. The essential details of the two sections are similar. A conductive layer (> 100 mS/m) is present between depths of 0 m and 20 m. There is a zone of elevated conductivity within this depth range in the centre of the line, and a second zone extending beyond the limit of the ground EM traverse to the east. The source of the extremely high conductivity (low resistivity) values below 40 m depth on the eastern and western ends of the ground EM resistivity section is unknown. They are not seen in any form on the resistivity section for “line 6693600 m N” (Figure 10), nor in the AEM data. They are most likely artifacts. There is a subtler enhancement in conductivity at depths of more than 40 m in the centre of the resistivity sections in Figures 8 and 10. Correlation of this feature across all lines enhances confidence in its validity, but does not preclude this feature from being a systematic artifact of the transformation to resistivity. This subtle enhancement at depth is not seen in the AEM data.

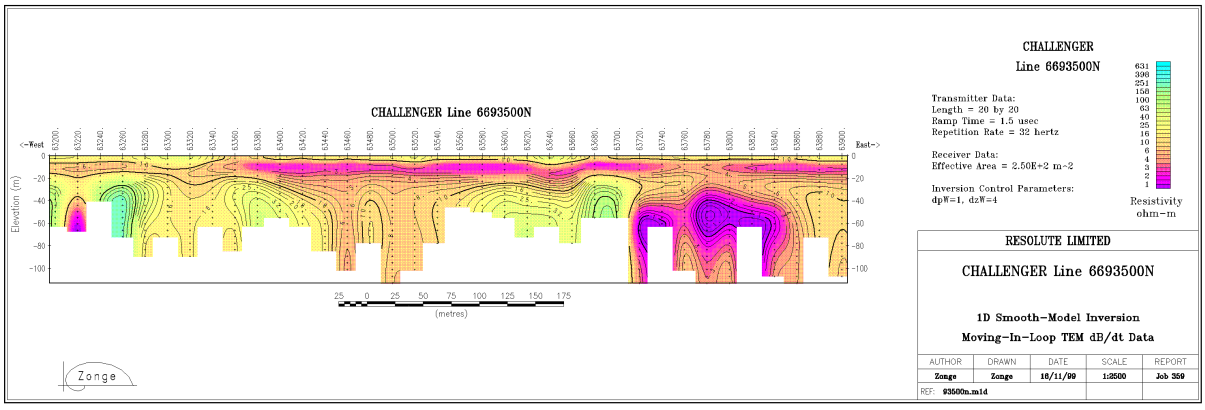

Figure 8. NanoTEM smooth model resistivity inversion section for “line 6693500mN”.

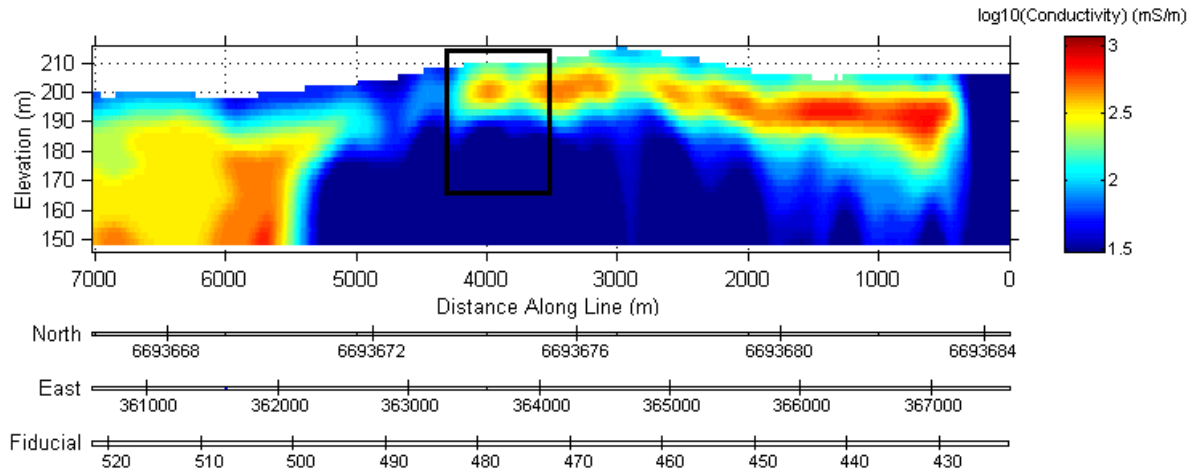

Figure 9. Conductivity section for the repeat line (6693650mN), flight 12. The location of the ground EM section in Figure 8 is indicated by the black rectangle.

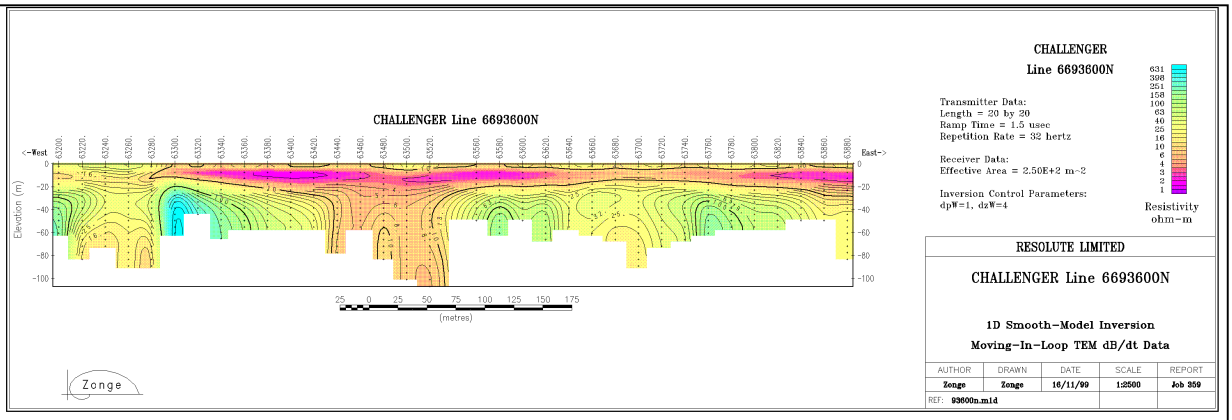

Figure 10. NanoTEM smooth model resistivity inversion section for "line 6693600mN".

A plan view slice through the ground EM resistivity data at 40 m depth was provided by the contractor (Figure 11). Discounting the strong anomaly in the south-east corner as spurious, the dominant feature is a north south trending zone of elevated conductivity. This same trend is well resolved in the conductance of the "conductive unit" image presented in Figure 12.

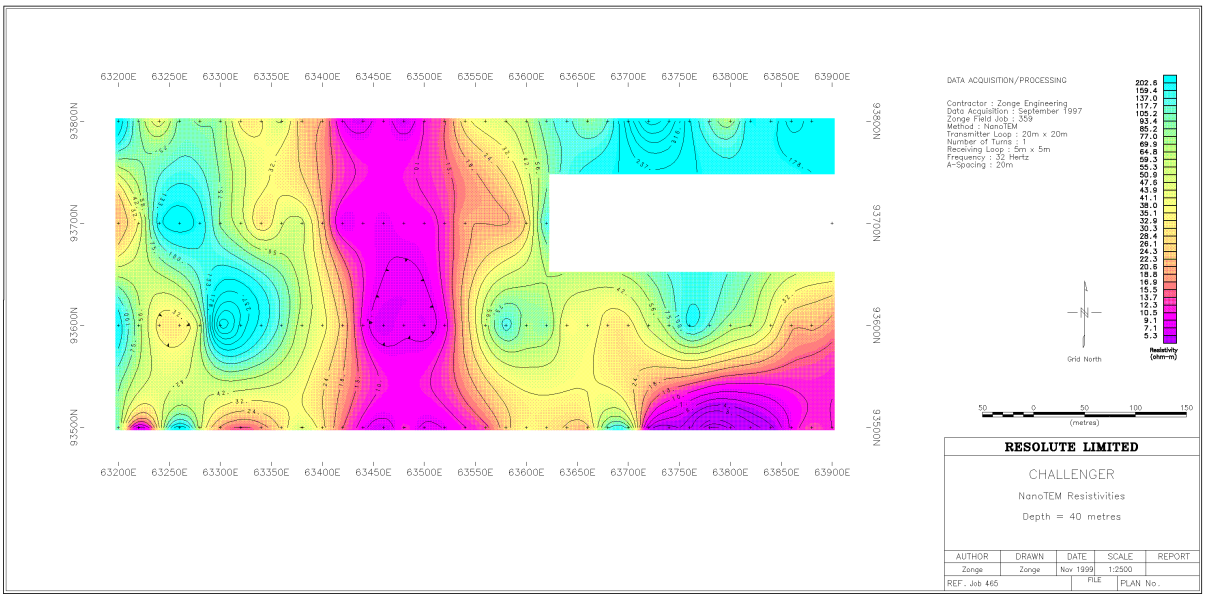

Figure 11. Horizontal slice at 40m depth through NanoTEM smooth model resistivity inversions. Note that the locations are AGD coordinates.

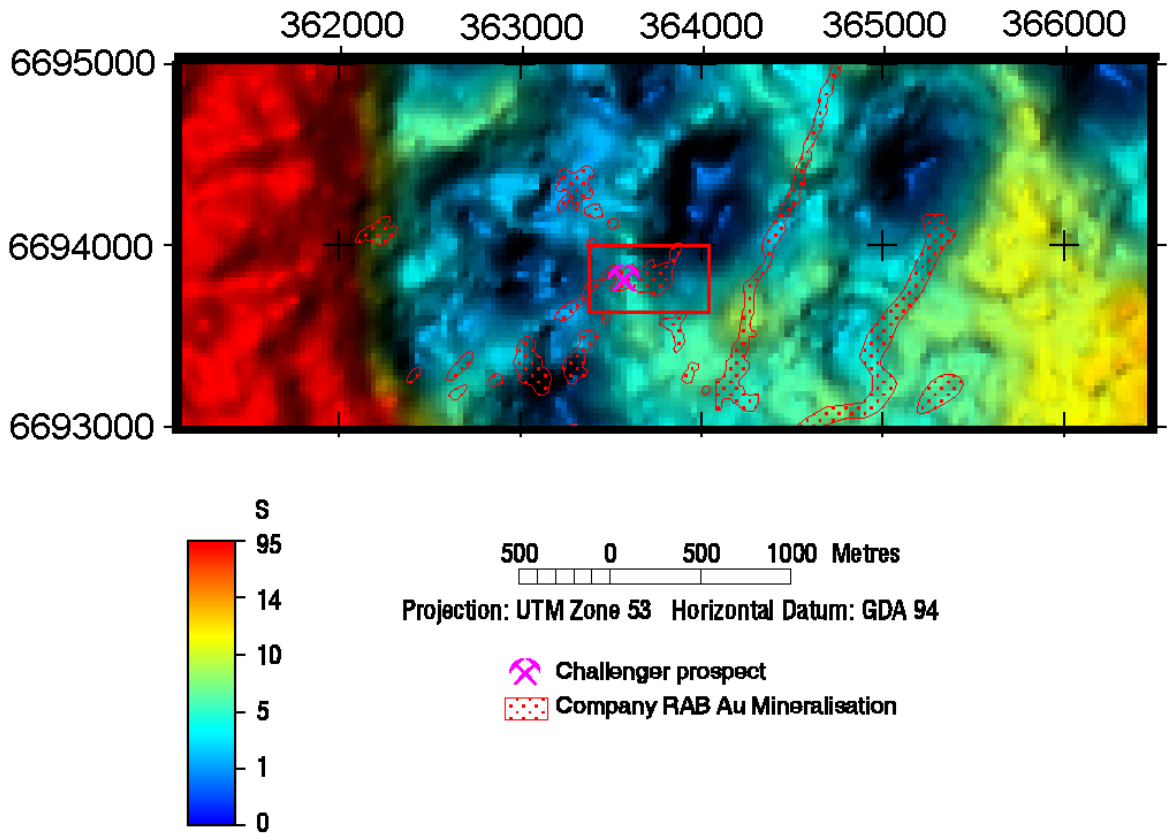

Figure 12. Conductance of "conductive unit" image for a subset of the AEM survey. The location of the ground EM resistivity slice shown in Figure 11 is indicated by the red rectangle.

4.1.4 Comparison of AEM conductivity information and drilling data

A large number of RAB and RC exploration holes have been drilled within a distance of 4 km of the Challenger deposit. The “depth to bedrock” values in the drilling database are in broad agreement with the predicted base of conductive material (Figure 13), a common observation in areas of conductive regolith. There are many irregularities and inconsistencies in the relationship at a local scale (hundreds of metres or less). These inconsistencies are a combination of shortcomings in the drillhole data and noise and artifacts in the conductivity values derived from AEM.

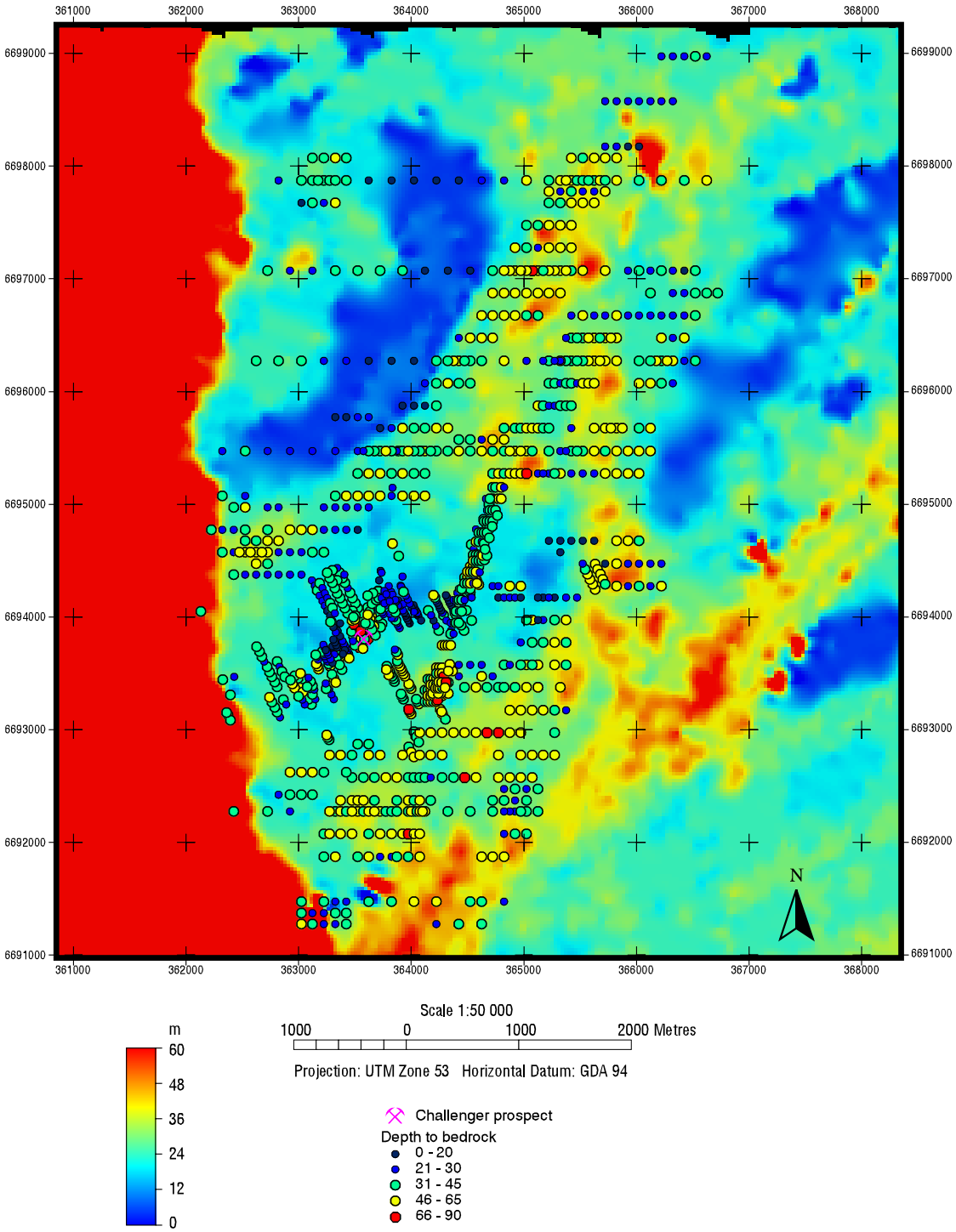

Figure 13. Depth to bedrock from drilling displayed over depth to base of “conductive unit” (0-60 m) image zoomed to the extent of the drilling data.

4.2 Assessment of Conductivity Distributions

A thorough assessment of the conductivity distributions in the survey area was made using conductivity sections for each flight line. The isosurfaces displayed in Figures 14 and 15 illustrate the general pattern of conductivity that were observed. The dominant features are a pair of deep north-south troughs filled with conductive material. Within these troughs, some vertical conductivity structure can be recognised (see Figure 6). Elsewhere, the vertical conductivity distributions appear relatively simple; a horizon of variable conductance (conductivity thickness product) is sandwiched between a near-surface resistive layer and a resistive bedrock halfspace. There are no strong bedrock conductors. The spatial patterns evident in the conductance images indicate that some of the conductive material is *in-situ* and that some is transported.

The granulite in the Challenger area is relatively homogeneous at scales relevant to the AEM survey (i.e., 10 m or more). A weak northeast grain is evident in the AEM data (Figure 14). This is consistent with the dominant dyke trend in the magnetic data. However, the main pattern displayed by *in situ* conductive material is one of equi-dimensional resistive patches surrounded by a mantle of conductive regolith. This is seen over a wide range of scales from hundreds of metres to many kilometres.

Known mineralisation would be expected to exhibit, at best, a weak conductivity enhancement in fresh rock brought about by small amounts of sulphides and graphite. A higher expectation was placed on recognising subtle zones of thicker conductive *in situ* regolith that may be developed over altered and mineralised rock.

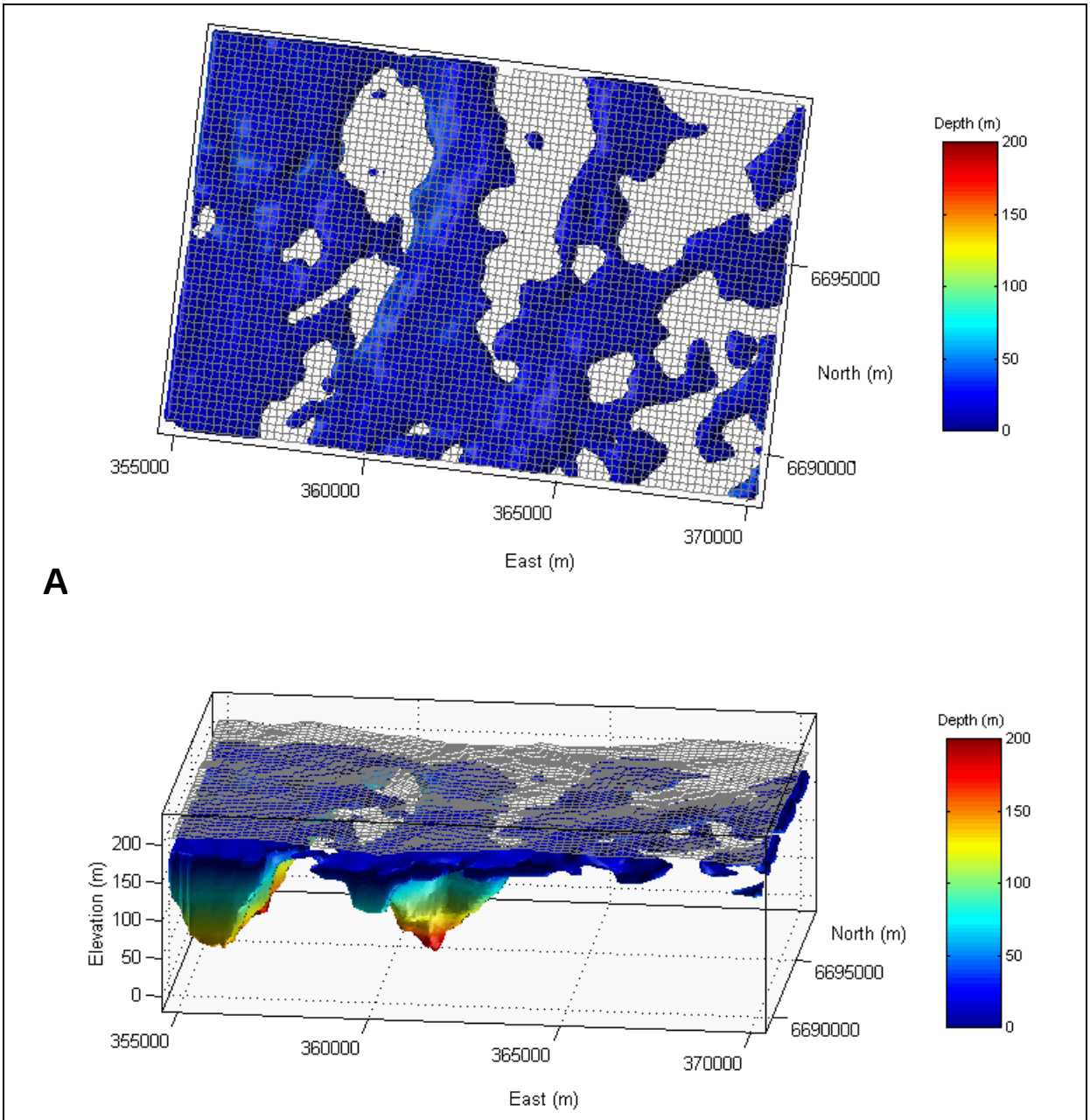

Figure 14. Conductivity isosurface perspective views using a 200 mS/m threshold to define the isosurface. Colouring based on depth below surface. A) Viewed from directly above on an azimuth of 173 degrees. B) Viewed from an azimuth of 173 degrees and an elevation of 17 degrees. The grey mesh represents the surface topography.

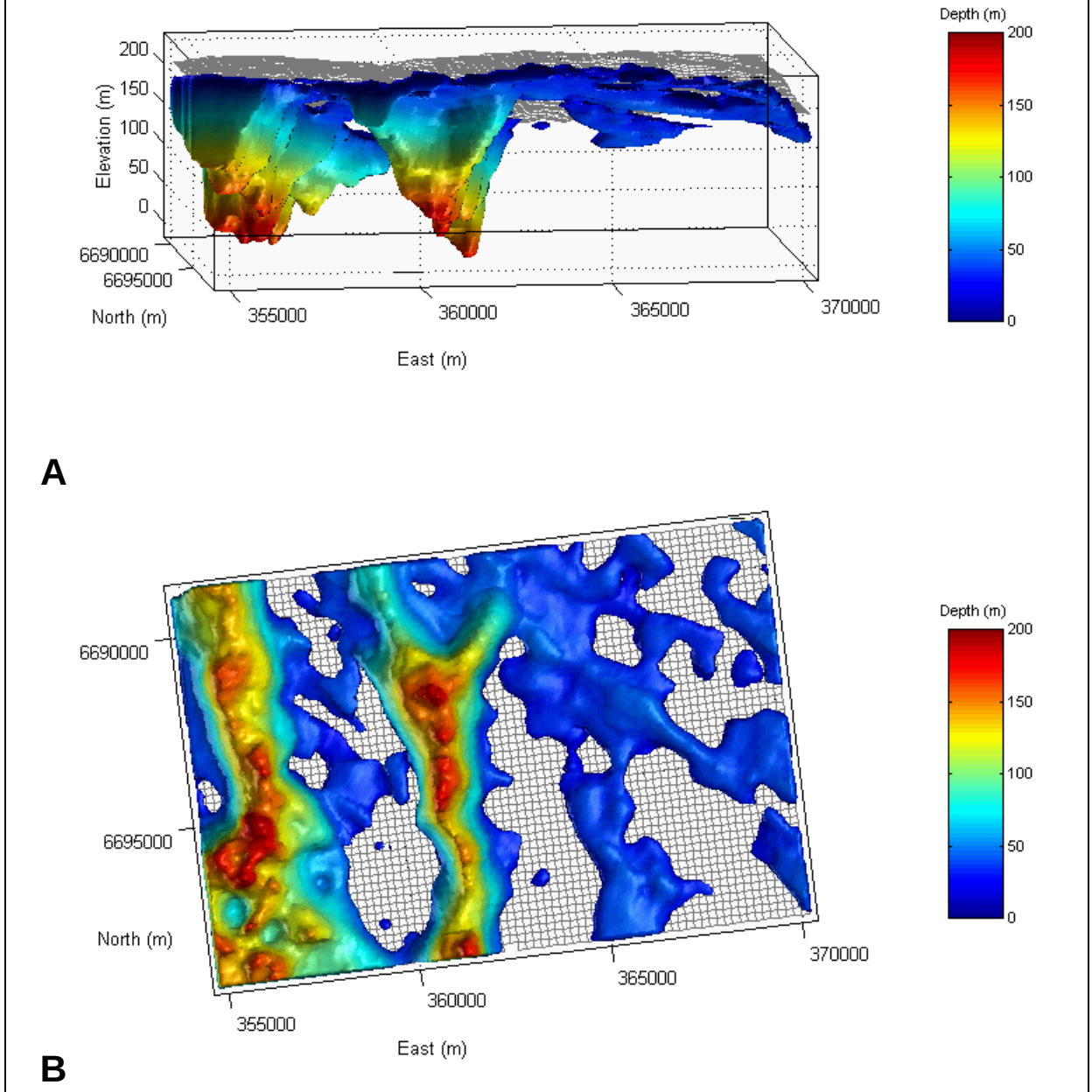

Figure 15. Conductivity isosurface perspective views using a 200 mS/m threshold to define the isosurface. Colouring based on depth below surface A) Viewed from an azimuth of 173 degrees and an elevation of -8 degrees. B) Viewed from directly below on an azimuth of 173 degrees. The grey mesh represents the surface topography.

4.3 Interpretation

4.3.1 Mapping Discrete Conductors

Although the search for confined high conductivity bodies was not the primary reason for acquiring AEM data in the Challenger area, the data were scanned for the presence of such discrete conductors. Discrete conductor mapping is a process that requires familiarity with the acquisition system and the expected response of that system to a variety of conductivity distributions (Lane, 2001). Experience plays a significant part in the success of this process.

Multi-plots (line by line profiles) are the main products used for interpretation of discrete conductors (Figure 16). In the case of the TEMPEST system, these plots contain a number of panels:

- a magnetics panel, with total magnetic intensity (TMI) and the first vertical derivative of TMI (1VDTMI),
- window amplitude profiles, generally compressed using the asinh function to give an overview of the variation of decay along each line, showing the response both before and after the application of an approximate correction for variations in the acquisition geometry,
- window amplitude profiles with linear scaling, restricted to the smaller amplitudes, important for identifying the response of discrete conductors,
- a transmitter loop panel, with actual terrain clearance, “standard” terrain clearance (referring to data following the application of approximate corrections for variations in acquisition geometry), altitude, pitch attitude and roll attitude
- a receiver coil panel, with a range of monitor values tracking sferics, coupling to the transmitter loop, low frequency signals induced by variations in the coupling of the receiver coils with the ambient magnetic field, powerline noise and coupling with VLF transmissions, and
- a CDI conductivity section (optional).

The transmitter loop and receiver coil panels help to determine the source of variations observed in the window amplitudes profiles (i.e., whether these are due to variations in the subsurface conductivity distribution or to variations in system geometry, receiver coil vibration, sferics etc).

Following manual identification of anomalous features on the multi-plots, automated characterisation of EM data in the immediate vicinity of each feature was used to assist with interpretation and prioritisation. Tables of anomaly characteristics were created, one each for X and Z components (for the same features). These are given in Appendix 2. Figure 17 shows the location of the features.

Priorities were assigned to the features in a subjective process that involves a number of factors, some of which are listed below:

- the expected response of the target,
- anomaly decay characteristics,
- response in the different components (X and Z),
- acquisition parameters in the vicinity of the features (e.g., terrain clearance),
- received data characteristics (e.g., sferic activity, coil motion activity),
- spatial extent (i.e., line to line correlation), and
- anomaly setting (particularly if the feature is located near the far edge of a patch of conductive cover).

Prioritisation can involve additional information (e.g., interpretation of magnetic data, more detailed geological interpretation of the survey area, geochemistry, ground geophysics, drilling of selected features) if these data are available and included in the scope of the interpretation project. A ‘global’ or ‘universal’ prioritisation is generally applied (ie the priority 1 features would be assigned this priority on any survey). Features assigned a priority of 1 are strong conductors with a high degree of certainty attached to the interpretation. Priority 2 features are either moderate conductors of high certainty or somewhat doubtful but strong conductors. Priority 3 features are weaker and/or have a low probability of being due to a real conductor.

There were no priority 1 or 2 features identified in the data. The most convincing and interesting features (because of line to line correlation) were a series of very weak responses forming a northeast trend near the northeast corner of the survey area (line 3007 through 3013).

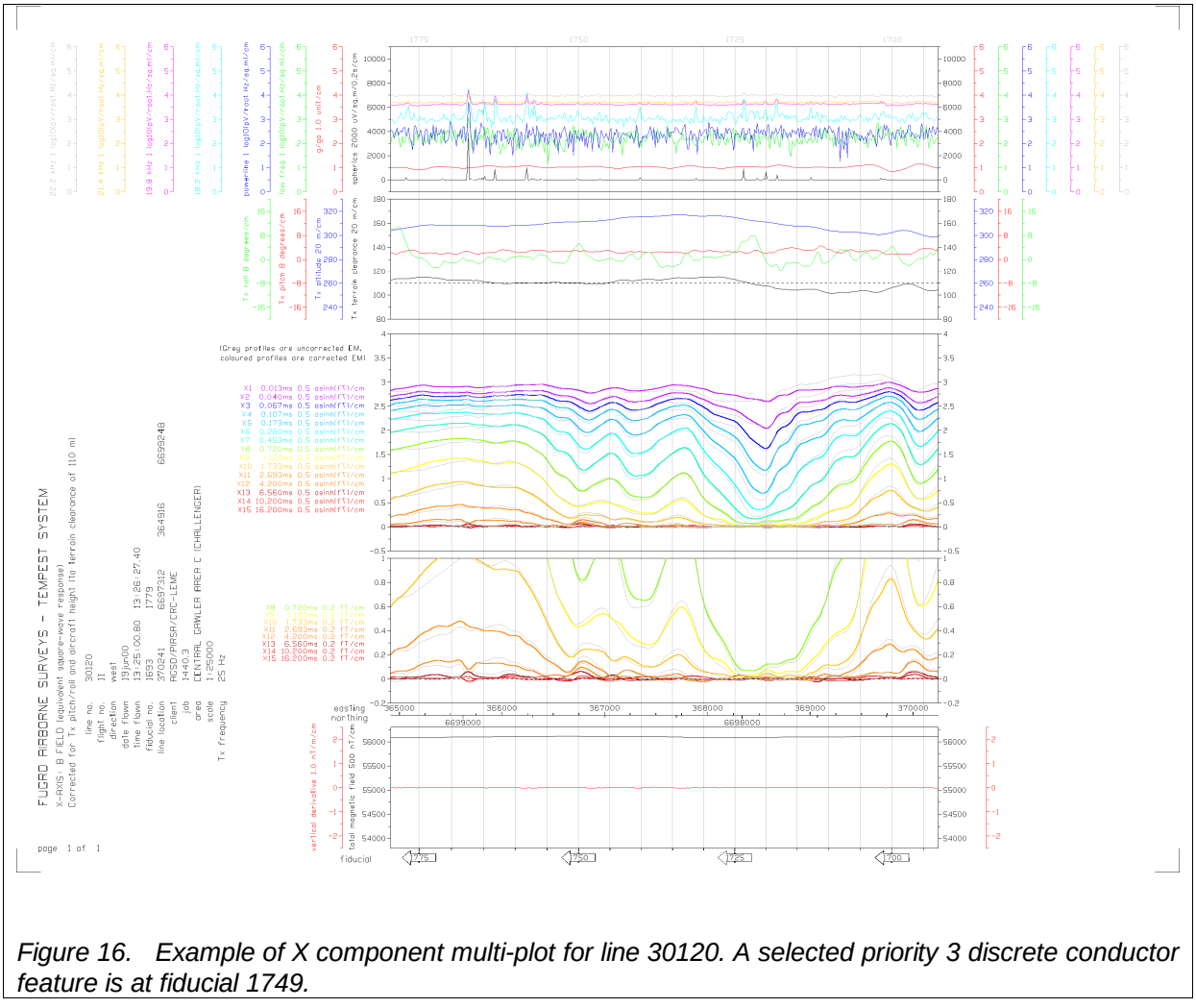

Figure 16. Example of X component multi-plot for line 30120. A selected priority 3 discrete conductor feature is at fiducial 1749.

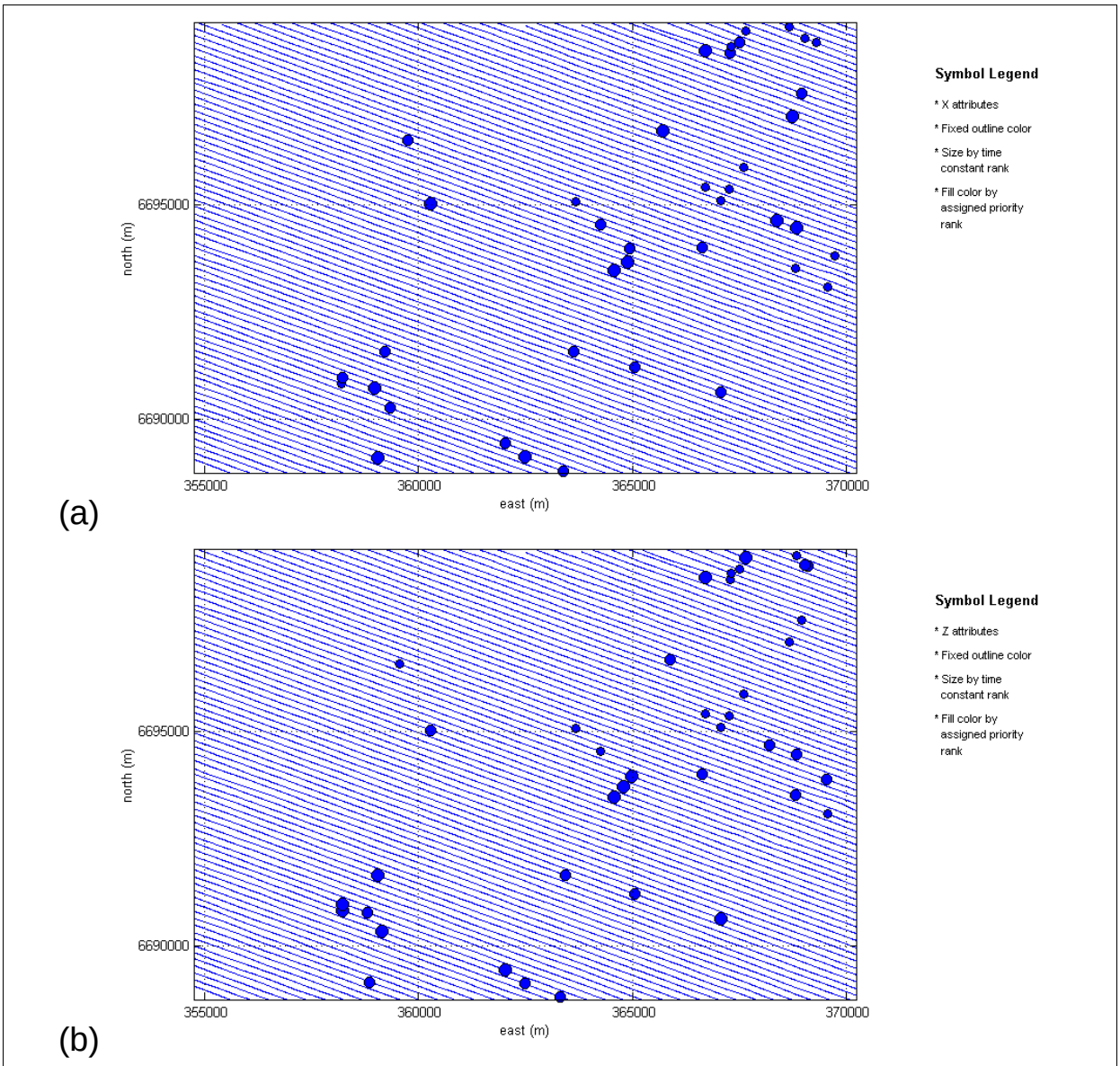

Figure 17. Flight path maps showing anomaly locations. Symbology determined from (a) X component attributes and (b) Z component attributes. Symbol size based on time constant rank with larger symbols for features with longer time constants. Symbol colour based on assigned priority, blue is for priority 3. Note there are no priority 1 and 2 features.

4.3.2 Mapping Geology

4.3.2.1 Interpretation Environment

The outputs from AEM surveys, and the inputs to the interpretation process, have traditionally been profiles of data for each flight line and located data files of windowed response amplitudes. This caters specifically for discrete conductor interpretation. A feature of the TEMPEST system is the provision of additional and modified outputs to facilitate mapping applications and the integration of AEM information with other data such as drilling information. For example, the measured response of the TEMPEST system is transformed to an equivalent square-wave B-field response and approximate corrections are applied for variations in the geometry of the acquisition system. This assists with imaging and subsequent manipulation of the data (e.g. principal component analysis). Further, the data are transformed to conductivity and depths using an approximate imaging technique, thus enabling AEM information to be related directly to subsurface drilling information.

There are a number of commercially available software tools to assist with AEM interpretation. These can be obtained from consultants and through collaborative research projects (e.g., AMIRA projects). Window response can be manipulated in aEMIT (AMIRA P476 project) and in modules of C-in-3D (FAS). Window response can also be transformed to conductivity using EMFlow (Encom) or inverted using layered models such as Air_Beo (AMIRA P223) or LEI (FAS). Image processing can be carried out using tools such as ERMapper or Geosoft. Plan view data from various sources can be integrated in a GIS (e.g., Arcview or MapInfo).

Although the practical conductivity transformation methods that can be applied to AEM data all contain a 1D assumption, there are certainly circumstances where visualisation of the conductivity data stitched together into a 3D gridded volume assists interpretation. The 3D distribution of conductivity can be displayed using programs such as Matlab, MVS, GeoExpress and Noesys. This functionality has been customised to some degree for AEM applications in the C-in-3D package (FAS). Some seismic interpretation packages and mine-modeling packages allow 3D gridded information to be combined with drilling data, but they are far from cheap and not customised in any fashion for conductivity data. The process of outlining features on horizontal and/or vertical sections and creating interpretive 3D objects is generally quite complex in these packages. Further work is required to simplify integration of conductivity and drilling information.

Several hybrid approaches were adopted within the GIS used in this workshop. AEM survey flight line vectors were hot-linked to conductivity section images that included profiles of the total magnetic intensity (TMI) and first vertical derivative of TMI (Figure 18). The conductivity data were also stitched together into a 3D gridded volume. East-west vertical slices were then generated at regular northing intervals and saved as image files (e.g., BMP format in this case). The image files were registered so that the top of the frame bordering the conductivity section corresponded to the plan view position of the section (Figure 19). A second set of these images was overlain with drilling information and registered in the same fashion as the clean sections.

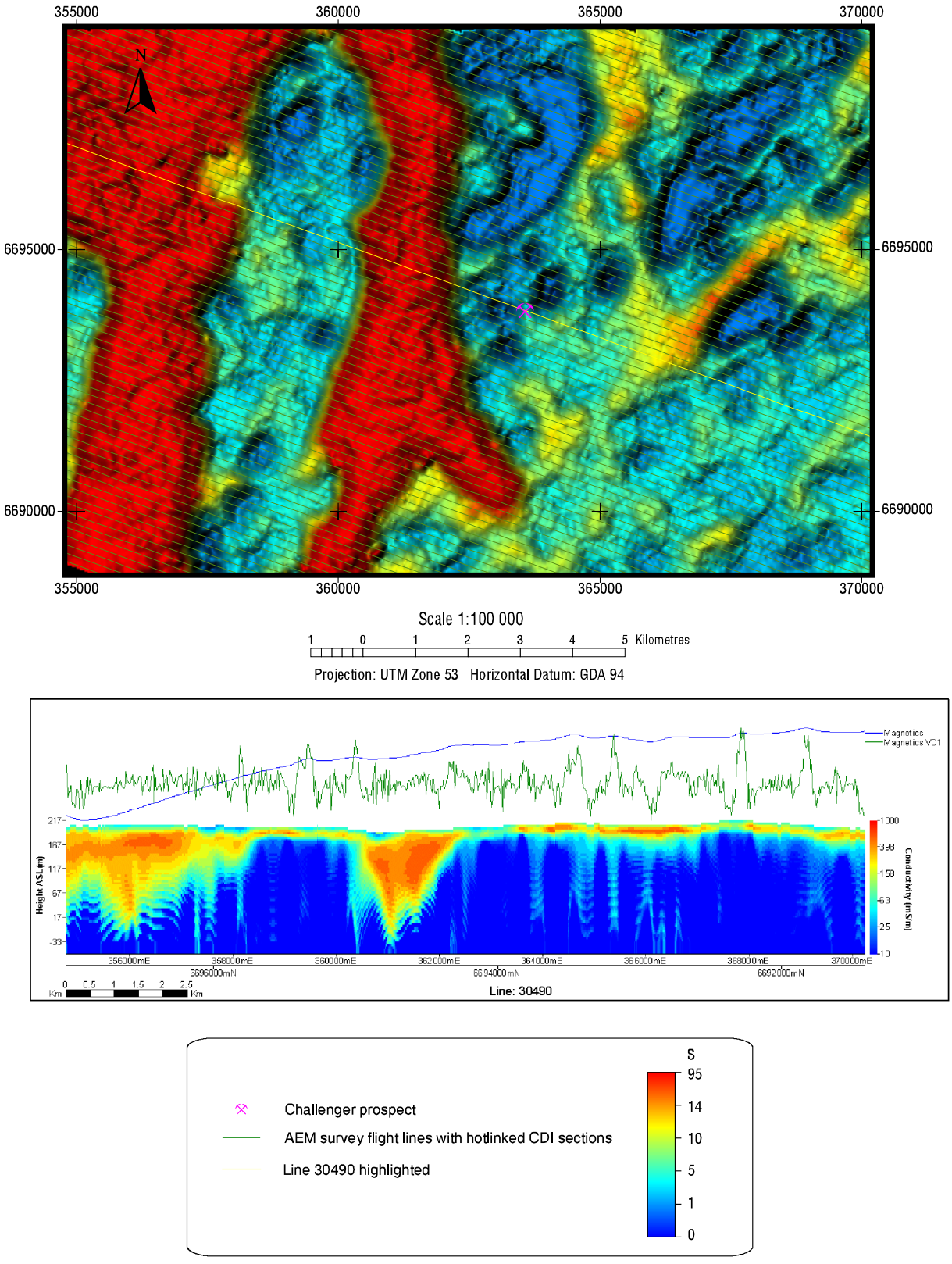

Figure 18. View of the GIS showing plan view conductance of "conductive unit" image, AEM survey flight lines (line 30490 highlighted) and the hot-linked conductivity section for flight line 30490. The conductivity section is overlain with lines showing the top and bottom of the "conductive unit". Profiles of TMI and the first vertical derivative of TMI are displayed above the conductivity section.

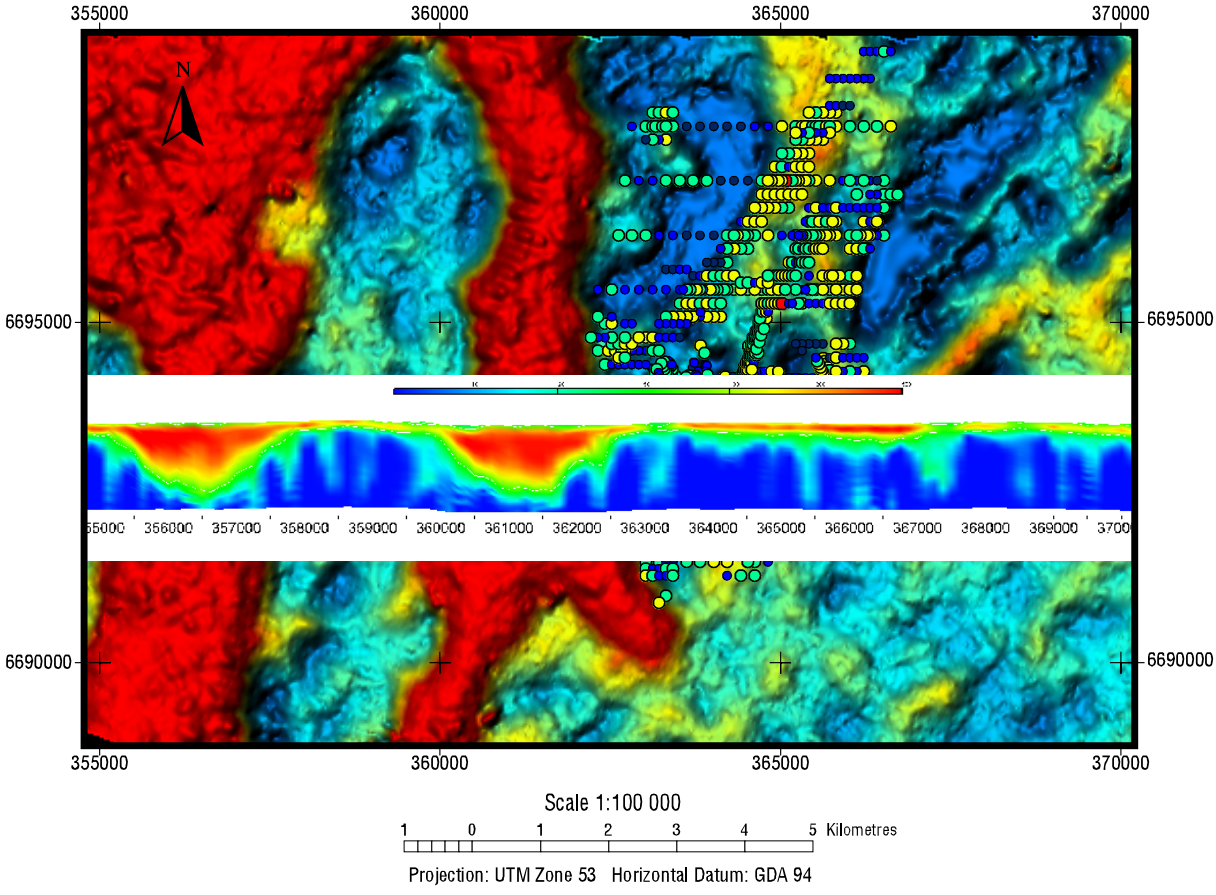

Figure 19. View of the GIS showing plan view conductance of "conductive unit" image, company drilling coded by depth to bedrock, and conductivity section for 6693600mN derived from a 3D conductivity grid.

4.3.2.2 GIS Themes

The data used in this workshop came from a number of sources (GA, PIRSA, CRC LEME, Dominion Mining). Where possible these data were loaded into the GIS (Arcview) to facilitate integrated interpretation. The GIS themes are listed in Appendix 3.

The data included:

Historical mineral exploration drilling and water bore locations (PIRSA)
Regional mapsheet, mineral exploration tenement outlines, road and drainage locations (PIRSA)
Regional geology (PIRSA)
Detailed aeromagnetic data over part of the AEM survey area (Company)
Surface geochemistry (Company)
RAB geochemistry (Company)
Depth of oxidation and depth to bedrock from drilling (Company)
Landsat TM imagery (CRC LEME)
Regolith mapping (CRC LEME)
Flight line and boundary information from the AEM survey (GA/PIRSA/CRC LEME)
Magnetic images from the AEM survey (GA/PIRSA/CRC LEME)
Derived surface topography images from the AEM survey (GA/PIRSA/CRC LEME)
Interval conductivity slices from the AEM survey (GA/PIRSA/CRC LEME)
Vertical conductivity slices from the AEM survey (GA/PIRSA/CRC LEME)
Vertical conductivity slices from the AEM survey combined with Company drilling information (GA/PIRSA/CRC LEME/Company)
Unit parameter images from the AEM survey (GA/PIRSA/CRC LEME)
Adaptive time constant images from the AEM survey (GA/PIRSA/CRC LEME)
Principal component images from the AEM survey (GA/PIRSA/CRC LEME)
Interval conductivity slices from the AEM survey (GA/PIRSA/CRC LEME)
Interpreted discrete conductors from the AEM survey (Workshop).

In the course of the workshop, magnetics and AEM interpretation layers were added to the GIS.

4.3.2.3 Interpretation

The workshop participants interpreted the data during the workshop. The GIS was displayed on a screen that everyone could see. One of the participants drew features in an annotation layer while the remainder of the participants debated the location and classification of the annotation elements. All of this took place after a session in which each participant had the opportunity to individually investigate the conductivity and magnetic susceptibility distributions as expressed by the products available in the GIS.

Selected views of the GIS showing the interpretation of aeromagnetic and AEM data are presented in Figures 22 to 35 in Appendix 4. Separate annotation themes for magnetic and AEM information were produced in order to allow for an investigation of the relationship between these two physical property distributions.

The magnetic data acquired with the AEM data show some large amplitude features in the extreme northwest corner of the survey area, probably related to BIF horizons (Figure 27). Elsewhere magnetic field relief was low except for a series of low to moderate amplitude linear magnetic highs. These linear features were subdivided on the basis of amplitude and strike direction. The majority are interpreted as dykes of varying age and composition.

There is more detail in the low level, closely spaced company magnetic data (as would be expected given that the data acquired during the AEM survey were collected at greater terrain clearance and wider line spacing). Patches of surficial magnetic deposits were mapped (Figure 25). These patches do not show any consistent relationship with the distribution of conductivity. Several low amplitude magnetic features with slightly broader wavelength were also recognised; one trending to the northeast *from* Challenger and several others located to the northeast *of* Challenger. At least two of these features may be related to pyrrhotite associated with Au mineralisation.

The most prominent features in the conductivity data are a pair of deep conductive troughs located in the western half of the survey area (Figure 31). The conductance values over these troughs are as high as 100 S. Conductivity depth imaging suggests depths of up to 200 m for widths as narrow as 2 km - indicating that the troughs have very steep sides. The troughs also have straight margins, which suggests partial structural control. The shape of the troughs is similar to the Blair Athol, Wolfang, and Miclere Permian Basins in the Clermont region of Queensland (Bruvel and Sorby, 1987; Wilton, 1995; Smith and Miller, 1995). These basins are of restricted extent - if a comparison with the troughs to the west of Challenger is to be pursued, it would be important to determine the extent of the troughs to the north and south of the survey area. The troughs at Challenger may have formed part of an extensive palaeochannel network. If this is the case, then simple pattern analysis would suggest that the flow direction was from the south to the north.

Broad (1km or more), irregular to dendritic areas of moderate conductance (up to 15 S) are also apparent in the AEM data, mostly in the eastern half of the survey area (Figure 31). These areas have characteristics consistent with conductive transported material. Conductivity sections and drilling information suggest that this material is up to 30 m thick.

Neither the deep troughs nor the shallower palaeo-drainage features can be identified from surface topography information obtained during the AEM survey (Figure 32). The eastern trough sits in a low part of the landscape and a portion of its western margin coincides with a north-northeast trending breakaway 5 m to 10 m in height. The western trough crosses one of the more elevated parts of the survey area. High frequency patterns in the magnetic data are muted over the troughs. The loss of short wavelength magnetic patterns is consistent with an increased depth to magnetic basement.

The nature of spatial patterning evident in the conductive zone over the reminder of the survey area would suggest that the observed variability in conductance is associated with variability in the nature of *in situ* weathered materials. These materials have conductivities ranging from 50 mS/m to 500 mS/m and thicknesses ranging from 0 m to 50 m. They manifest as small isolated patches of conductive near-surface materials, conductive near-surface materials along linear trends and breaks, and resistive areas where conductive materials are very thin or absent. The latter group includes small resistive areas that are roughly equi-dimensional and which range in diameter from about 200 m to 1000 m (Figure 29). Diffuse discontinuities in conductance patterns across the survey area were also identified.

The source of the variability in the nature of *in situ* regolith materials is unknown. The bedrock is uniformly resistive, however it is probable that weathering may have picked out subtle but important variations in bedrock composition and/or structure. For example, the conductive material along linear trends and breaks may be associated with deeper weathering along faults or shear zones. These faults may be an exploration target if they acted as pathways for the redistribution of gold and sulfides during the late fluid infiltration event identified by Andrew Tompkins (Section 3.2). However, Challenger is located on a conductive lineament which, it has been argued, is associated with deeper weathering due to the presence of sulfides in leucosomes which formed as a consequence of the partial melt of the proto-ore during the Sleafordian Orogeny (Section 3). Thus, conductive linears may form

because of compositional variability in the bedrock, and in the Challenger area this variability may be associated with the presence of metal sulfides.

The AEM data from around Challenger has been imaged so that the resistive areas with little or no conductive cover have yellow/orange/red colouring, and the conductive areas – where the cover is deeper – have blue/cyan colouring (Figure 20). This colour scheme is the inverse of the conventional approach. This image suggests that the weathering is defining resistant masses of a resistive rock type. The rock may be a variant of the granulite gneiss or, as was suggested during the workshop, it may be a felsic mass derived from the silicate melt formed by granulite facies metamorphism during the Sleafordian Orogeny. As the melt may have carried Au, this rock may be mineralised. Unfortunately the drillhole database was not adequate to test this hypothesis. It was agreed that careful reappraisal of the existing drill core is required.

The Challenger setting (conductive linears and curvi-linears in amongst a number of equi-dimensional resistive patches 500 m to 1000 m in diameter) is not unique in the survey area. The Challenger deposit sits on the flanks of a topographic high and this fact, along with the absence of significant transported material over the high, probably aided its discovery through surface geochemical sampling.

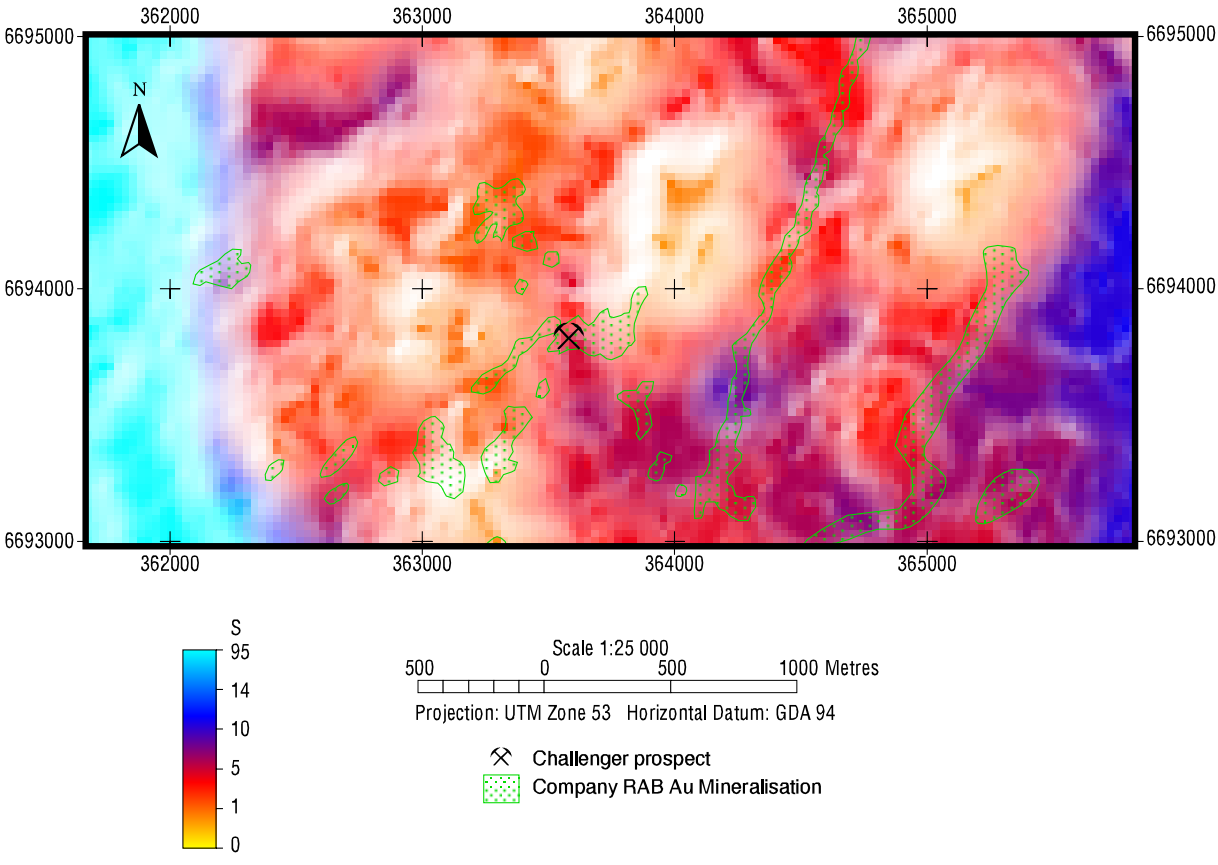

Figure 20. Conductance of "conductive unit" image for a subset of the AEM survey. In this image areas of low conductance are shown in yellow/orange/red and areas of high conductance are shown in blue/cyan. Note this colour scheme is the inverse of the usual red-blue high-low colour scheme used for geophysical data.

5 Conclusions from the Workshop

The workshop helped all participants, including the leaders, to learn something about AEM and its application in a difficult exploration environment.

The conductivity distribution lacked discrete bedrock conductors and was dominated by near-surface conductors of broad spatial extent relative to the footprint of the TEMPEST AEM system. Hence, the conditions were appropriate for the use of a 1D approximate transformation to conductivity. The simple vertical conductivity structure revealed on most of the conductivity sections allowed summary parameters such as “conductive unit” parameters to be used to summarise the conductivity information in plan view images.

In many regolith dominated terrains, the base of conductive near-surface material corresponds in depth to the transition of saprolite into saprock or bedrock (e.g., Worrall et al., 2001). The mapped base of conductive material in the Challenger area has broad similarities with the depth to bedrock from drilling. However, there are many examples of disagreement that would require checking of both AEM and drilling data before the true extent of the relationship could be deduced. The absence of cheap and convenient software tools for working with AEM data, conductivity sections and drillholes is frustrating when trying to investigate detailed relationships between predicted conductivity and drilling information. Further work is required in this area in order to facilitate the integration of AEM data into geoscience projects.

Spatial patterning in the conductivity distribution in plan and section view enabled conductive transported material to be recognised. This material covers approximately half of the survey area. This finding has important implications for the interpretation of results from surface geochemical surveys. A re-assessment of the geochemical patterns and surface regolith mapping in the light of the interpretation produced during the workshop is warranted.

Recognition of the presence of transported material up to 30 m or more in thickness also has direct implications for the economics of gold resource exploitation. Dominion is focussing on exploring for shallow resources that can be mined from open-pits. Knowledge of the areas without thick transported material at an early stage in exploration would have made exploration more efficient.

The host sequence to the Challenger mineralisation is granulite metamorphic facies gneiss comprising mafic and ultramafic protoliths, but the distribution of rock types and their relationships have not been mapped. There is considerable variability in the conductance of regolith materials derived from the weathering of the gneiss. The source of this variability is unknown, but it may reflect subtle changes in bedrock composition and/or structure. The variations mapped using the conductivity data would assist and provide context if bedrock samples from exploration drilling were to be reappraised.

Prior to the AEM survey, ground EM and electrical measurements had identified that the sub-crop of the main Challenger mineralisation was located within a trough of conductive regolith. The AEM survey re-confirmed this observation and, by covering a much larger area, placed this observation in a broader context. This setting was observed elsewhere in the survey area, and could be used as part of a multi-faceted targeting strategy for selecting areas for further exploration.

Multi-plot profiles from the AEM survey were scanned for discrete conductor anomalies. Only a handful of low priority features were returned. Most of these features were spatially

isolated, casting further doubt over their validity. A cluster of features near the northeast corner of the survey area was the most promising target. The Challenger mineralisation contains some sulphides and graphite, but not enough to generate a detectable conductivity or chargeability response during trial ground EM or electrical surveys. The weak conductors identified from the AEM survey may still be prospective as potential sites for mineralisation associated with enhanced sulphide and/or graphite content.

Water for mineral processing is a valuable commodity in the Challenger area. Soon after the release of products from the AEM survey, the data were used to site a bore designed to test for water in the deep conductive trough west of the Challenger resource. Conductivity sections derived from the AEM data indicated that the trough was around 200 m deep. The water bore encountered 180 m of clay and coal or lignite over 30 m of sand. A scoured unconformity was present at the base of the sand. The hole finished in gneissic material at 216 m. Abundant water was present in the basal sands. The saline water-saturated sands and overlying clays account for the elevated conductivity of the trough. The accuracy of the prediction of depth to the base of the trough is a testament to the advances in AEM acquisition and processing. Further acquisition of AEM data to the north and south of the present survey boundary would be warranted if it were important to map the full extent of the trough for water resource estimation purposes. The survey could provide details of the extent and cross-sectional area of the water-bearing sands.

6 Acknowledgments

The enthusiastic participation of all who attended the workshop is gratefully acknowledged. We are particularly grateful to Sue Daly (PIRSA). Dominion and Resolute generously provided geophysical and drilling data for the workshop. Roger Skirrow (GA), Tony Poustie (Dominion), Andrew Tompkins (ANU), Peter Williams (Resolute), David Gray (CRC LEME/CSIRO) and John Wilford (CRC LEME/GA) each made presentations. Pre- and post-workshop efforts by Ross Brodie, Peter Milligan and, particularly, Matti Peljo and Lindsay Highet enabled the workshop participants to utilise a first class array of products in the GIS and to present some of the views of the GIS in this report.

7 References

Bonwick, C., 1997, Discovery of the Challenger Gold Deposit - Implications for future exploration on the Gawler Craton: New Generation Gold Mines '97, Case Histories of Discovery, AMF.

Bruvel, F.J., and Sorby, L.A., 1987, Departmental airborne geophysical test survey in the Clermont area: Queensland Government Mining Journal, April 1987, 128-131.

Daly, S. J., Fanning, C. M., and Fairclough, M. C., 1998, Tectonic evolution and exploration potential of the Gawler Craton: AGSO Journal of Australian Geology and Geophysics, v. 17, no. 3, p. 145-168.

Drexel, J.F., Preiss, W.V., and Parker, A.J., 1993, The geology of South Australia: South Australia Geological Survey Bulletin 54.

Lane, R., (editor), 2001, Guide to the TEMPEST AEM System: Fugro Airborne Surveys.

Lane, R., Green, A., Golding, C., Owers, M., Pik, P., Plunkett, C., Sattel, D., and Thorn, B., 2000, An example of 3D conductivity mapping using the TEMPEST airborne electromagnetic system: Exploration Geophysics, 31, 162-172.

Lane, R., and Pracilio, G., 2000, Visualisation of sub-surface conductivity derived from airborne EM: SAGEEP 2000, 101-111.

Lawrie, K.C., Munday, T.J., Dent, D.L., Gibson, D.L., Brodie, R.C., Wilford, J., Reilly, N.S., and Chan, R.A., 2000, A 'Geological Systems' approach to understanding the processes involved in land and water salinisation in areas of complex regolith - the Gilmore Project, central-west NSW: AGSO Research Newsletter, 32, 13-15, 26-32.

Lintern, M.J., and Sheard, M.J., 1999, Regolith studies related to the Challenger Gold Deposit, Gawler Craton, South Australia: Geochemistry and stratigraphy of the Challenger Gold Deposit: CRC LEME Open Report 78.

Raiche, A., 1998, Modelling the time-domain response of AEM systems: Exploration Geophysics 29, 103-106.

Smith, R.D.C. & Miller, D.E., 1995. The Blair Athol coal mine. In: Follington, I.L., Beeston, J.W. & Hamilton, L.H. (eds.), Bowen Basin Symposium 1995 Proceedings, Mackay, Qld, 1-3 October, 1995, Geological Society of Australia Coal Geology Group, 265-270.

Wilton, R., 1995. The Wolfang coal deposit. In: Follington, I.L., Beeston, J.W. & Hamilton, L.H. (eds.), Bowen Basin Symposium 1995 Proceedings, Mackay, Qld, 1-3 October, 1995, Geological Society of Australia Coal Geology Group, 459-462.

Worrall, L., Lane, R., Meyers, J., Whitaker, A., 2001, Exploring through cover - the integrated interpretation of high resolution aeromagnetic, airborne electromagnetic and ground gravity data from the Grant's Patch area, Eastern Goldfields Province, Archaean Yilgarn Craton, Part A: Mapping geology using airborne electromagnetics (TEMPEST): Extended Abstract submitted for ASEG 15th Geophysical Conference and Exhibition, August 2001, Brisbane.

Appendix 1 - Acquisition Summary for Challenger TEMPEST AEM Data

Job Number	1440.3
Survey Company	FUGRO AIRBORNE SURVEYS
Date Flown/Compiled	June 2000
Client	AGSO/PIRSA/CRC LEME
Area Name	CENTRAL GAWLER AREA C (CHALLENGER), SA
Total Survey Length	1130 kilometres
Traverse Line Spacing	150 metres
Tie Line Spacing	3300 metres
Traverse Line Direction	110 - 290 degrees
Tie Line Direction	020 - 200 degrees
Terrain Clearance	110 metres
EM System	25Hz TEMPEST
Navigation	Real-time differential GPS
Datum and Projection	GDA94 (MGA Zone 53)

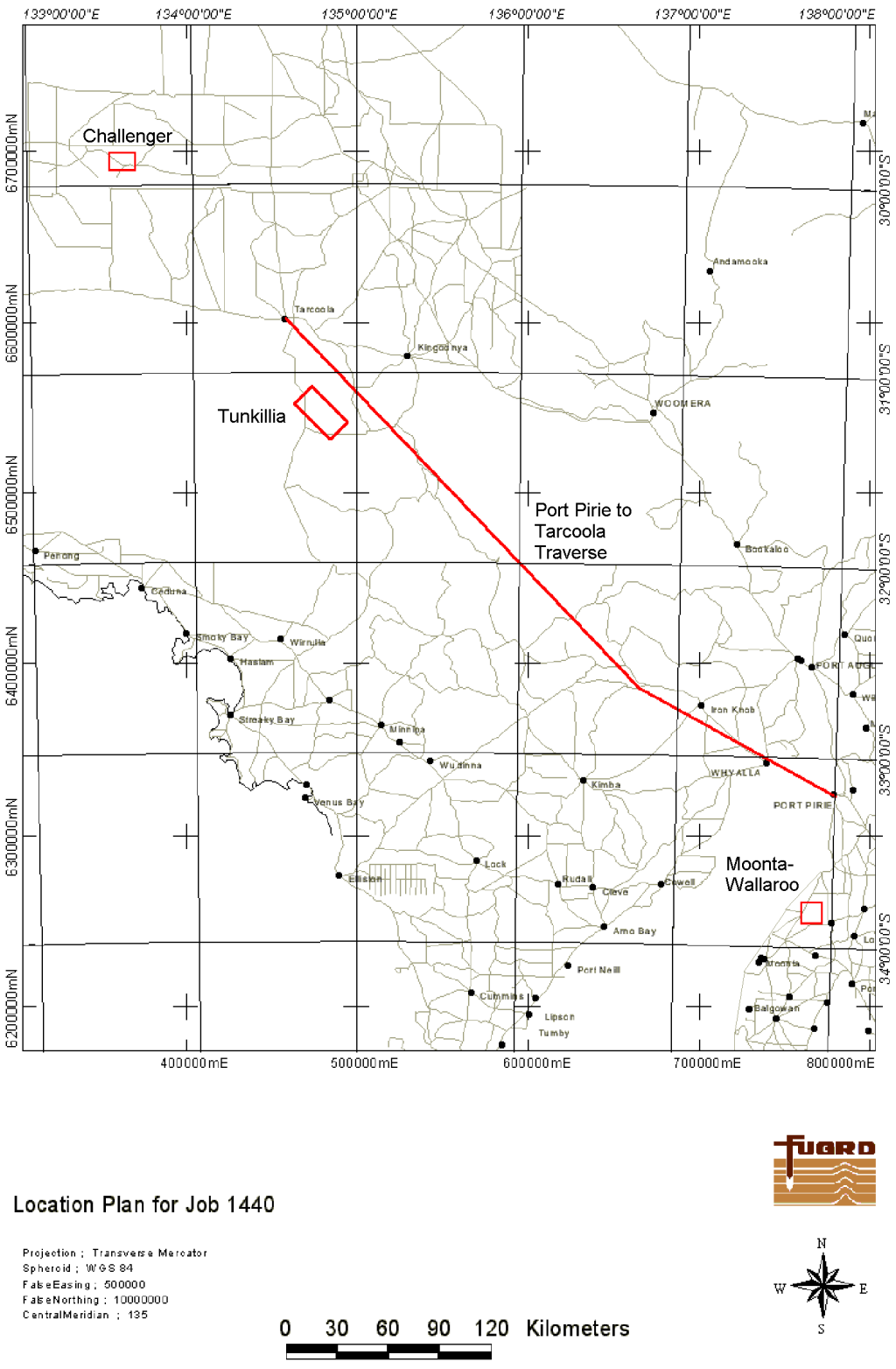

Figure 21. Location Plan for TEMPEST Job 1440.

Appendix 2 – Discrete Conductor Anomaly Characteristics

X component

Line	Fiducial (s)	East (m)	North (m)	Surface Elevation (m)	Terrain Clearance (m)	Component	Threshold (fT)	Search Half-width (s)	# Windows for TC Calculation	Last Window Above Threshold	Time Constant (ms)	Specified Line	Specified Fiducial	Priority
30040	964.4	368672	6699165	200.2	114.5	1	0.1	1.5	3	9	0.52	30040	963.0	3
30050	1040.4	369038	6698887	199.2	109.1	1	0.1	1.5	3	10	1.00	30050	1039.0	3
30050	1044.4	369312	6698784	197.4	109.8	1	0.1	1.5	3	10	0.73	30050	1043.0	3
30070	1222.4	367651	6699059	200.5	112.4	1	0.1	1.5	3	10	1.08	30070	1221.0	3
30090	1412.4	367506	6698784	201.6	108.1	1	0.1	1.5	3	10	1.26	30090	1411.0	3
30100	1549.4	367318	6698701	201.0	109.8	1	0.1	1.5	3	10	1.18	30100	1548.0	3
30110	1618.4	367290	6698549	199.6	112.3	1	0.1	1.5	3	11	1.42	30110	1617.0	3
30120	1750.4	366721	6698599	197.7	110.3	1	0.1	1.5	3	12	2.68	30120	1749.0	3
30130	1854.4	368978	6697608	199.3	113.3	1	0.1	1.5	3	11	1.29	30130	1853.0	3
30170	2322.4	368739	6697069	200.7	110.7	1	0.1	1.5	3	12	3.31	30170	2321.0	3
30260	1347.0	365713	6696732	196.0	114.9	1	0.1	1.5	3	12	2.85	30260	1346.0	3
30270	1613.4	367618	6695875	201.5	110.2	1	0.1	1.5	3	10	0.71	30270	1612.0	3
30310	2468.4	367265	6695362	200.4	109.8	1	0.1	1.5	3	10	0.90	30310	2467.0	3
30320	2582.4	366710	6695412	201.6	107.6	1	0.1	1.5	3	9	0.58	30320	2581.0	3
30330	2930.4	367080	6695116	200.6	109.1	1	0.1	1.5	3	10	0.81	30330	2929.0	3
30330	2951.4	368395	6694631	199.6	115.8	1	0.1	1.5	3	12	2.93	30330	2950.0	3
30330	2958.4	368835	6694465	200.6	114.0	1	0.1	1.5	3	14	12.55	30330	2957.0	3
30350	3473.4	369735	6693823	201.7	116.5	1	0.1	1.5	3	10	0.66	30350	3472.0	3
30390	4482.4	368819	6693527	205.6	108.9	1	0.1	1.5	3	10	0.93	30390	4481.0	3
30400	4528.2	369578	6693085	205.8	111.1	1	0.1	1.5	3	10	0.70	30400	4527.0	3
30410	4852.4	359738	6696510	196.6	113.9	1	0.1	1.5	3	11	1.72	30410	4851.0	3
30410	4915.4	363670	6695075	203.9	109.5	1	0.1	1.5	3	10	0.76	30410	4914.0	3
30410	4963.4	366635	6694001	204.3	113.8	1	0.1	1.5	3	12	2.01	30410	4962.0	3

30430	892.4	364249	6694550	209.2	104.7	1	0.1	1.5	3	11	1.79	30430	891.0	3
30450	1435.6	364932	6693984	210.9	105.9	1	0.1	1.5	3	11	1.27	30450	1435.0	3
30470	1965.4	364899	6693679	211.8	107.9	1	0.1	1.5	3	13	6.12	30470	1964.0	3
30490	2435.4	360268	6695042	198.5	116.9	1	0.1	1.5	3	13	8.18	30490	2434.0	3
30490	2498.4	364563	6693479	211.3	106.3	1	0.1	1.5	3	13	6.10	30490	2497.0	3
30610	801.4	367084	6690644	212.0	116.5	1	0.1	1.5	3	11	1.57	30610	800.0	3
30620	959.4	365061	6691221	212.5	110.6	1	0.1	1.5	3	12	1.58	30620	958.0	3
30630	1281.4	363627	6691587	209.9	110.7	1	0.1	1.5	3	12	2.43	30630	1280.0	3
30730	3736.4	359204	6691591	203.8	115.3	1	0.1	1.5	3	12	2.15	30730	3735.0	3
30791	474.4	358225	6690991	209.2	113.8	1	0.1	1.5	3	11	1.52	30791	473.0	3
30791	485.0	358966	6690730	206.1	117.5	1	0.1	1.5	3	13	4.92	30791	484.0	3
30800	684.4	358199	6690843	208.5	105.5	1	0.1	1.5	3	11	1.17	30800	683.0	3
30800	618.4	362029	6689446	202.6	110.5	1	0.1	1.5	3	12	2.33	30800	617.0	3
30810	818.4	359333	6690274	201.1	118.1	1	0.1	1.5	3	12	2.53	30810	817.0	3
30810	863.4	362490	6689126	204.9	111.2	1	0.1	1.5	3	12	3.13	30810	862.0	3
30810	876.4	363391	6688799	207.1	110.1	1	0.1	1.5	3	12	1.96	30810	875.0	3
30890	1876.4	359054	6689101	203.2	112.4	1	0.1	1.5	3	13	5.53	30890	1875.0	3

(column 1) line
(column 2) fid (of the location within the search window with the longest time constant)
(column 3) east (of the location within the search window with the longest time constant)
(column 4) north (of the location within the search window with the longest time constant)
(column 5) surface topography (of the location within the search window with the longest time constant)
(column 6) terrain clearance (of the location within the search window with the longest time constant)
(column 7) component (1=X, 2=Y, 3=Z)
(column 8) threshold for window amplitude and time constant
(column 9) half-width for search (fiducial units)
(column 10) number of windows for time constant calculation
(column 11) last window above threshold
(column 12) time constant for last windows above threshold (ms)
(column 13) line (as specified in the input)
(column 14) fid (as specified in the input)
(column 15) priority (1, 2 or 3, with 1 being the highest priority)
(undefined -99999)
Parallax suitable for horizontal / broad bodies applied to the window amplitudes.

Z component

Line	Fiducial (s)	East (m)	North (m)	Surface Elevation (m)	Terrain Clearance (m)	Component	Threshold (fT)	Search Half-width (s)	# Windows for TC Calculation	Last Window Above Threshold	Time Constant (ms)	Specified Line	Specified Fiducial	Priority
30040	961.6	368845	6699104	200.6	113.6	3	0.1	1.5	3	10	0.52	30040	963.0	3
30050	1040.4	369038	6698887	199.2	109.1	3	0.1	1.5	3	11	1.15	30050	1039.0	3
30050	1041.6	369120	6698857	200.5	108.4	3	0.1	1.5	3	11	1.25	30050	1043.0	3
30070	1222.4	367651	6699059	200.5	112.4	3	0.1	1.5	3	12	2.86	30070	1221.0	3
30090	1412.4	367506	6698784	201.6	108.1	3	0.1	1.5	3	11	1.05	30090	1411.0	3
30100	1549.4	367318	6698701	201.0	109.8	3	0.1	1.5	3	10	0.77	30100	1548.0	3
30110	1618.4	367290	6698549	199.6	112.3	3	0.1	1.5	3	10	0.67	30110	1617.0	3
30120	1750.4	366721	6698599	197.7	110.3	3	0.1	1.5	3	12	1.78	30120	1749.0	3
30130	1854.4	368978	6697608	199.3	113.3	3	0.1	1.5	3	10	0.63	30130	1853.0	3
30170	2321.6	368684	6697089	201.4	109.0	3	0.1	1.5	3	10	0.66	30170	2321.0	3
30260	1344.6	365873	6696675	196.8	115.0	3	0.1	1.5	3	12	1.68	30260	1346.0	3
30270	1613.4	367618	6695875	201.5	110.2	3	0.1	1.5	3	10	0.61	30270	1612.0	3
30310	2468.4	367265	6695362	200.4	109.8	3	0.1	1.5	3	10	0.68	30310	2467.0	3
30320	2582.4	366710	6695412	201.6	107.6	3	0.1	1.5	3	9	0.40	30320	2581.0	3
30330	2930.4	367080	6695116	200.6	109.1	3	0.1	1.5	3	10	0.66	30330	2929.0	3
30330	2948.6	368220	6694699	200.4	115.4	3	0.1	1.5	3	12	1.15	30330	2950.0	3
30330	2958.4	368835	6694465	200.6	114.0	3	0.1	1.5	3	12	1.43	30330	2957.0	3
30350	3470.6	369561	6693887	202.4	116.6	3	0.1	1.5	3	12	1.21	30350	3472.0	3
30390	4482.4	368819	6693527	205.6	108.9	3	0.1	1.5	3	11	1.08	30390	4481.0	3
30400	4528.4	369564	6693090	205.7	111.1	3	0.1	1.5	3	11	0.99	30400	4527.0	3
30410	4849.6	359564	6696574	197.7	111.3	3	0.1	1.5	3	11	0.94	30410	4851.0	3
30410	4915.4	363670	6695075	203.9	109.5	3	0.1	1.5	3	10	0.67	30410	4914.0	3
30410	4963.4	366635	6694001	204.3	113.8	3	0.1	1.5	3	12	1.61	30410	4962.0	3
30430	892.4	364249	6694550	209.2	104.7	3	0.1	1.5	3	11	1.04	30430	891.0	3
30450	1436.4	364986	6693964	210.5	106.1	3	0.1	1.5	3	12	1.83	30450	1435.0	3
30470	1963.8	364792	6693717	212.8	106.2	3	0.1	1.5	3	13	2.76	30470	1964.0	3

30490	2435.4	360268	6695042	198.5	116.9	3	0.1	1.5	3	12	1.22	30490	2434.0	3
30490	2498.4	364563	6693479	211.3	106.3	3	0.1	1.5	3	14	7.33	30490	2497.0	3
30610	801.4	367084	6690644	212.0	116.5	3	0.1	1.5	3	12	1.82	30610	800.0	3
30620	959.4	365061	6691221	212.5	110.6	3	0.1	1.5	3	12	1.37	30620	958.0	3
30630	1278.6	363430	6691660	207.5	113.1	3	0.1	1.5	3	12	1.43	30630	1280.0	3
30730	3734.0	359033	6691654	205.9	115.1	3	0.1	1.5	3	14	6.20	30730	3735.0	3
30791	474.4	358225	6690991	209.2	113.8	3	0.1	1.5	3	12	1.87	30791	473.0	3
30791	482.6	358800	6690793	209.0	114.6	3	0.1	1.5	3	12	1.44	30791	484.0	3
30800	684.2	358210	6690839	208.5	105.5	3	0.1	1.5	3	13	2.99	30800	683.0	3
30800	618.4	362029	6689446	202.6	110.5	3	0.1	1.5	3	12	1.77	30800	617.0	3
30810	815.6	359140	6690349	205.4	113.5	3	0.1	1.5	3	14	6.35	30810	817.0	3
30810	863.4	362490	6689126	204.9	111.2	3	0.1	1.5	3	12	1.59	30810	862.0	3
30810	875.2	363308	6688828	206.6	109.4	3	0.1	1.5	3	12	1.40	30810	875.0	3
30890	1873.6	358854	6689170	203.2	114.0	3	0.1	1.5	3	12	1.37	30890	1875.0	3

(column 1) line
(column 2) fid (of the location within the search window with the longest time constant)
(column 3) east (of the location within the search window with the longest time constant)
(column 4) north (of the location within the search window with the longest time constant)
(column 5) surface topography (of the location within the search window with the longest time constant)
(column 6) terrain clearance (of the location within the search window with the longest time constant)
(column 7) component (1=X, 2=Y, 3=Z)
(column 8) threshold for window amplitude and time constant
(column 9) half-width for search (fiducial units)
(column 10) number of windows for time constant calculation
(column 11) last window above threshold
(column 12) time constant for last windows above threshold (ms)
(column 13) line (as specified in the input)
(column 14) fid (as specified in the input)
(column 15) priority (1, 2 or 3, with 1 being the highest priority)
(undefined -99999)
Parallax suitable for horizontal / broad bodies applied to the window amplitudes.

Appendix 3 – Listing of GIS Themes

Arcview

ARCVIEW THEME	FILENAME	FILETYPE	DESCRIPTION	DATASET SOURCE
Challenger prospect	gis/pirsa/ch_prospect.shp	ESRI shape file - Point	Location and basic information for Challenger prospect	PIRSA
Discrete_cond.shp	gis/workshop_interp/discrete_cond.shp	ESRI shape file - Point	Discrete conductors interpreted at workshop	AEM Workshop
Magnetics Interpretation	gis/workshop_interp/revised_mag2.shp	ESRI shape file - Arc	Magnetics interpretation from workshop	AEM Workshop
Aem_mag_poly2.shp	gis/workshop_interp/aem_mag_poly2.shp	ESRI shape file - Polygon	High frequency magnetic response - interpretation from workshop	AEM Workshop
AEM interpretation - lines	gis/workshop_interp/aemint_l.shp	ESRI shape file - Arc	AEM interpretation from workshop	AEM Workshop
AEM interpretation - polygons	gis/workshop_interp/aemint_p2.shp	ESRI shape file - Polygon	AEM interpretation from workshop	AEM Workshop
Hotlinked CDI slices	gis/aem/aem_lines.shp	ESRI shape file - Arc	CDI sections (GIF images) hotlinked to AEM survey flight lines	GA/PIRSA/CRC LEME
Company surface Au	gis/company_data/min_footprints/dd_surface.shp	ESRI shape file - Arc	Company provided datasets	Dominion Mining Ltd
Company supergene Au	gis/company_data/min_footprints/dd_supergene.shp	ESRI shape file - Arc	Company provided datasets	Dominion Mining Ltd
Company basement Au	gis/company_data/min_footprints/dd_shallow.shp	ESRI shape file - Arc	Company provided datasets	Dominion Mining Ltd
Company all footprints	gis/company_data/min_footprints/dd_allft.shp	ESRI shape file - Arc	Company provided datasets	Dominion Mining Ltd
Company gravity interp	gis/company_data/gravity/gravity_interp_polyline.shp	ESRI shape file - Arc	Company provided datasets	Dominion Mining Ltd
Company gravity highs	gis/company_data/gravity/grav_highs_region.shp	ESRI shape file - Polygon	Company provided datasets	Dominion Mining Ltd
Company RAB AC DHs	gis/company_data/drilling/dd_rab_ac_point.shp	ESRI shape file - Point	Company provided datasets	Dominion Mining Ltd
Company RC DDH	gis/company_data/drilling/dd_rc_ddh_pt.shp	ESRI shape file - Point	Company provided datasets	Dominion Mining Ltd
Company RAB Au Mineralisation	gis/company_data/drilling/dd_chal_rab_au_min.shp	ESRI shape file - Polygon	Company provided datasets	Dominion Mining Ltd
Local Calcrete	gis/company_data/calcrete/dd_calc_point.shp	ESRI shape file - Point	Company provided datasets	Dominion Mining Ltd
Depth to oxidation	gis/company_data/depth_to_oxidation/dd_mwoxchpt.shp	ESRI shape file - Point	Company provided datasets	Dominion Mining Ltd
Depth to bedrock	gis/company_data/depth_to_oxidation/dd_dp_to_bdrk.shp	ESRI shape file - Point	Company provided datasets	Dominion Mining Ltd
Company ne_struct	gis/company_data/aeromag/dd_ne_struct.shp	ESRI shape file - Arc	Company provided datasets	Dominion Mining Ltd
Company aeromag contours	gis/company_data/aeromag/dd_aeromag_contour_ln.shp	ESRI shape file - Arc	Company provided datasets	Dominion Mining Ltd
Geochem samples	gis/pirsa/geochem.shp	ESRI shape file - Point	Subseted data from PIRSA's "South Australia GIS"	PIRSA
DH - strat logs	gis/pirsa/dh_strat.shp	ESRI shape file - Point	Subseted data from PIRSA's "South Australia GIS"	PIRSA
DH - mineral exploration	gis/pirsa/dhexplor.shp	ESRI shape file - Point	Subseted data from PIRSA's "South Australia GIS"	PIRSA
DH - water wells	gis/pirsa/dh_water.shp	ESRI shape file - Point	Subseted data from PIRSA's "South Australia GIS"	PIRSA
Regolith - alluvial sediments	gis/regolith/rego_dd.shp	ESRI shape file - Polygon	Regolith data from CRC LEME's "Gawler GIS"	CRC LEME

ARCVIEW THEME	FILENAME	FILETYPE	DESCRIPTION	DATASET SOURCE
Regolith - colluvial sediments	gis/regolith/rego_dd.shp	ESRI shape file - Polygon	Regolith data from CRC LEME's "Gawler GIS"	CRC LEME
Regolith - lags	gis/regolith/rego_dd.shp	ESRI shape file - Polygon	Regolith data from CRC LEME's "Gawler GIS"	CRC LEME
Regolith - saprolite minor indurated sediments	gis/regolith/rego_dd.shp	ESRI shape file - Polygon	Regolith data from CRC LEME's "Gawler GIS"	CRC LEME
Regolith polygons	gis/regolith/rego_dd.shp	ESRI shape file - Polygon	Regolith data from CRC LEME's "Gawler GIS"	CRC LEME
Regional geology	gis/pirsa/ch_reg_geol.shp	ESRI shape file - Polygon	Subseted data from PIRSA's "South Australia GIS"	PIRSA
1 2M Geology	gis/pirsa/ch_geol2m.shp	ESRI shape file - Polygon	Subseted data from PIRSA's "South Australia GIS"	PIRSA
1 250k maps	gis/pirsa/ch_maps250k.shp	ESRI shape file - Polygon	Subseted data from PIRSA's "South Australia GIS"	PIRSA
1 100k maps	gis/pirsa/ch_maps100k.shp	ESRI shape file - Polygon	Subseted data from PIRSA's "South Australia GIS"	PIRSA
Historical SML's	gis/pirsa/ch_his_sml.shp	ESRI shape file - Polygon	Subseted data from PIRSA's "South Australia GIS"	PIRSA
Historical EL's	gis/pirsa/ch_his_el.shp	ESRI shape file - Polygon	Subseted data from PIRSA's "South Australia GIS"	PIRSA
Exploration licences	gis/pirsa/ch_exp_lic.shp	ESRI shape file - Polygon	Subseted data from PIRSA's "South Australia GIS"	PIRSA
Localities	gis/pirsa/ch_localities.shp	ESRI shape file - Point	Subseted data from PIRSA's "South Australia GIS"	PIRSA
Roads	gis/pirsa/ch_roads.shp	ESRI shape file - Arc	Subseted data from PIRSA's "South Australia GIS"	PIRSA
Drainage	gis/pirsa/ch_drain.shp	ESRI shape file - Arc	Subseted data from PIRSA's "South Australia GIS"	PIRSA
Clip_poly.shp	gis/pirsa/clip_poly.shp	ESRI shape file - Polygon	Clip polygon used to subset PIRSA data	GA/PIRSA/CRC LEME
AEM area outline	gis/aem/aem_bdy.shp	ESRI shape file - Polygon	AEM survey area outline	GA/PIRSA/CRC LEME
AEM flight lines	gis/aem/aem_lines.shp	ESRI shape file - Arc	AEM survey flight lines	GA/PIRSA/CRC LEME
AEM fid's	gis/aem/aem_fids.shp	ESRI shape file - Point	AEM survey fiducials	GA/PIRSA/CRC LEME
Geol interp (P Lyons)	gis/pirsa/solgeol.shp	ESRI shape file - Polygon	Interpreted solid geology of Mulgathing Complex (preliminary)	GA
Derived surface topography (NE)	gis/images/der_sur_top_gs_ne.bil	BIL image	AEM survey processed images	GA/PIRSA/CRC LEME
Derived surface topography (NW)	gis/images/der_sur_top_gs_nw.bil	BIL image	AEM survey processed images	GA/PIRSA/CRC LEME
AEM TMI (rtp) (E)	gis/images/tmi-rtp-e.bil	BIL image	AEM survey processed images	GA/PIRSA/CRC LEME
AEM TMI (rtp) (N)	gis/images/tmi-rtp-n.bil	BIL image	AEM survey processed images	GA/PIRSA/CRC LEME
AEM 1VD TMI (rtp)	gis/images/tmi-rtp-1vd.bil	BIL image	AEM survey processed images	GA/PIRSA/CRC LEME
AEM 1VD TMI (agc) (NSg)	gis/images/chal_agc_23_nsg.bil	BIL image	AEM survey processed images	GA/PIRSA/CRC LEME
AEM 1VD TMI (agc) (EWg)	gis/images/chal_agc_23_ewg.bil	BIL image	AEM survey processed images	GA/PIRSA/CRC LEME
AEM 1VD TMI (agc)	gis/images/chal_agc_23.bil	BIL image	AEM survey processed images	GA/PIRSA/CRC LEME
Company IVD TMI	gis/images/company-tmi_1vd_utm53.bil	BIL image	Company provided datasets	Dominion Mining Ltd
Company TMI (NW)	gis/images/company-tmi-nw_utm53.bil	BIL image	Company provided datasets	Dominion Mining Ltd
Company TMI (E)	gis/images/company-tmi-e_utm53.bil	BIL image	Company provided datasets	Dominion Mining Ltd
Company TMI (N)	gis/images/company-tmi-n_utm53.bil	BIL image	Company provided datasets	Dominion Mining Ltd

ARCVIEW THEME	FILENAME	FILETYPE	DESCRIPTION	DATASET SOURCE
Gawler Landsat TM	gis/regolith/gawler_landsat.bil	BIL image	Regolith data from CRC LEME's "Gawler GIS"	CRC LEME
Conductance_company_2vd_trans.bil	gis/images/conductance_company_2vd_trans.bil	BIL image	AEM survey processed images	GA/PIRSA/CRC LEME
Conductance_company_1vd_trans.bil	gis/images/conductance_company_1vd_trans.bil	BIL image	AEM survey processed images	GA/PIRSA/CRC LEME
Interval conductivity 0-10m	gis/images/intcond-0-10.bil	BIL image	AEM survey processed images	GA/PIRSA/CRC LEME
Interval conductivity 10-20m	gis/images/intcond-10-20.bil	BIL image	AEM survey processed images	GA/PIRSA/CRC LEME
Interval conductivity 20-30m	gis/images/intcond-20-30.bil	BIL image	AEM survey processed images	GA/PIRSA/CRC LEME
Interval conductivity 30-40m	gis/images/intcond-30-40.bil	BIL image	AEM survey processed images	GA/PIRSA/CRC LEME
Interval conductivity 40-50m	gis/images/intcond-40-50.bil	BIL image	AEM survey processed images	GA/PIRSA/CRC LEME
Interval conductivity 50-60m	gis/images/intcond-50-60.bil	BIL image	AEM survey processed images	GA/PIRSA/CRC LEME
Interval conductivity 60-70m	gis/images/intcond-60-70.bil	BIL image	AEM survey processed images	GA/PIRSA/CRC LEME
Interval conductivity 70-80m	gis/images/intcond-70-80.bil	BIL image	AEM survey processed images	GA/PIRSA/CRC LEME
Interval conductivity 80-90m	gis/images/intcond-80-90.bil	BIL image	AEM survey processed images	GA/PIRSA/CRC LEME
Interval conductivity 90-100m	gis/images/intcond-90-100.bil	BIL image	AEM survey processed images	GA/PIRSA/CRC LEME
Interval conductivity 0-10m (NW)	gis/images/intcond-0-10-nw.bil	BIL image	AEM survey processed images	GA/PIRSA/CRC LEME
Interval conductivity 10-20m (NW)	gis/images/intcond-10-20-nw.bil	BIL image	AEM survey processed images	GA/PIRSA/CRC LEME
Interval conductivity 20-30m (NW)	gis/images/intcond-20-30-nw.bil	BIL image	AEM survey processed images	GA/PIRSA/CRC LEME
Interval conductivity 30-40m (NW)	gis/images/intcond-30-40-nw.bil	BIL image	AEM survey processed images	GA/PIRSA/CRC LEME
Depth to top of conductive unit	gis/images/dtop.bil	BIL image	AEM survey processed images	GA/PIRSA/CRC LEME
Depth to base of conductive unit 0-220m	gis/images/dbottom-0-220.bil	BIL image	AEM survey processed images	GA/PIRSA/CRC LEME
Depth to base of conductive unit 0-60m	gis/images/dbottom-0-60.bil	BIL image	AEM survey processed images	GA/PIRSA/CRC LEME
Thickness of conductive unit 0-220m	gis/images/thickness-0-220.bil	BIL image	AEM survey processed images	GA/PIRSA/CRC LEME
Thickness of conductive unit 0-60m	gis/images/thickness-0-60.bil	BIL image	AEM survey processed images	GA/PIRSA/CRC LEME
Conductance of conductive unit (NE)	gis/images/conductance-ne.bil	BIL image	AEM survey processed images	GA/PIRSA/CRC LEME
Conductance of conductive unit (NW)	gis/images/conductance-nw.bil	BIL image	AEM survey processed images	GA/PIRSA/CRC LEME
Adaptive time constant (NE)	gis/images/adaptive-tc-ne.bil	BIL image	AEM survey processed images	GA/PIRSA/CRC LEME
Adaptive time constant (NW)	gis/images/adaptive-tc-nw.bil	BIL image	AEM survey processed images	GA/PIRSA/CRC LEME
Principal components over TMI	gis/images/challenger_pcs_mag.bil	BIL image	AEM survey processed images	GA/PIRSA/CRC LEME
Principal components	gis/images/challenger_pcs.bil	BIL image	AEM survey processed images	GA/PIRSA/CRC LEME
6697500N.bmp	gis/dh_sections/6697500N.bmp	BITMAP image	Regridded CDI data (MVS software) sectioned to northings	GA/PIRSA/CRC LEME
6697000N.bmp	gis/dh_sections/6697000N.bmp	BITMAP image	Regridded CDI data (MVS software) sectioned to northings	GA/PIRSA/CRC LEME
6696500N.bmp	gis/dh_sections/6696500N.bmp	BITMAP image	Regridded CDI data (MVS software) sectioned to northings	GA/PIRSA/CRC LEME
6696000N.bmp	gis/dh_sections/6696000N.bmp	BITMAP image	Regridded CDI data (MVS software) sectioned to northings	GA/PIRSA/CRC LEME

ARCVIEW THEME	FILENAME	FILETYPE	DESCRIPTION	DATASET SOURCE
6695500N.bmp	gis/dh_sections/6695500N.bmp	BITMAP image	Regridded CDI data (MVS software) sectioned to northings	GA/PIRSA/CRC LEME
6695000N.bmp	gis/dh_sections/6695000N.bmp	BITMAP image	Regridded CDI data (MVS software) sectioned to northings	GA/PIRSA/CRC LEME
6694800N.bmp	gis/dh_sections/6694800N.bmp	BITMAP image	Regridded CDI data (MVS software) sectioned to northings	GA/PIRSA/CRC LEME
6694600N.bmp	gis/dh_sections/6694600N.bmp	BITMAP image	Regridded CDI data (MVS software) sectioned to northings	GA/PIRSA/CRC LEME
6694400N.bmp	gis/dh_sections/6694400N.bmp	BITMAP image	Regridded CDI data (MVS software) sectioned to northings	GA/PIRSA/CRC LEME
6694200N.bmp	gis/dh_sections/6694200N.bmp	BITMAP image	Regridded CDI data (MVS software) sectioned to northings	GA/PIRSA/CRC LEME
6694000N.bmp	gis/dh_sections/6694000N.bmp	BITMAP image	Regridded CDI data (MVS software) sectioned to northings	GA/PIRSA/CRC LEME
6693800N.bmp	gis/dh_sections/6693800N.bmp	BITMAP image	Regridded CDI data (MVS software) sectioned to northings	GA/PIRSA/CRC LEME
6693600N.bmp	gis/dh_sections/6693600N.bmp	BITMAP image	Regridded CDI data (MVS software) sectioned to northings	GA/PIRSA/CRC LEME
6693400N.bmp	gis/dh_sections/6693400N.bmp	BITMAP image	Regridded CDI data (MVS software) sectioned to northings	GA/PIRSA/CRC LEME
6693200N.bmp	gis/dh_sections/6693200N.bmp	BITMAP image	Regridded CDI data (MVS software) sectioned to northings	GA/PIRSA/CRC LEME
6693000N.bmp	gis/dh_sections/6693000N.bmp	BITMAP image	Regridded CDI data (MVS software) sectioned to northings	GA/PIRSA/CRC LEME
6692800N.bmp	gis/dh_sections/6692800N.bmp	BITMAP image	Regridded CDI data (MVS software) sectioned to northings	GA/PIRSA/CRC LEME
6692600N.bmp	gis/dh_sections/6692600N.bmp	BITMAP image	Regridded CDI data (MVS software) sectioned to northings	GA/PIRSA/CRC LEME
6692400N.bmp	gis/dh_sections/6692400N.bmp	BITMAP image	Regridded CDI data (MVS software) sectioned to northings	GA/PIRSA/CRC LEME
6692200N.bmp	gis/dh_sections/6692200N.bmp	BITMAP image	Regridded CDI data (MVS software) sectioned to northings	GA/PIRSA/CRC LEME
6692000N.bmp	gis/dh_sections/6692000N.bmp	BITMAP image	Regridded CDI data (MVS software) sectioned to northings	GA/PIRSA/CRC LEME
6691500N.bmp	gis/dh_sections/6691500N.bmp	BITMAP image	Regridded CDI data (MVS software) sectioned to northings	GA/PIRSA/CRC LEME
6691000N.bmp	gis/dh_sections/6691000N.bmp	BITMAP image	Regridded CDI data (MVS software) sectioned to northings	GA/PIRSA/CRC LEME
6690500N.bmp	gis/dh_sections/6690500N.bmp	BITMAP image	Regridded CDI data (MVS software) sectioned to northings	GA/PIRSA/CRC LEME
6690000N.bmp	gis/dh_sections/6690000N.bmp	BITMAP image	Regridded CDI data (MVS software) sectioned to northings	GA/PIRSA/CRC LEME
6689500N.bmp	gis/dh_sections/6689500N.bmp	BITMAP image	Regridded CDI data (MVS software) sectioned to northings	GA/PIRSA/CRC LEME
S6695000N.bmp	gis/dh_sections/slices/s6695000N.bmp	BITMAP image	Regridded CDI data (MVS software) sectioned to northings	GA/PIRSA/CRC LEME
S6694800N.bmp	gis/dh_sections/slices/s6694800N.bmp	BITMAP image	Regridded CDI data (MVS software) sectioned to northings	GA/PIRSA/CRC LEME
S6694600N.bmp	gis/dh_sections/slices/s6694600N.bmp	BITMAP image	Regridded CDI data (MVS software) sectioned to northings	GA/PIRSA/CRC LEME
S6694400N.bmp	gis/dh_sections/slices/s6694400N.bmp	BITMAP image	Regridded CDI data (MVS software) sectioned to northings	GA/PIRSA/CRC LEME
S6694000N.bmp	gis/dh_sections/slices/s6694000N.bmp	BITMAP image	Regridded CDI data (MVS software) sectioned to northings	GA/PIRSA/CRC LEME
S6693800N.bmp	gis/dh_sections/slices/s6693800N.bmp	BITMAP image	Regridded CDI data (MVS software) sectioned to northings	GA/PIRSA/CRC LEME
S6693600N.bmp	gis/dh_sections/slices/s6693600N.bmp	BITMAP image	Regridded CDI data (MVS software) sectioned to northings	GA/PIRSA/CRC LEME
S6693400N.bmp	gis/dh_sections/slices/s6693400N.bmp	BITMAP image	Regridded CDI data (MVS software) sectioned to northings	GA/PIRSA/CRC LEME
S6693200N.bmp	gis/dh_sections/slices/s6693200N.bmp	BITMAP image	Regridded CDI data (MVS software) sectioned to northings	GA/PIRSA/CRC LEME
S6693000N.bmp	gis/dh_sections/slices/s6693000N.bmp	BITMAP image	Regridded CDI data (MVS software) sectioned to northings	GA/PIRSA/CRC LEME

ARCVIEW THEME	FILENAME	FILETYPE	DESCRIPTION	DATASET SOURCE
S6692800N.bmp	gis/dh_sections/slices/s6692800N.bmp	BITMAP image	Regridded CDI data (MVS software) sectioned to northings	GA/PIRSA/CRC LEME
S6692600N.bmp	gis/dh_sections/slices/s6692600N.bmp	BITMAP image	Regridded CDI data (MVS software) sectioned to northings	GA/PIRSA/CRC LEME
S6692400N.bmp	gis/dh_sections/slices/s6692400N.bmp	BITMAP image	Regridded CDI data (MVS software) sectioned to northings	GA/PIRSA/CRC LEME
S6692200N.bmp	gis/dh_sections/slices/s6692200N.bmp	BITMAP image	Regridded CDI data (MVS software) sectioned to northings	GA/PIRSA/CRC LEME
S6692000N.bmp	gis/dh_sections/slices/s6692000N.bmp	BITMAP image	Regridded CDI data (MVS software) sectioned to northings	GA/PIRSA/CRC LEME

Mapinfo

MAPINFO LAYER	FILENAME	FILETYPE	DESCRIPTION	DATASET SOURCE
ch_prospect	pirsa\ch_prospect.tab	MAPINFO table - Point	Location and basic information for Challenger prospect	PIRSA
discrete_cond	workshop_interp\discrete_cond.tab	MAPINFO table - Point	Discrete conductors interpreted at workshop	AEM Workshop
mag_interp	workshop_interp\revised_mag2.tab	MAPINFO table - Arc	Magnetics interpretation from workshop	AEM Workshop
aem_mag_poly	workshop_interp\aem_mag_poly2.tab	MAPINFO table - Polygon	High frequency magnetic response - interpretation from workshop	AEM Workshop
aem_interp_ln	workshop_interp\aemint_l.tab	MAPINFO table - Arc	AEM interpretation from workshop	AEM Workshop
aem_interp_po	workshop_interp\aemint_p2.tab	MAPINFO table - Polygon	AEM interpretation from workshop	AEM Workshop
Hotlinked_CDI_sections	aem\aem_lines.tab	MAPINFO table - Arc	CDI sections (GIF images) hotlinked to AEM survey flight lines	GA/PIRSA/CRC LEME
Co_surface	company_data\min_footprints\dd_surface.tab	MAPINFO table - Arc	Company provided datasets	Dominion Mining Ltd
Co_supergene	company_data\min_footprints\dd_supergene.tab	MAPINFO table - Arc	Company provided datasets	Dominion Mining Ltd
Co_shallow	company_data\min_footprints\dd_shallow.tab	MAPINFO table - Arc	Company provided datasets	Dominion Mining Ltd
Co_all_footprints	company_data\min_footprints\dd_allft.tab	MAPINFO table - Arc	Company provided datasets	Dominion Mining Ltd
gravity_interp_polyline	company_data\gravity\gravity_interp_polyline.tab	MAPINFO table - Arc	Company provided datasets	Dominion Mining Ltd
grav_highs_region	company_data\gravity\grav_highs_region.tab	MAPINFO table - Polygon	Company provided datasets	Dominion Mining Ltd
Co_rab_ac_pt	company_data\drilling\dd_rab_ac_point.tab	MAPINFO table - Point	Company provided datasets	Dominion Mining Ltd
Co_rc_ddh_pt	company_data\drilling\dd_rc_ddh_pt.tab	MAPINFO table - Point	Company provided datasets	Dominion Mining Ltd
Co_rab_au_min	company_data\drilling\dd_chal_rab_au_min.tab	MAPINFO table - Polygon	Company provided datasets	Dominion Mining Ltd
Co_calcrete_pt	company_data\calcrete\dd_calc_point.tab	MAPINFO table - Point	Company provided datasets	Dominion Mining Ltd
depth_to_oxid_pt	company_data\depth_to_oxidation\dd_mwoxchpt.tab	MAPINFO table - Point	Company provided datasets	Dominion Mining Ltd
depth_to_bedrock_pt	company_data\depth_to_oxidation\dd_dp_to_bdrk.tab	MAPINFO table - Point	Company provided datasets	Dominion Mining Ltd
Co_NE__struct	company_data\aeromag\dd_ne_struct.tab	MAPINFO table - Arc	Company provided datasets	Dominion Mining Ltd
Co_aeromag_contours	company_data\aeromag\dd_aeromag_contour_ln.tab	MAPINFO table - Arc	Company provided datasets	Dominion Mining Ltd
geochem	pirsa\geochem.tab	MAPINFO table - Point	Subseted data from PIRSA's "South Australia GIS"	PIRSA
dh_strat	pirsa\dh_strat.tab	MAPINFO table - Point	Subseted data from PIRSA's "South Australia GIS"	PIRSA
dhexplor	pirsa\dhexplor.tab	MAPINFO table - Point	Subseted data from PIRSA's "South Australia GIS"	PIRSA
dh_water	pirsa\dh_water.tab	MAPINFO table - Point	Subseted data from PIRSA's "South Australia GIS"	PIRSA
Regolith - alluvial sediments	regolith\rego_dd.tab	MAPINFO table - Polygon	Regolith data from CRC LEME's "Gawler GIS"	CRC LEME
Regolith - colluvial sediments	regolith\rego_dd.tab	MAPINFO table - Polygon	Regolith data from CRC LEME's "Gawler GIS"	CRC LEME
Regolith - lags	regolith\rego_dd.tab	MAPINFO table - Polygon	Regolith data from CRC LEME's "Gawler GIS"	CRC LEME
Regolith - saprolite minor indurated	regolith\rego_dd.tab	MAPINFO table - Polygon	Regolith data from CRC LEME's "Gawler GIS"	CRC LEME

MAPINFO LAYER	FILENAME	FILETYPE	DESCRIPTION	DATASET SOURCE
sediments				
regolith_po	regolith\rego_dd.tab	MAPINFO table - Polygon	Regolith data from CRC LEME's "Gawler GIS"	CRC LEME
ch_reg_geol	pirsa\ch_reg_geol.tab	MAPINFO table - Polygon	Subseted data from PIRSA's "South Australia GIS"	PIRSA
ch_geol2m	pirsa\ch_geol2m.tab	MAPINFO table - Polygon	Subseted data from PIRSA's "South Australia GIS"	PIRSA
ch_maps250k	pirsa\ch_maps250k.tab	MAPINFO table - Polygon	Subseted data from PIRSA's "South Australia GIS"	PIRSA
ch_maps100k	pirsa\ch_maps100k.tab	MAPINFO table - Polygon	Subseted data from PIRSA's "South Australia GIS"	PIRSA
ch_his_sml	pirsa\ch_his_sml.tab	MAPINFO table - Polygon	Subseted data from PIRSA's "South Australia GIS"	PIRSA
ch_his_el	pirsa\ch_his_el.tab	MAPINFO table - Polygon	Subseted data from PIRSA's "South Australia GIS"	PIRSA
ch_exp_lic	pirsa\ch_exp_lic.tab	MAPINFO table - Polygon	Subseted data from PIRSA's "South Australia GIS"	PIRSA
ch_localities	pirsa\ch_localities.tab	MAPINFO table - Point	Subseted data from PIRSA's "South Australia GIS"	PIRSA
ch_roads	pirsa\ch_roads.tab	MAPINFO table - Arc	Subseted data from PIRSA's "South Australia GIS"	PIRSA
ch_drain	pirsa\ch_drain.tab	MAPINFO table - Arc	Subseted data from PIRSA's "South Australia GIS"	PIRSA
clip_poly	pirsa\clip_poly.tab	MAPINFO table - Polygon	Clip polygon used to subset PIRSA data	GA/PIRSA/CRC LEME
AEM_survey_area	aem\aem_bdy.tab	MAPINFO table - Polygon	AEM survey area outline	GA/PIRSA/CRC LEME
aem_fids	aem\aem_fids.tab	MAPINFO table - Point	AEM survey fiducials	GA/PIRSA/CRC LEME
solgeol	pirsa\solgeol.tab	MAPINFO table - Polygon	Interpreted solid geology of Mulgathing Complex (preliminary)	GA
der_sur_top_gs_ne	images\der_sur_top_gs_ne.bil	BIL image	Derived surface topography (NE)	GA/PIRSA/CRC LEME
der_sur_top_gs_nw	images\der_sur_top_gs_nw.bil	BIL image	Derived surface topography (NW)	GA/PIRSA/CRC LEME
tmi_rtp_e	images\tmi-rtp-e.bil	BIL image	AEM TMI (rtp) (E)	GA/PIRSA/CRC LEME
tmi_rtp_n	images\tmi-rtp-n.bil	BIL image	AEM TMI (rtp) (N)	GA/PIRSA/CRC LEME
tmi_rtp_1vd	images\tmi-rtp-1vd.bil	BIL image	AEM 1VD TMI (rtp)	GA/PIRSA/CRC LEME
chal_agc_23_nsg	images\chal_agc_23_nsg.bil	BIL image	AEM 1VD TMI (agc) (NSg)	GA/PIRSA/CRC LEME
chal_agc_23_ewg	images\chal_agc_23_ewg.bil	BIL image	AEM 1VD TMI (agc) (EWg)	GA/PIRSA/CRC LEME
chal_agc_23	images\chal_agc_23.bil	BIL image	AEM 1VD TMI (agc)	GA/PIRSA/CRC LEME
company_tmi_1vd_utm53	images\company-tmi_1vd_utm53.bil	BIL image	Company IVD TMI	Dominion Mining Ltd
company_tmi_nw_utm53	images\company-tmi-nw_utm53.bil	BIL image	Company TMI (NW)	Dominion Mining Ltd
company_tmi_e_utm53	images\company-tmi-e_utm53.bil	BIL image	Company TMI (E)	Dominion Mining Ltd
company_tmi_n_utm53	images\company-tmi-n_utm53.bil	BIL image	Company TMI (N)	Dominion Mining Ltd
gawler_landsat	regolith\gawler_landsat.bil	BIL image	Gawler Landsat TM	CRC LEME
conductance_company_2vd_trans	images\conductance_company_2vd_trans.bil	BIL image	Conductance_company_2vd_trans.bil	GA/PIRSA/CRC LEME
conductance_company_1vd_trans	images\conductance_company_1vd_trans.bil	BIL image	Conductance_company_1vd_trans.bil	GA/PIRSA/CRC LEME
intcond_0_10	images\intcond-0-10.bil	BIL image	Interval conductivity 0-10m	GA/PIRSA/CRC LEME

MAPINFO LAYER	FILENAME	FILETYPE	DESCRIPTION	DATASET SOURCE
intcond_10_20	images\intcond-10-20.bil	BIL image	Interval conductivity 10-20m	GA/PIRSA/CRC LEME
intcond_20_30	images\intcond-20-30.bil	BIL image	Interval conductivity 20-30m	GA/PIRSA/CRC LEME
intcond_30_40	images\intcond-30-40.bil	BIL image	Interval conductivity 30-40m	GA/PIRSA/CRC LEME
intcond_40_50	images\intcond-40-50.bil	BIL image	Interval conductivity 40-50m	GA/PIRSA/CRC LEME
intcond_50_60	images\intcond-50-60.bil	BIL image	Interval conductivity 50-60m	GA/PIRSA/CRC LEME
intcond_60_70	images\intcond-60-70.bil	BIL image	Interval conductivity 60-70m	GA/PIRSA/CRC LEME
intcond_70_80	images\intcond-70-80.bil	BIL image	Interval conductivity 70-80m	GA/PIRSA/CRC LEME
intcond_80_90	images\intcond-80-90.bil	BIL image	Interval conductivity 80-90m	GA/PIRSA/CRC LEME
intcond_90_100	images\intcond-90-100.bil	BIL image	Interval conductivity 90-100m	GA/PIRSA/CRC LEME
intcond_0_10_nw	images\intcond-0-10-nw.bil	BIL image	Interval conductivity 0-10m (NW)	GA/PIRSA/CRC LEME
intcond_10_20_nw	images\intcond-10-20-nw.bil	BIL image	Interval conductivity 10-20m (NW)	GA/PIRSA/CRC LEME
intcond_20_30_nw	images\intcond-20-30-nw.bil	BIL image	Interval conductivity 20-30m (NW)	GA/PIRSA/CRC LEME
intcond_30_40_nw	images\intcond-30-40-nw.bil	BIL image	Interval conductivity 30-40m (NW)	GA/PIRSA/CRC LEME
dtop	images\dtop.bil	BIL image	Depth to top of conductive unit	GA/PIRSA/CRC LEME
dbottom_0_220	images\dbottom-0-220.bil	BIL image	Depth to base of conductive unit 0-220m	GA/PIRSA/CRC LEME
dbottom_0_60	images\dbottom-0-60.bil	BIL image	Depth to base of conductive unit 0-60m	GA/PIRSA/CRC LEME
thickness_0_220	images\thickness-0-220.bil	BIL image	Thickness of conductive unit 0-220m	GA/PIRSA/CRC LEME
thickness_0_60	images\thickness-0-60.bil	BIL image	Thickness of conductive unit 0-60m	GA/PIRSA/CRC LEME
conductance_ne	images\conductance-ne.bil	BIL image	Conductance of conductive unit (NE)	GA/PIRSA/CRC LEME
conductance_nw	images\conductance-nw.bil	BIL image	Conductance of conductive unit (NW)	GA/PIRSA/CRC LEME
adaptive_tc_ne	images\adaptive-tc-ne.bil	BIL image	Adaptive time constant (NE)	GA/PIRSA/CRC LEME
adaptive_tc_nw	images\adaptive-tc-nw.bil	BIL image	Adaptive time constant (NW)	GA/PIRSA/CRC LEME
challenger_pcs_mag	images\challenger_pcs_mag.bil	BIL image	Principal components over TMI	GA/PIRSA/CRC LEME
challenger_pcs	images\challenger_pcs.bil	BIL image	Principal components	GA/PIRSA/CRC LEME
6697500N	dh_sections\6697500N.bmp	BITMAP image	Regridded CDI data (MVS software) sectioned to northings	GA/PIRSA/CRC LEME
6697000N	dh_sections\6697000N.bmp	BITMAP image	Regridded CDI data (MVS software) sectioned to northings	GA/PIRSA/CRC LEME
6696500N	dh_sections\6696500N.bmp	BITMAP image	Regridded CDI data (MVS software) sectioned to northings	GA/PIRSA/CRC LEME
6696000N	dh_sections\6696000N.bmp	BITMAP image	Regridded CDI data (MVS software) sectioned to northings	GA/PIRSA/CRC LEME
6695500N	dh_sections\6695500N.bmp	BITMAP image	Regridded CDI data (MVS software) sectioned to northings	GA/PIRSA/CRC LEME
6695000N	dh_sections\6695000N.bmp	BITMAP image	Regridded CDI data (MVS software) sectioned to northings	GA/PIRSA/CRC LEME
6694800N	dh_sections\6694800N.bmp	BITMAP image	Regridded CDI data (MVS software) sectioned to northings	GA/PIRSA/CRC LEME
6694600N	dh_sections\6694600N.bmp	BITMAP image	Regridded CDI data (MVS software) sectioned to northings	GA/PIRSA/CRC LEME

MAPINFO LAYER	FILENAME	FILETYPE	DESCRIPTION	DATASET SOURCE
6694400N	dh_sections\6694400N.bmp	BITMAP image	Regridded CDI data (MVS software) sectioned to northings	GA/PIRSA/CRC LEME
6694200N	dh_sections\6694200N.bmp	BITMAP image	Regridded CDI data (MVS software) sectioned to northings	GA/PIRSA/CRC LEME
6694000N	dh_sections\6694000N.bmp	BITMAP image	Regridded CDI data (MVS software) sectioned to northings	GA/PIRSA/CRC LEME
6693800N	dh_sections\6693800N.bmp	BITMAP image	Regridded CDI data (MVS software) sectioned to northings	GA/PIRSA/CRC LEME
6693600N	dh_sections\6693600N.bmp	BITMAP image	Regridded CDI data (MVS software) sectioned to northings	GA/PIRSA/CRC LEME
6693400N	dh_sections\6693400N.bmp	BITMAP image	Regridded CDI data (MVS software) sectioned to northings	GA/PIRSA/CRC LEME
6693200N	dh_sections\6693200N.bmp	BITMAP image	Regridded CDI data (MVS software) sectioned to northings	GA/PIRSA/CRC LEME
6693000N	dh_sections\6693000N.bmp	BITMAP image	Regridded CDI data (MVS software) sectioned to northings	GA/PIRSA/CRC LEME
6692800N	dh_sections\6692800N.bmp	BITMAP image	Regridded CDI data (MVS software) sectioned to northings	GA/PIRSA/CRC LEME
6692600N	dh_sections\6692600N.bmp	BITMAP image	Regridded CDI data (MVS software) sectioned to northings	GA/PIRSA/CRC LEME
6692400N	dh_sections\6692400N.bmp	BITMAP image	Regridded CDI data (MVS software) sectioned to northings	GA/PIRSA/CRC LEME
6692200N	dh_sections\6692200N.bmp	BITMAP image	Regridded CDI data (MVS software) sectioned to northings	GA/PIRSA/CRC LEME
6692000N	dh_sections\6692000N.bmp	BITMAP image	Regridded CDI data (MVS software) sectioned to northings	GA/PIRSA/CRC LEME
6691500N	dh_sections\6691500N.bmp	BITMAP image	Regridded CDI data (MVS software) sectioned to northings	GA/PIRSA/CRC LEME
6691000N	dh_sections\6691000N.bmp	BITMAP image	Regridded CDI data (MVS software) sectioned to northings	GA/PIRSA/CRC LEME
6690500N	dh_sections\6690500N.bmp	BITMAP image	Regridded CDI data (MVS software) sectioned to northings	GA/PIRSA/CRC LEME
6690000N	dh_sections\6690000N.bmp	BITMAP image	Regridded CDI data (MVS software) sectioned to northings	GA/PIRSA/CRC LEME
6689500N	dh_sections\6689500N.bmp	BITMAP image	Regridded CDI data (MVS software) sectioned to northings	GA/PIRSA/CRC LEME
S6695000N	dh_sections\slices\s6695000N.bmp	BITMAP image	Regridded CDI data (MVS software) sectioned to northings	GA/PIRSA/CRC LEME
S6694800N	dh_sections\slices\s6694800N.bmp	BITMAP image	Regridded CDI data (MVS software) sectioned to northings	GA/PIRSA/CRC LEME
S6694600N	dh_sections\slices\s6694600N.bmp	BITMAP image	Regridded CDI data (MVS software) sectioned to northings	GA/PIRSA/CRC LEME
S6694400N	dh_sections\slices\s6694400N.bmp	BITMAP image	Regridded CDI data (MVS software) sectioned to northings	GA/PIRSA/CRC LEME
S6694000N	dh_sections\slices\s6694000N.bmp	BITMAP image	Regridded CDI data (MVS software) sectioned to northings	GA/PIRSA/CRC LEME
S6693800N	dh_sections\slices\s6693800N.bmp	BITMAP image	Regridded CDI data (MVS software) sectioned to northings	GA/PIRSA/CRC LEME
S6693600N	dh_sections\slices\s6693600N.bmp	BITMAP image	Regridded CDI data (MVS software) sectioned to northings	GA/PIRSA/CRC LEME
S6693400N	dh_sections\slices\s6693400N.bmp	BITMAP image	Regridded CDI data (MVS software) sectioned to northings	GA/PIRSA/CRC LEME
S6693200N	dh_sections\slices\s6693200N.bmp	BITMAP image	Regridded CDI data (MVS software) sectioned to northings	GA/PIRSA/CRC LEME
S6693000N	dh_sections\slices\s6693000N.bmp	BITMAP image	Regridded CDI data (MVS software) sectioned to northings	GA/PIRSA/CRC LEME
S6692800N	dh_sections\slices\s6692800N.bmp	BITMAP image	Regridded CDI data (MVS software) sectioned to northings	GA/PIRSA/CRC LEME
S6692600N	dh_sections\slices\s6692600N.bmp	BITMAP image	Regridded CDI data (MVS software) sectioned to northings	GA/PIRSA/CRC LEME
S6692400N	dh_sections\slices\s6692400N.bmp	BITMAP image	Regridded CDI data (MVS software) sectioned to northings	GA/PIRSA/CRC LEME
S6692200N	dh_sections\slices\s6692200N.bmp	BITMAP image	Regridded CDI data (MVS software) sectioned to northings	GA/PIRSA/CRC LEME

MAPINFO LAYER	FILENAME	FILETYPE	DESCRIPTION	DATASET SOURCE
S6692000N	dh_sections\slices\s6692000N.bmp	BITMAP image	Regridded CDI data (MVS software) sectioned to northings	GA/PIRSA/CRC LEME

Appendix 4 – Snapshots from the GIS

Data from the vicinity of the Challenger Deposit

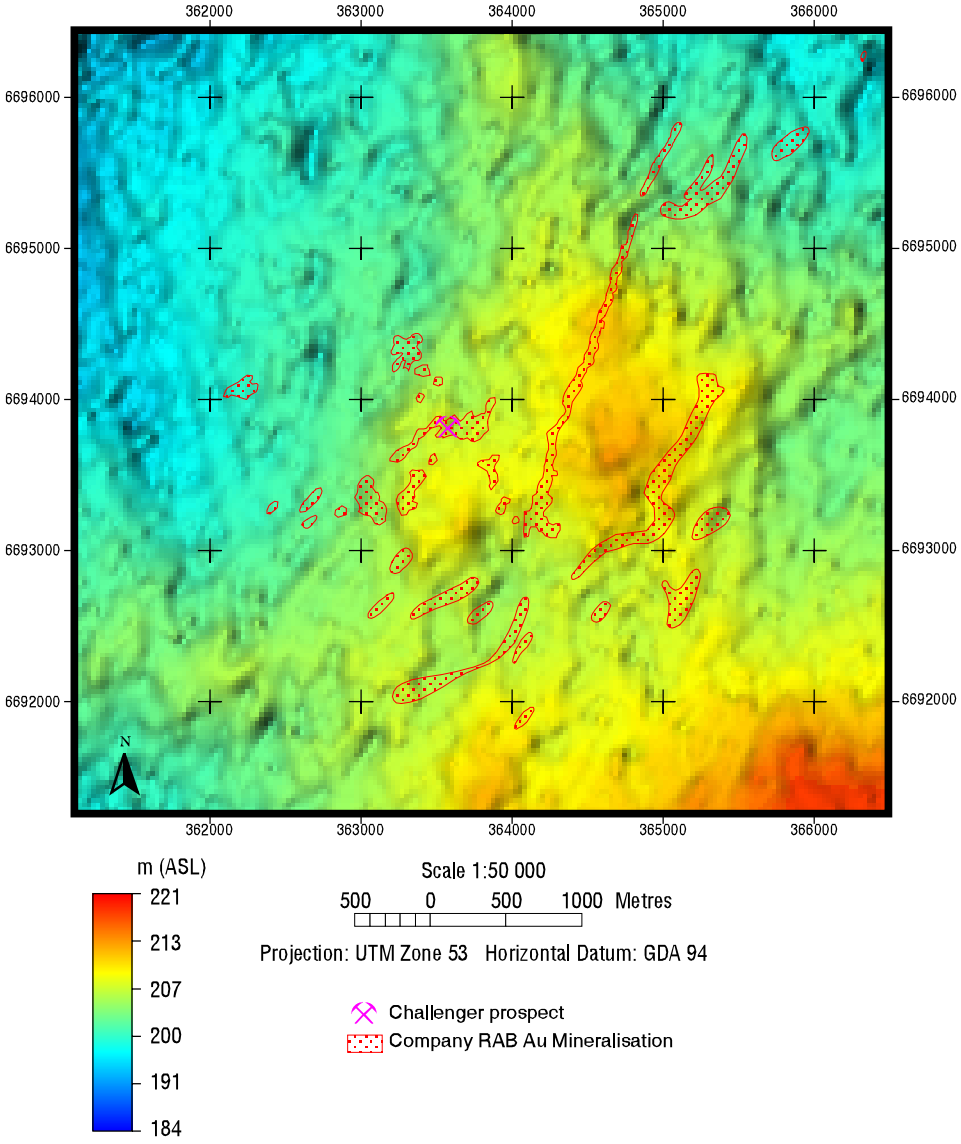

Figure 22. Surface topography derived from the AEM survey overlain by the distribution of gold within the regolith.

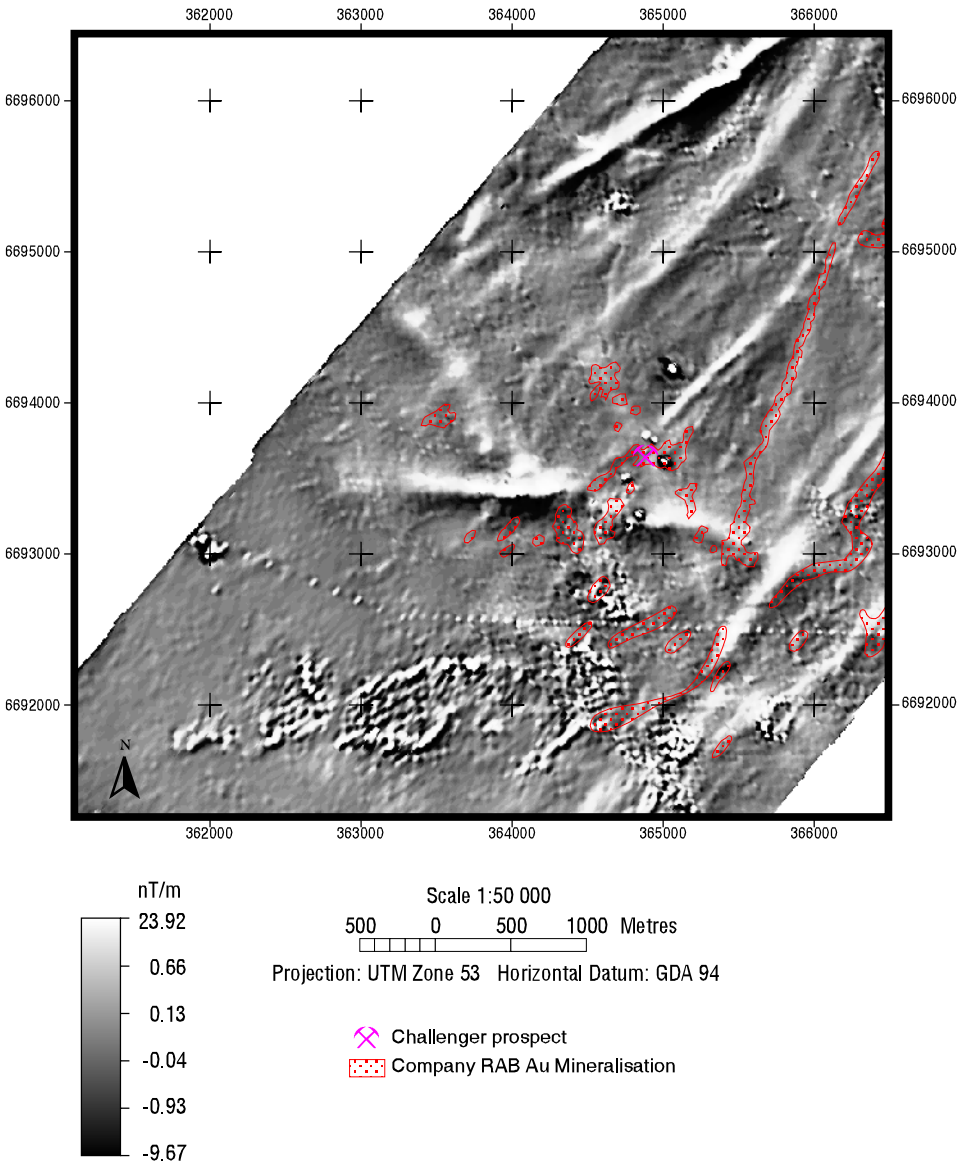

Figure 23. First vertical derivative of total magnetic intensity, derived from the high-resolution company data, overlain by the distribution of gold within the regolith.

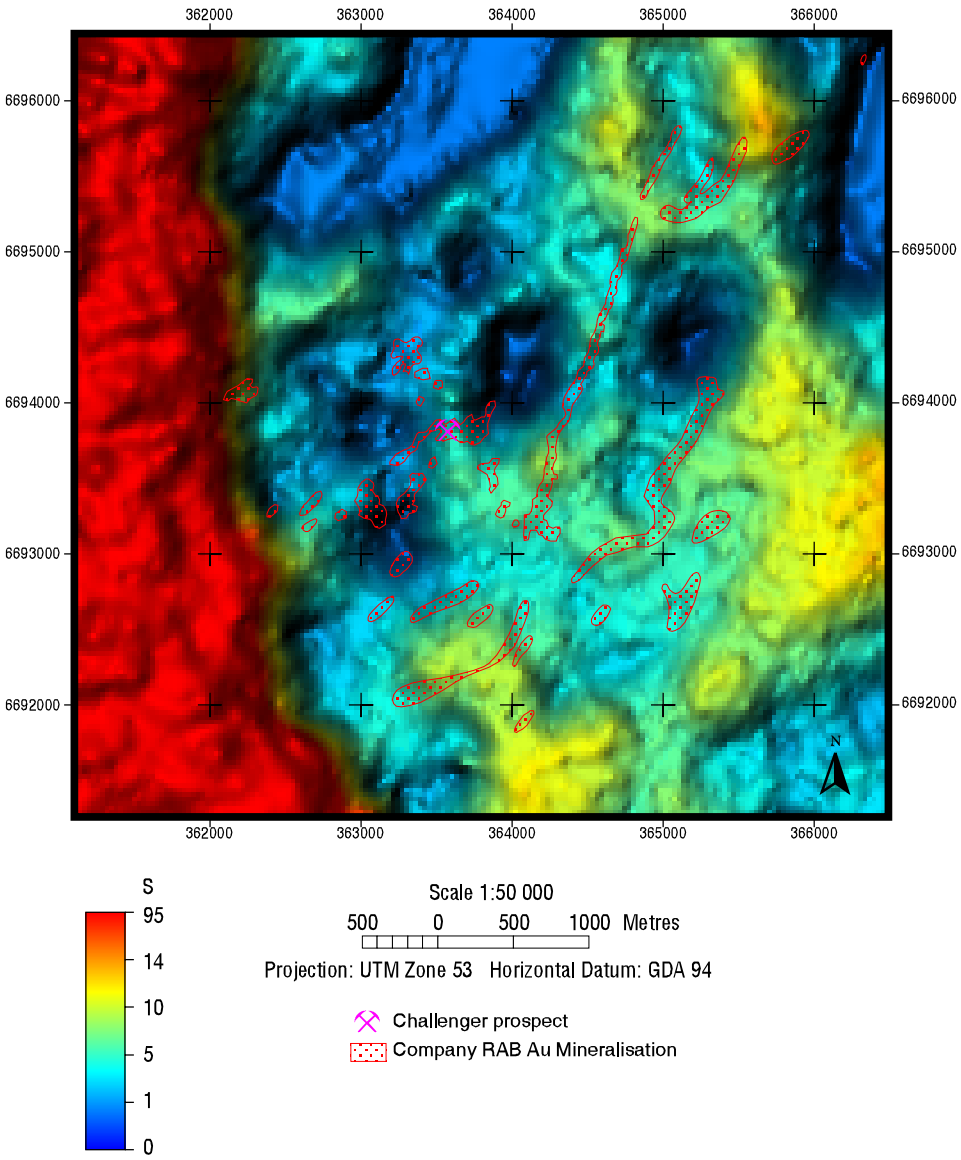

Figure 24. Conductance of "conductive unit" derived from the AEM survey overlain by the distribution of gold within the regolith. .

Images overlain by the Magnetics Interpretation

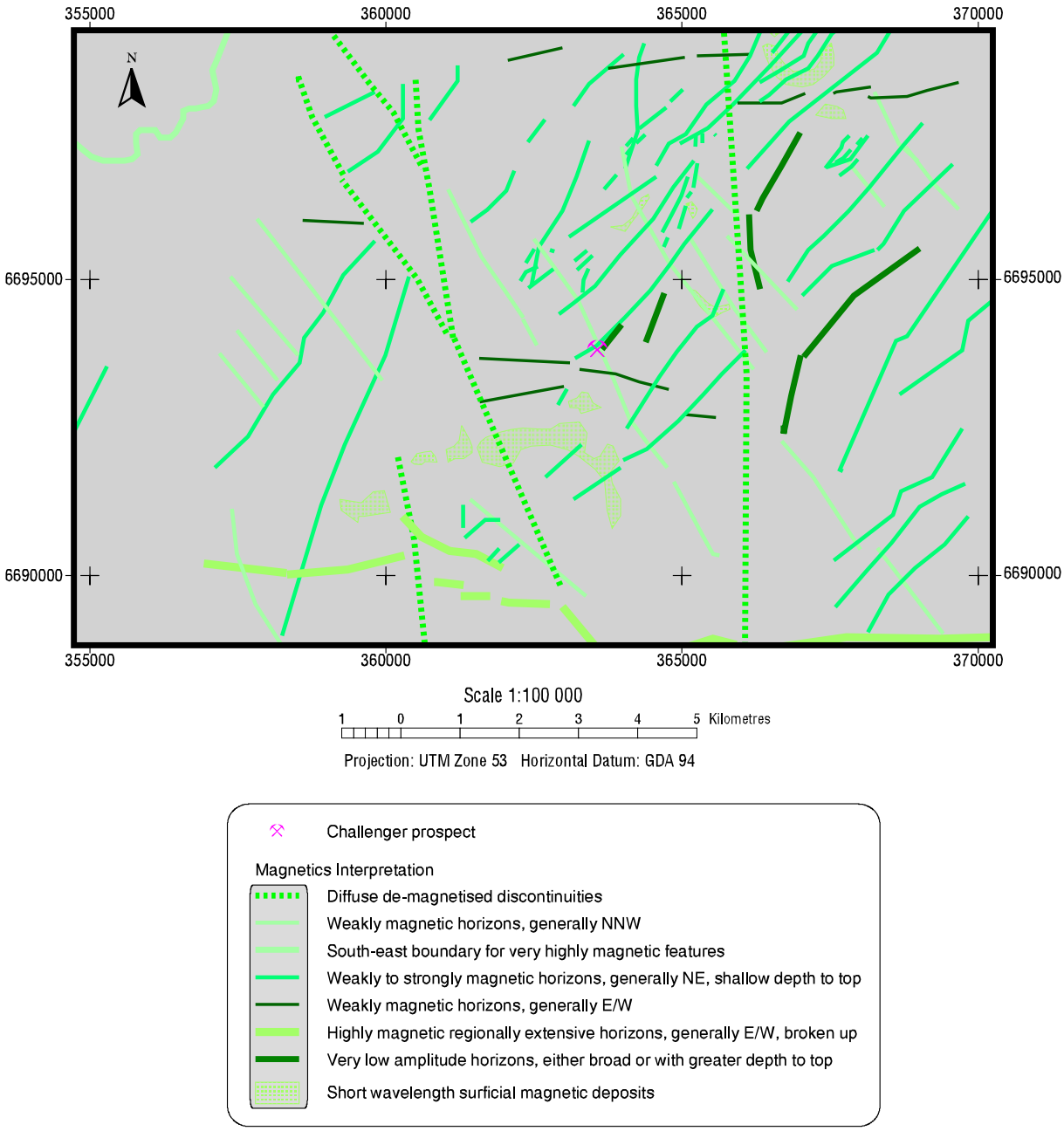

Figure 25. Interpretation of magnetics data from the survey area (high resolution company data and data acquired with the AEM survey).

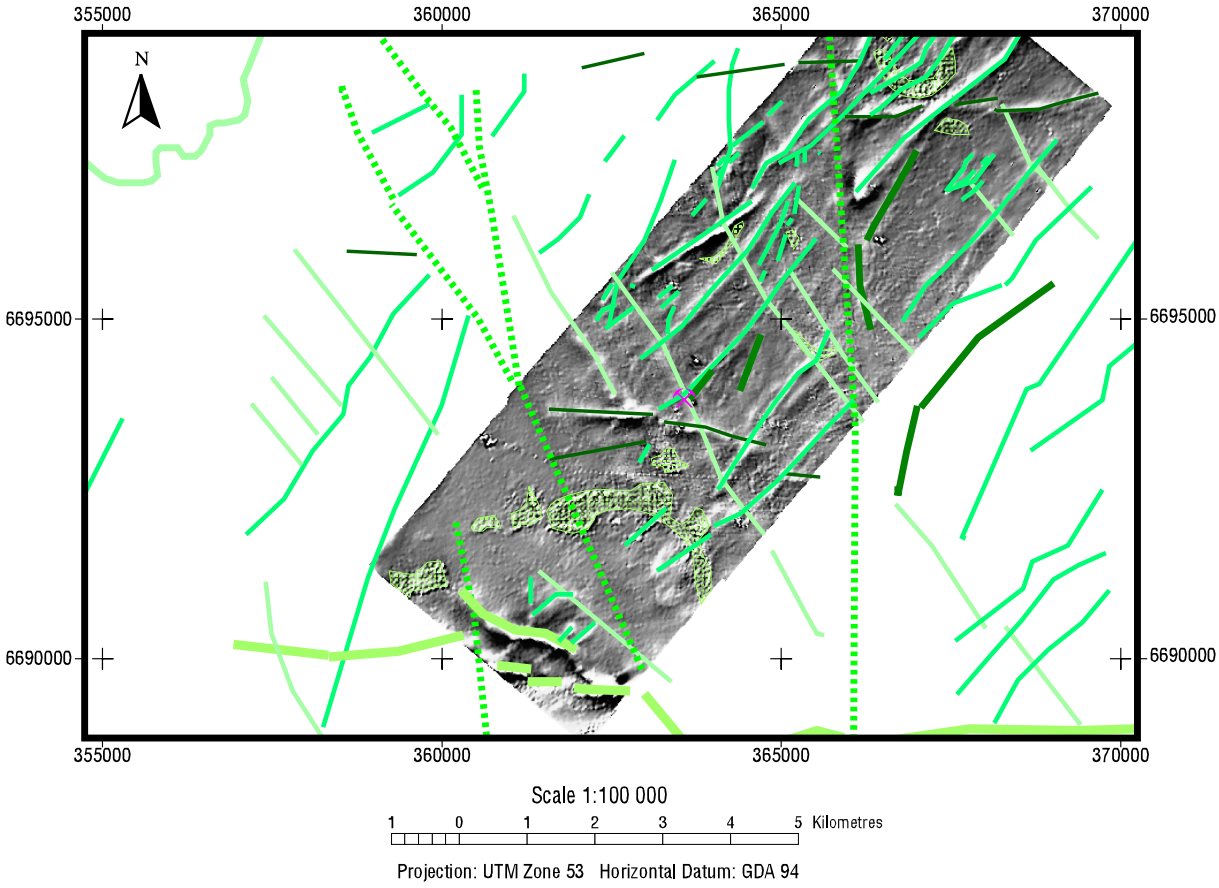

Figure 26. First vertical derivative of total magnetic intensity derived from the company survey overlain by the interpretation of the combined data.

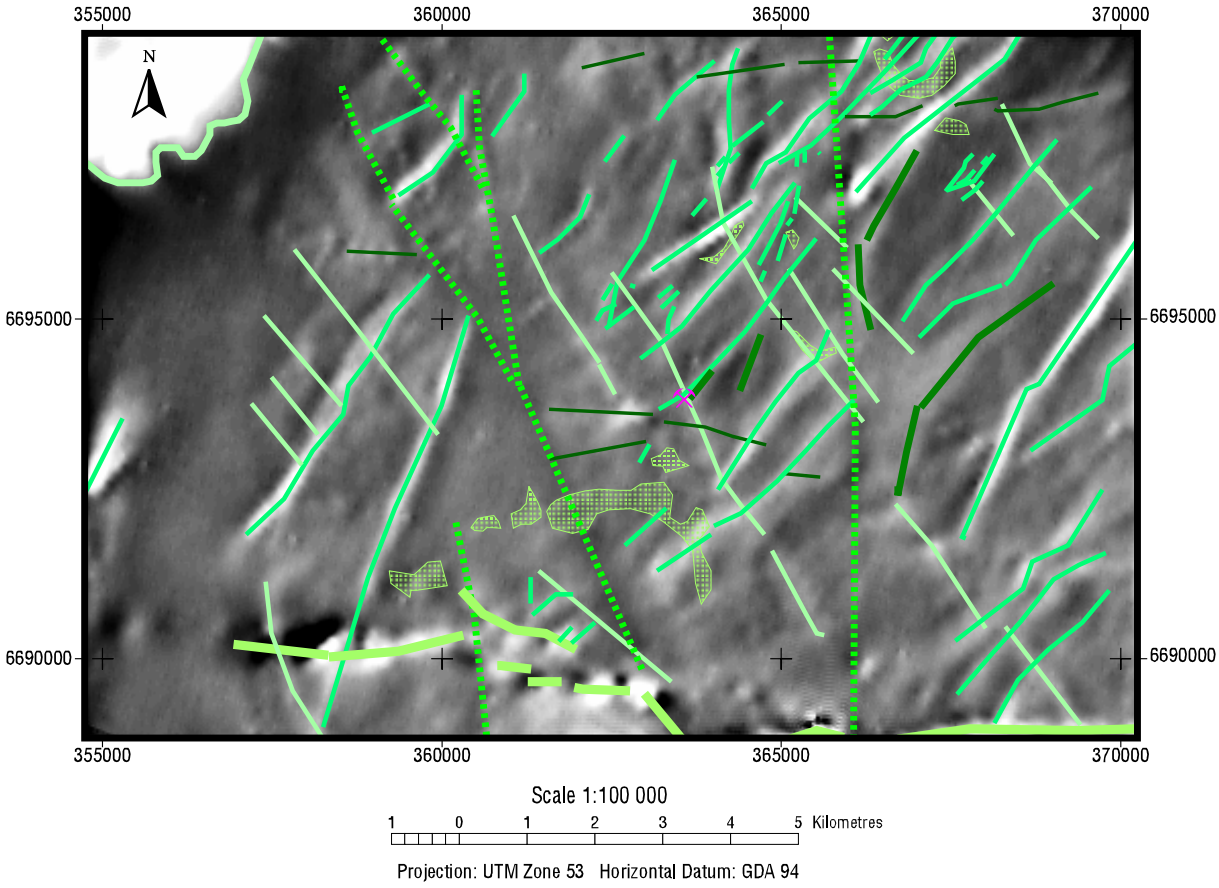

Figure 27. First vertical derivative of total magnetic intensity derived from the AEM survey overlain by the interpretation of the combined data.

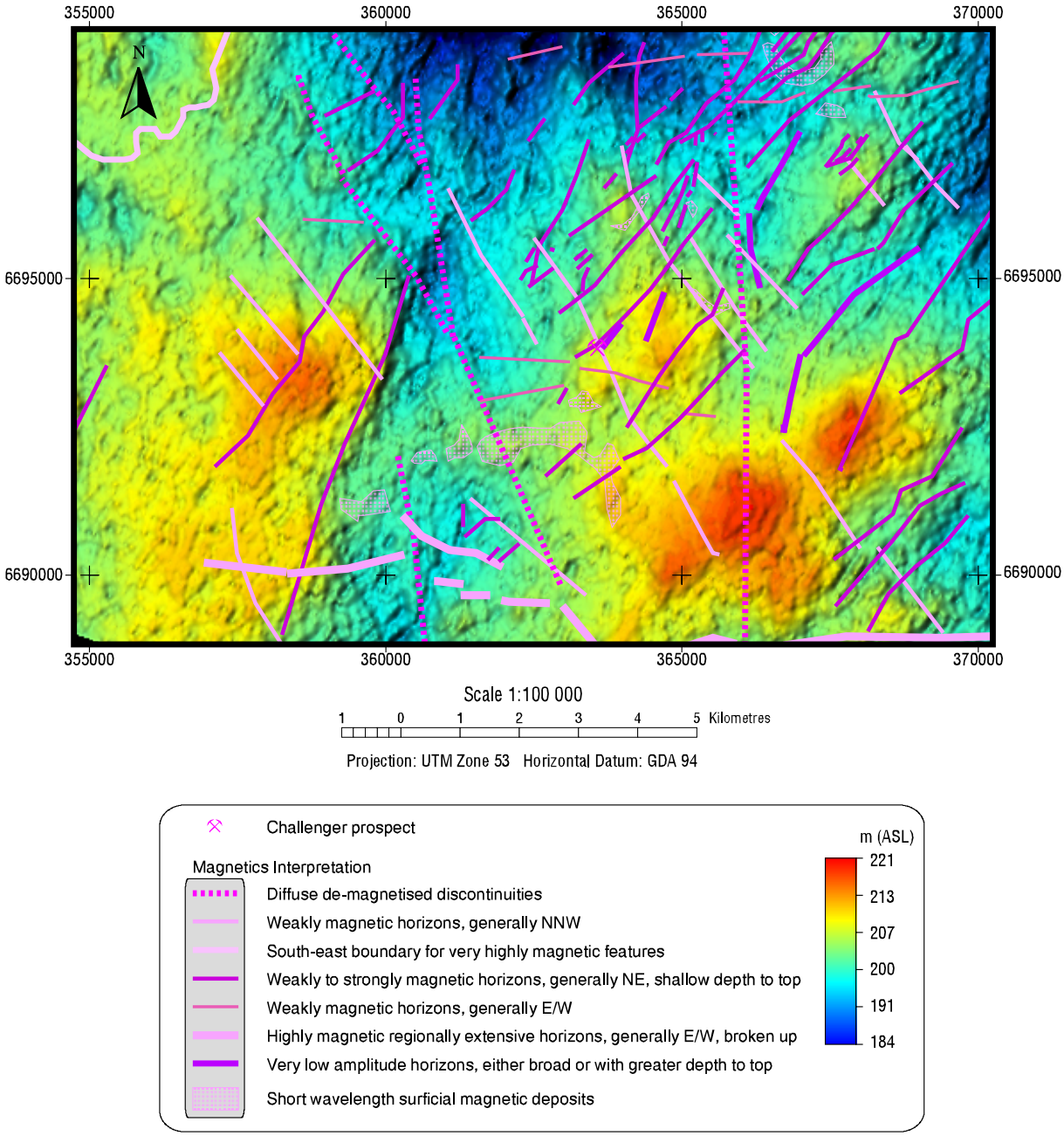

Figure 28. Surface topography derived from the AEM survey overlain by the magnetics interpretation.

.

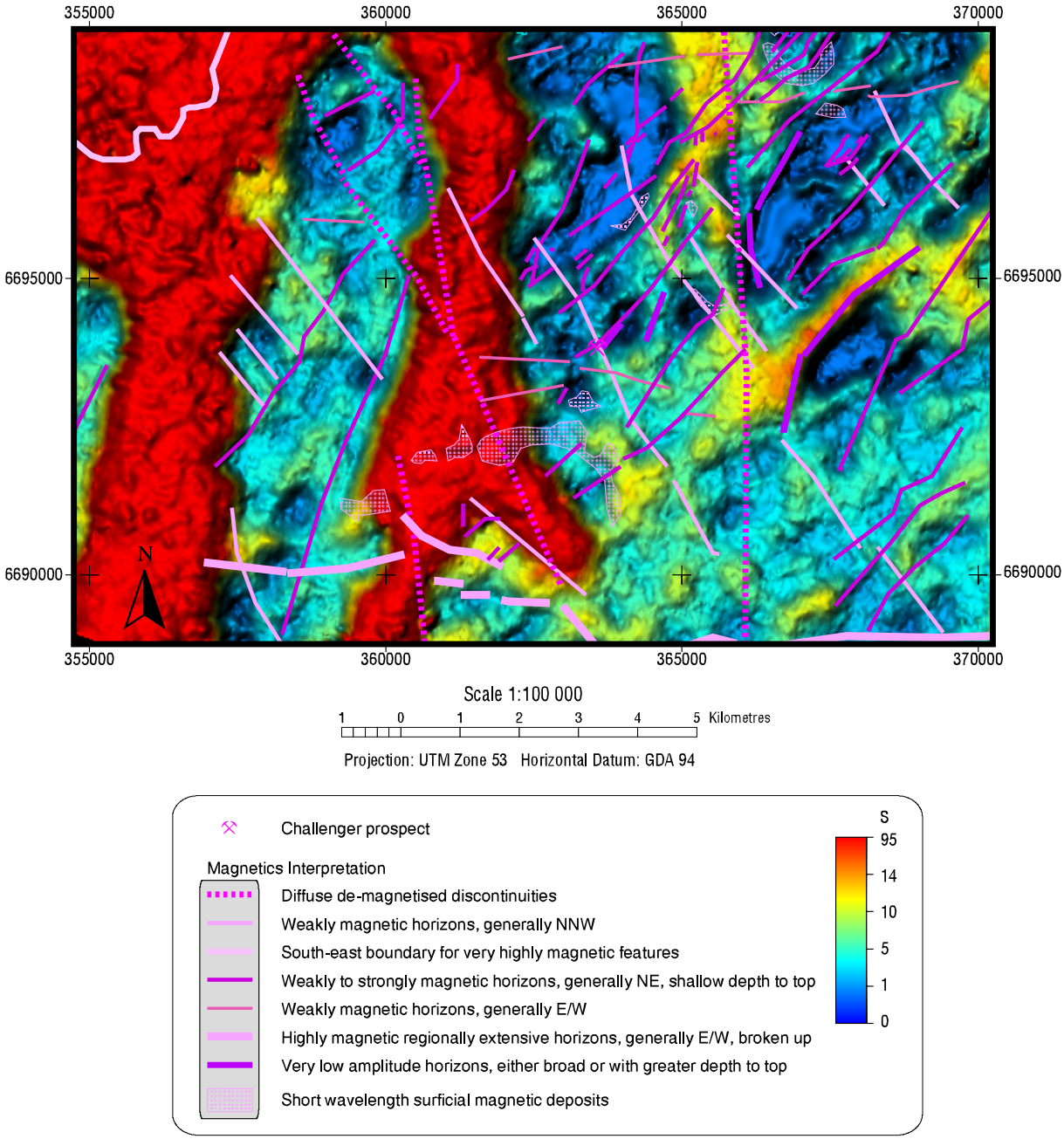

Figure 29. Conductance of "conductive unit" derived from the AEM survey overlain by the interpretation of the magnetic data.

Images overlain by the AEM Interpretation

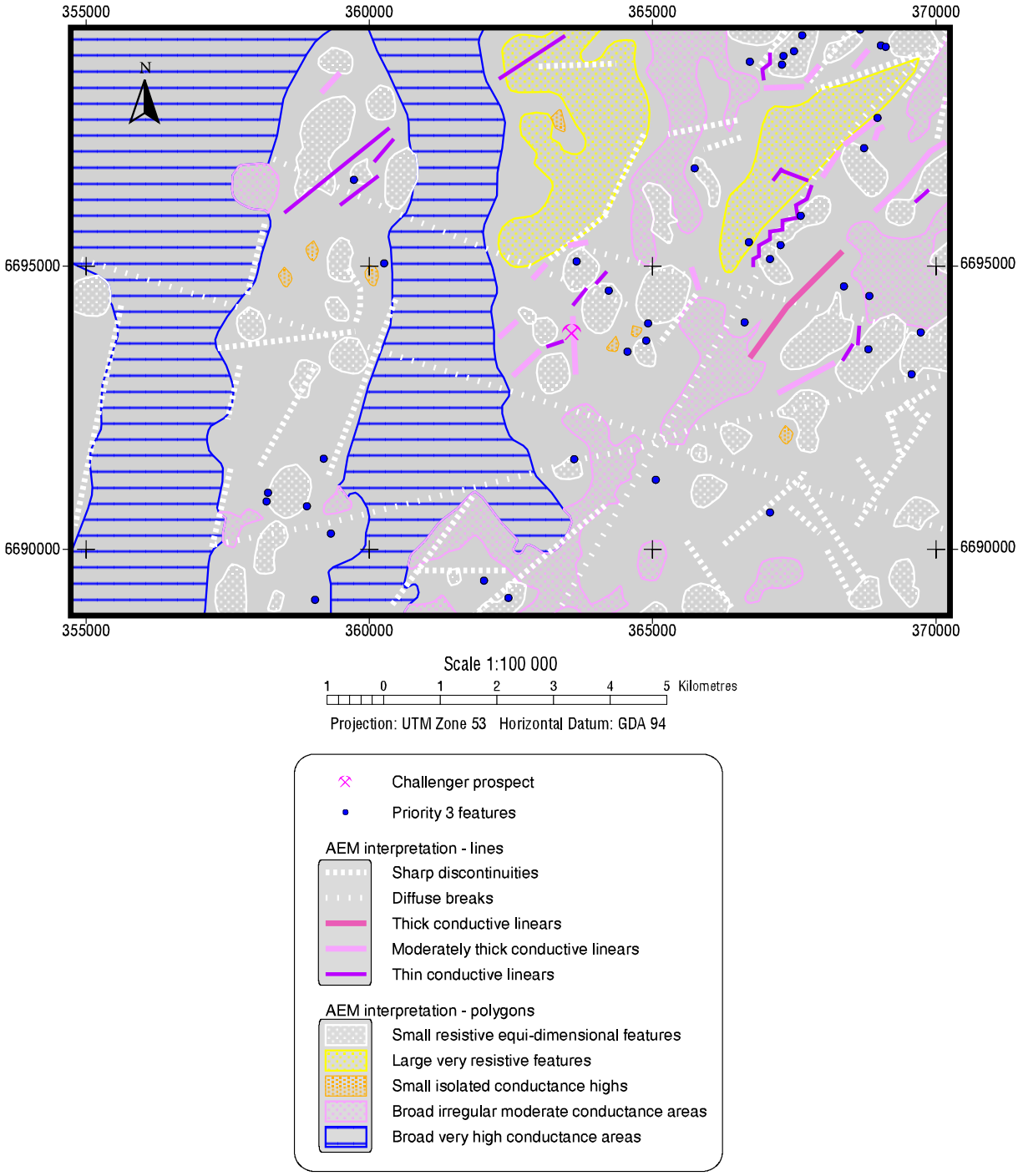

Figure 30. Interpretation of the AEM data.

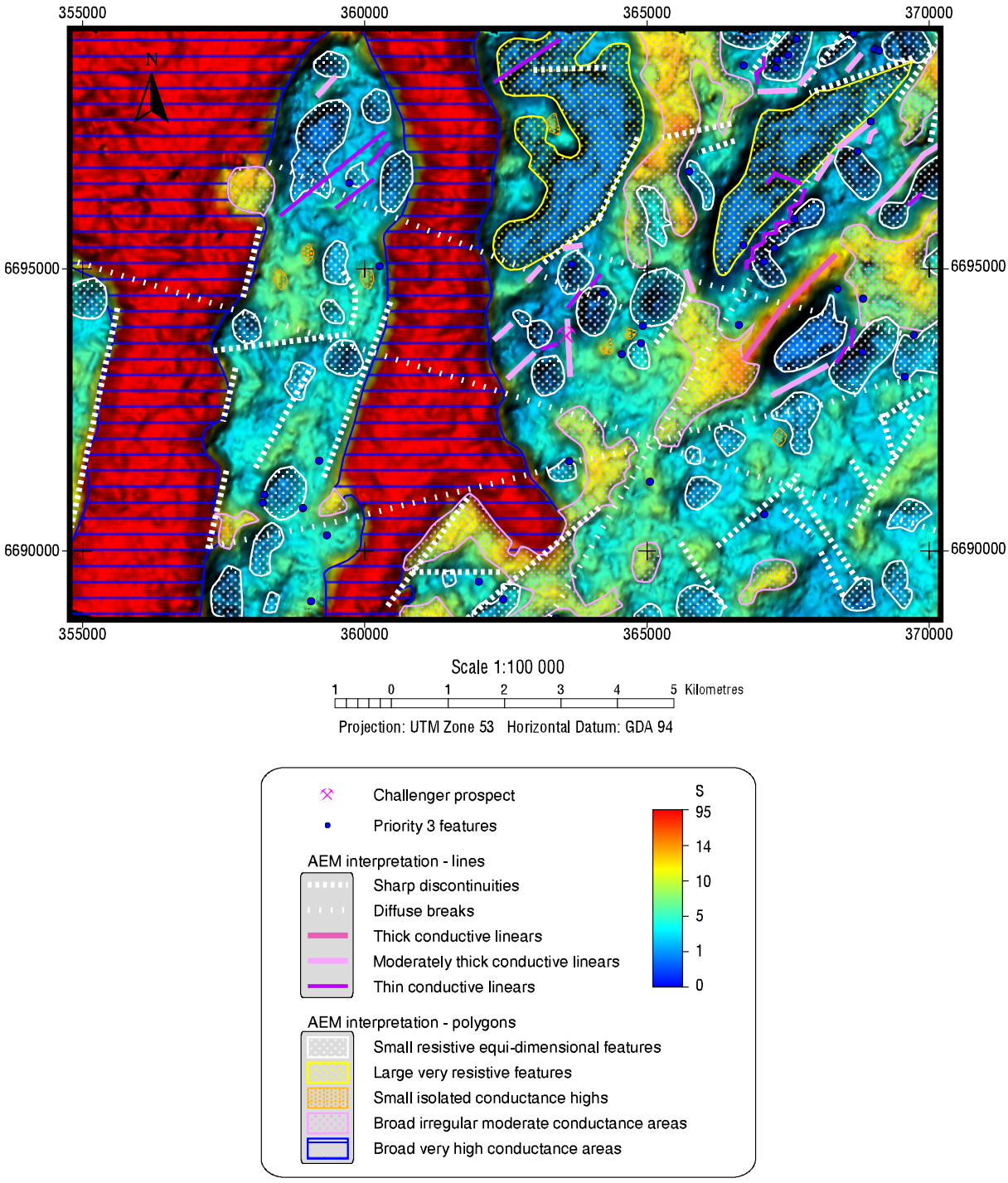

Figure 31. Conductance of "conductive unit" derived from the AEM survey overlain by the AEM interpretation.

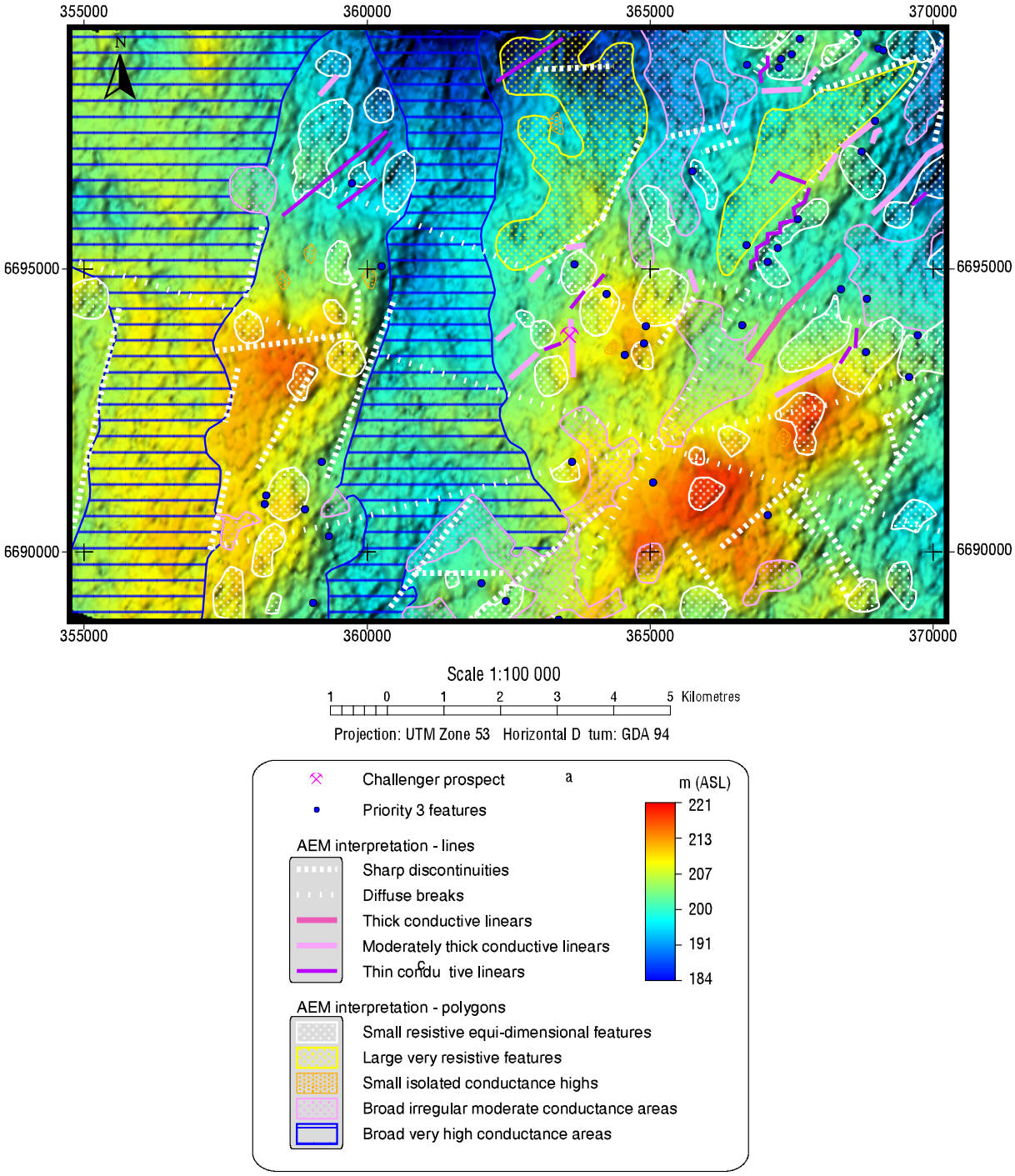

Figure 32. Surface topography derived from the AEM survey overlain by the AEM interpretation.

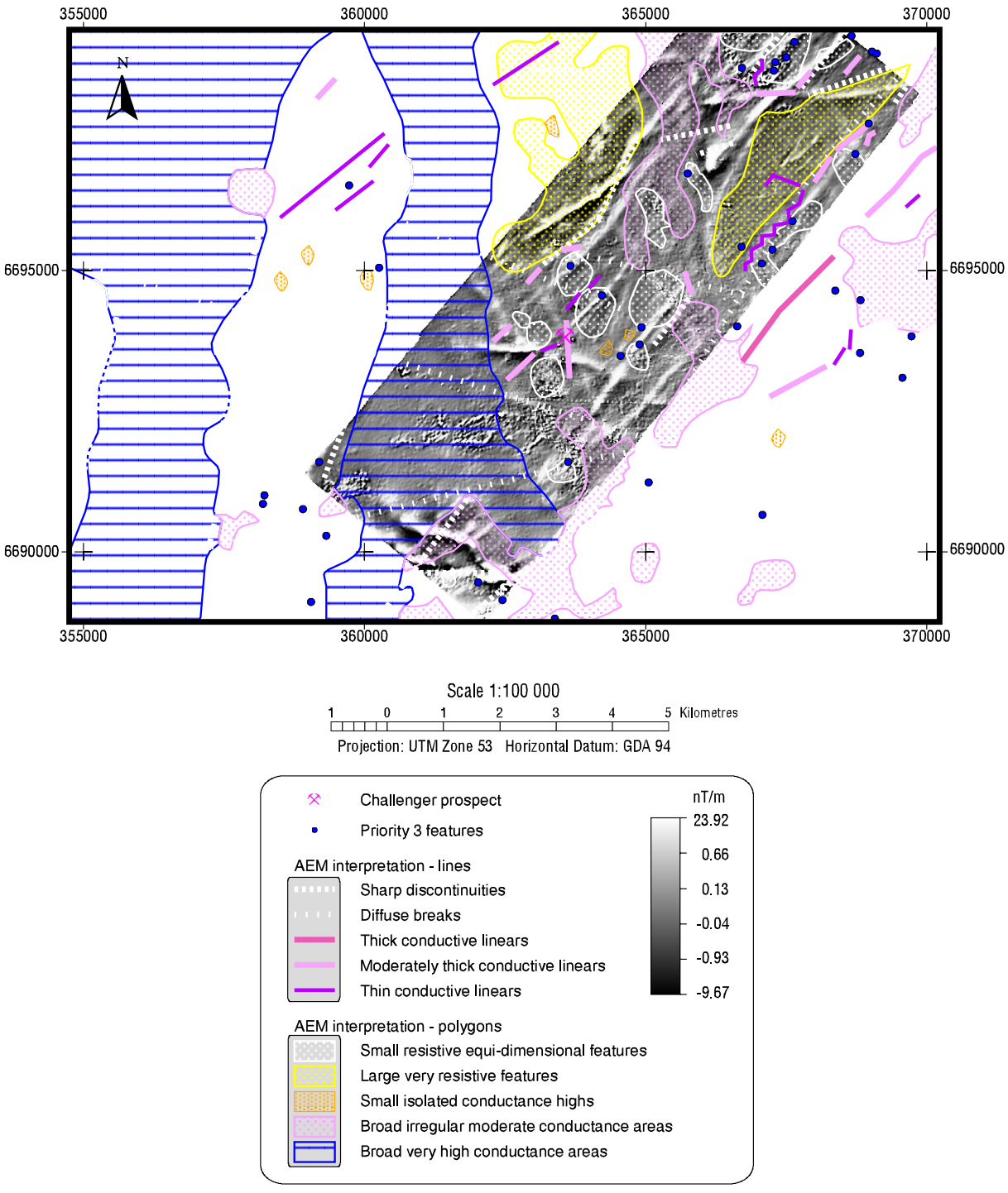

Figure 33. First vertical derivative of total magnetic intensity derived from the company magnetic survey overlain by the AEM interpretation.

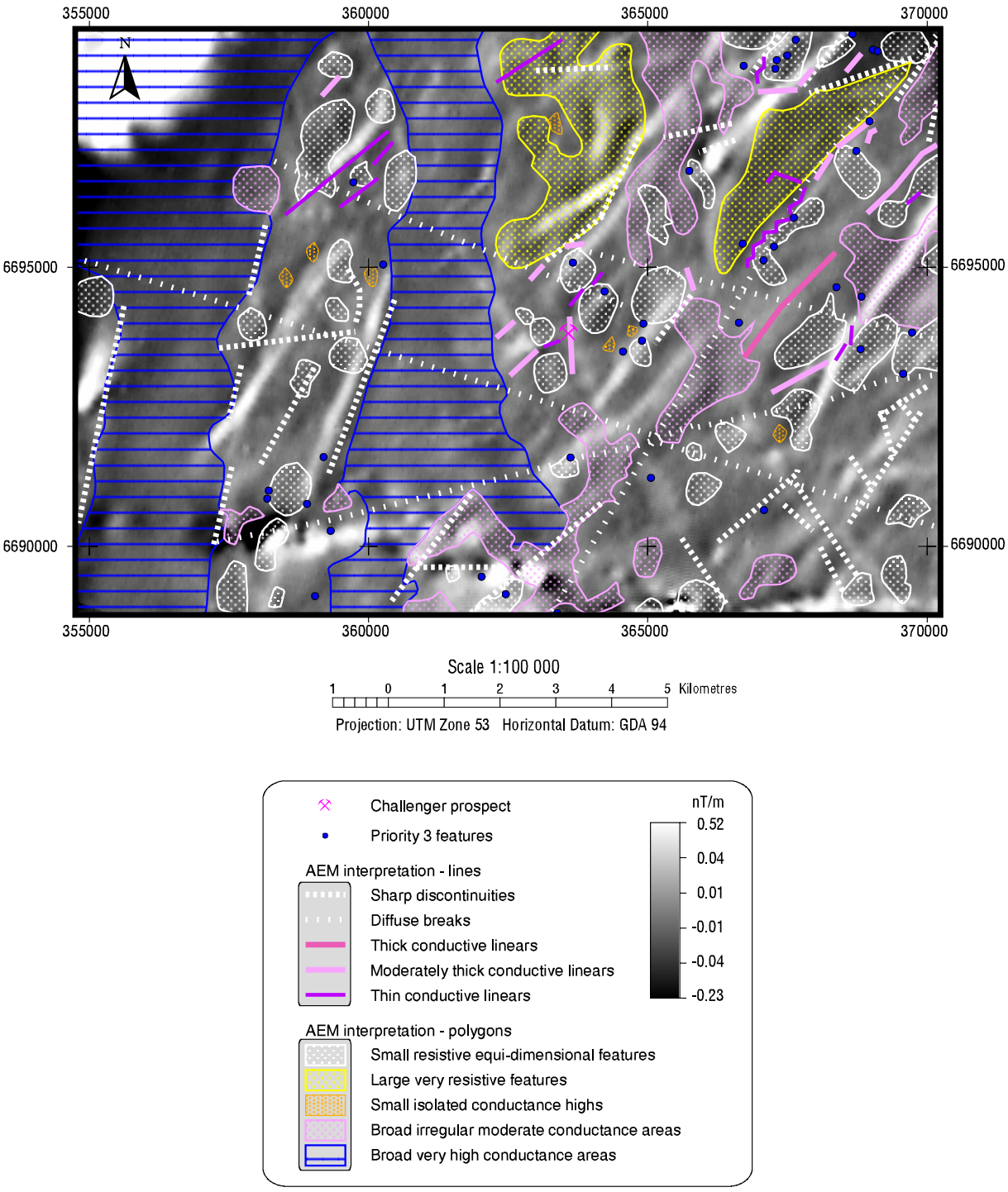

Figure 34. First vertical derivative of total magnetic intensity derived from the AEM survey overlain by the AEM interpretation.

Magnetics and AEM Interpretations

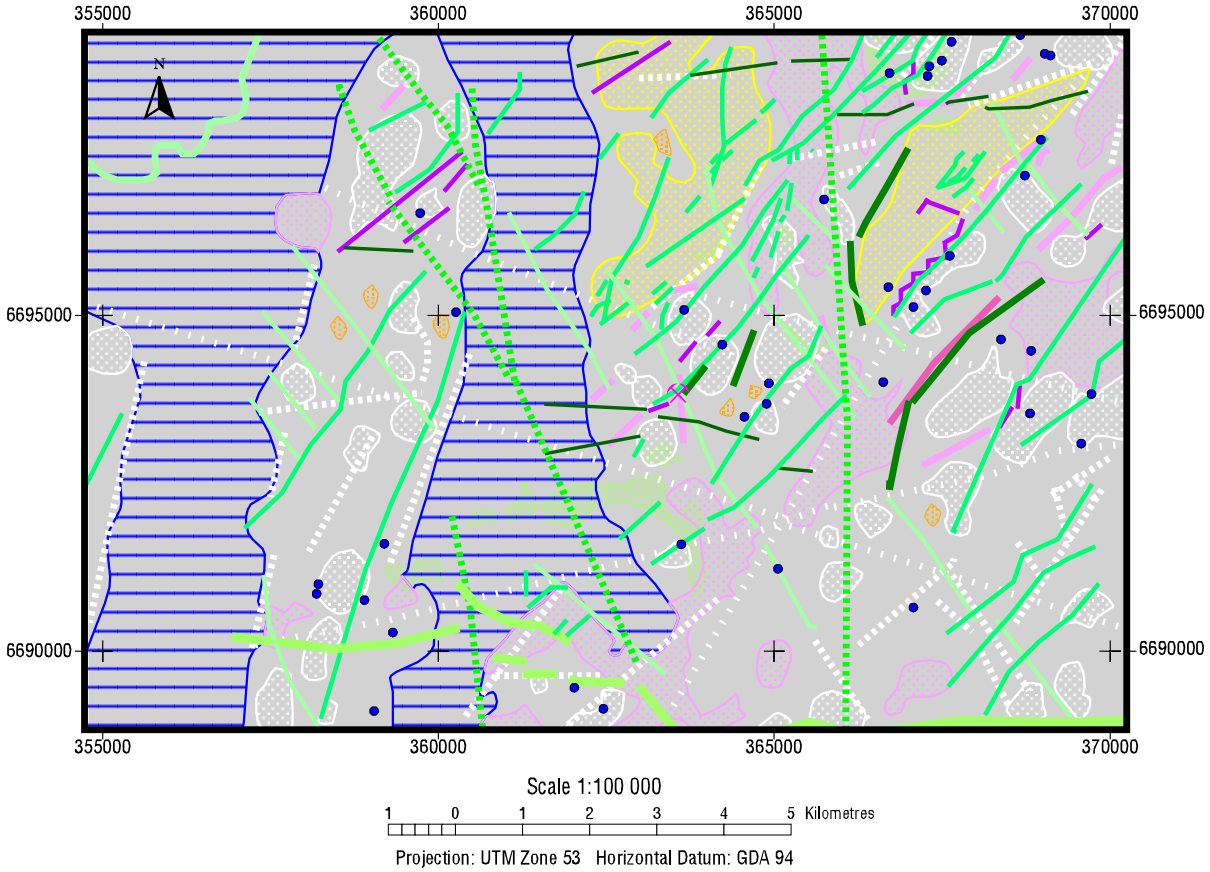

Challenger prospect

Magnetics Interpretation

- Diffuse de-magnetised discontinuities
- Weakly magnetic horizons, generally NNW
- South-east boundary for very highly magnetic features
- Weakly to strongly magnetic horizons, generally NE, shallow depth to top
- Weakly magnetic horizons, generally E/W
- Highly magnetic regionally extensive horizons, generally E/W, broken up
- Very low amplitude horizons, either broad or with greater depth to top
- Short wavelength surficial magnetic deposits

Challenger prospect

Priority 3 features

AEM interpretation - lines

- Sharp discontinuities
- Diffuse breaks
- Thick conductive linears
- Moderately thick conductive linears
- Thin conductive linears

AEM interpretation - polygons

- Small resistive equi-dimensional features
- Large very resistive features
- Small isolated conductance highs
- Broad irregular moderate conductance areas
- Broad very high conductance areas

Figure 35. AEM and Magnetics interpretations combined.